Science & Technology Facilities Council

Technical Report
RAL-TR-2013-016

Neutrons at ESS-Bilbao: From Production to Utilisation

JP de Vicente, F Fernandez-Alonso, F Sordo, FJ Bermejo

December 2013

Enquiries concerning this report should be addressed to:

RAL Library
STFC Rutherford Appleton Laboratory
Harwell Oxford
Didcot
OX11 0QX

Tel: +44(0)1235 445384
Fax: +44(0)1235 446403
email: libraryral@stfc.ac.uk

Science and Technology Facilities Council reports are available online at: http://epubs.stfc.ac.uk

ISSN 1358-6254

Neutrons at ESS-Bilbao: from Production to Utilisation

J.P. de Vicente[1,2]
F. Fernandez-Alonso[3]
F. Sordo[1,2]
F.J. Bermejo[4]

2013

[1] Instituto de Fusion Nuclear, Jose Gutierrez Abascal, 2 28006 Madrid, Spain

[2] Consorcio ESS-Bilbao, Paseo Landabarri, 2 E-48940 Leioa, Biscay, Spain

[3] ISIS Facility, Rutherford Appleton Laboratory, Chilton, Didcot, Oxfordshire OX11 0QX, United Kingdom

[4] Instituto de Estructura de la Materia, Consejo Superior de Investigaciones Cientificas, Serrano, 121 28006 Madrid, Spain

«Neutrons tell you where the atoms are
and what the atoms do»

C. Shull and B. Brockhouse
Nobel Prize Laureates in Physics 1994

Edited by LaTeX

Contents

List of Figures

PART 1: NEUTRONS AT ESS-BILBAO: FROM PRODUCTION TO UTILISATION

PART 2: SUPPLEMENTARY INFORMATION

List of Tables

FOREWORD

Collaborative efforts between the Neutronics and Target Design Group at the Instituto de Fusión Nuclear and the Molecular Spectroscopy Group at the ISIS Pulsed Neutron and Muon Source date back to 2012 in the context of the ESS-Bilbao project. The rationale for these joint activities was twofold, namely: to assess the realm of applicability of the low-energy neutron source proposed by ESS-Bilbao - for details, see [1]; and to explore instrument capabilities for pulsed-neutron techniques in the range 0.05-3 ms, a time range where ESS-Bilbao and ISIS could offer a significant degree of synergy and complementarity. As part of this collaboration, J.P. de Vicente has spent a three-month period within the ISIS Molecular Spectroscopy Group, to gain hands-on experience on the practical aspects of neutron-instrument design and the requisite neutron-transport simulations. To date, these activities have resulted in a joint MEng thesis [2] as well as a number of publications and contributions to national and international conferences [3, 4, 5, 6].

Building upon these previous works, the primary aim of this report is to provide a self-contained discussion of general criteria for instrument selection at ESS-Bilbao, the first accelerator-driven, low-energy neutron source designed in Spain. To this end, Chapter 1 provides a brief overview of the current design parameters of the accelerator and target station. Neutron moderation is covered in Chapter 2, where we take a closer look at two possible target-moderator-reflector configurations and pay special attention to the spectral and temporal characteristics of the resulting neutron pulses. This discussion provides a necessary starting point to assess the operation of ESSB in short- and long-pulse modes. These considerations are further explored in Chapter 3, dealing with the primary characteristics of ESS-Bilbao as a short- or long-pulse facility in terms of accessible dynamic range and spectral resolution. Other practical aspects including background suppression and the use of fast choppers are also discussed. The guiding principles introduced in the first three chapters are put to use in Chapter 4 where we analyse in some detail the capabilities of a small-angle scattering instrument, as well as how specific scientific requirements can be mapped onto the optimal use of ESS-Bilbao for condensed-matter research. Part 2 of the report contains additional supporting documentation, including a description of the ESSB McStas component, a detailed characterisation of moderator response and neutron pulses, and estimates of parameters associated with the design and operation of neutron choppers.

In closing this brief foreword, we wish to thank both ESS-Bilbao and ISIS for their continuing encouragement and support along the way.

Acronyms

AC Advanced configuration

BC Baseline configuration

ESSB ESS-Bilbao

FWHM full-width-at-half-maximum

HWHM half-width-at-half-maximum

ISIS-TS2 ISIS Target Station 2

LAP Line shape Asymmetry Parameter

LPM Long-Pulse Mode

NPF Neutron-Pulse Falling edge

NPR Neutron-Pulse Rising edge

nUN non-Useful Neutrons

SNP Symmetrized Neutron Pulse

SPM Short-Pulse Mode

TMR Target-Moderator-Reflector

TOF Time of Flight

TS Target Station

UN Useful Neutrons

WAP Width Asymmetry Parameter

PART 1: NEUTRONS AT ESS-BILBAO: FROM PRODUCTION TO UTILISATION

1 THE ESS-BILBAO PROJECT

1.1 Brief historical overview

The use of neutrons for condensed-matter research followed the development of fission reactors in the 1940s, just a decade after the discovery of this elusive particle by Chadwick in 1932. In the 1970s, the possibility of using particle accelerators to drive neutron production became a reality and led to the construction of large-scale accelerator-based neutron facilities in Japan, USA, and the United Kingdom. Second-generation spallation sources using higher-intensity proton accelerators followed at the end of the last century with the construction of the Spallation Neutron Source (SNS) at Oak Ridge (USA) and the Materials and Life Science Experimental Facility in J-PARC (Japan), efforts soon to be emulated by the China Spallation Neutron Source (CSNS) currently under construction in Guandong Province near Hong Kong.

The possibility of building a European Spallation Source (ESS) [7] was first explored in the 1990s. During the early 2000s, a number of European cities including Bilbao (Spain) presented their candidature to host the ESS, and this process led to the decision in 2009 to build the ESS in Lund (Sweden). At the time of writing, the ESS-Bilbao (ESSB) project seeks to complement this wider pan-European initiative via the construction and operation of a smaller neutron source in Spain. While the higher-intensity ESS is expected to be fully operational a decade from now, ESSB could start operations as early as 2016. With this lower-scale infrastructure development at a national level, the ESSB and its associated neutron community in Spain will be in a strong position to support at various levels the development of more ambitious European efforts.

In the above context, it is important to stress that ESSB will not be a spallation neutron source per se, but rather a far more compact one where neutrons are produced via direct (p,n) reactions at significantly lower proton energies [8] . A similar approach to neutron production is used at LENS at the University of Indiana in the USA [9] , although its total neutron output remains significantly lower than the calculated source term of $\sim 10^{15}\ n\ s^{-1}$ for ESSB [1]. Moreover, the construction and subsequent operation of ESSB stands as a reference project within the current Spanish roadmap of scientific infrastructures. Upon its completion, its primeary remit will be to support both the Spanish scientific community as well as the ESS project.

1.2 Facilities

The ESSB facility will be hosted on the Leioa campus of the University of the Basque Country (UPV/EHU), near Bilbao (Spain). The layout of the main building is shown in Figure 1-1, highlighting its primary components.

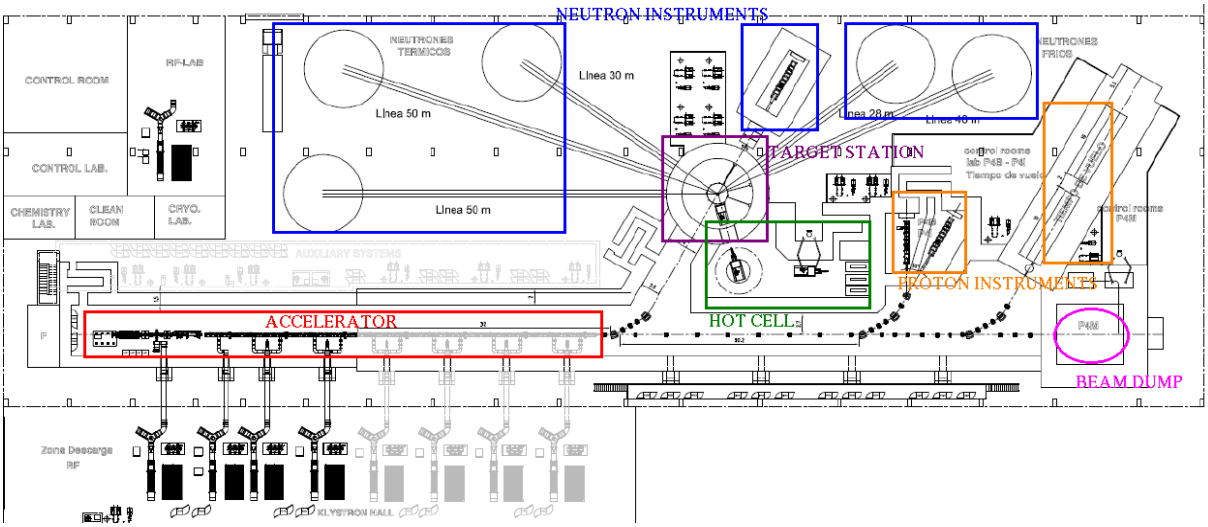

Figure 1-1: Layout for the ESSB facility.

As detailed in Fig. 1-1, a proton **accelerator** goes along the main building, accelerating protons up to 50 MeV before they are bent and directed towards the neutron **target station** (TS). The TS is roughly located at the center of the main building. Neutrons produced at the TS can then be guided into a series of **neutron instruments** arranged radially relative to the TS monolith. **Proton instruments** are placed further downstream along the primary proton-beam direction. A **hot cell** sits next to the TS for the storage and subsequent decay of activated materials and components. Finally, a **beam dump** (BD) is located along the line of sight of the proton LINAC. The main components of the ESSB facility are summarized in more detail below.

1.2.1 ACCELERATOR

The proton LINAC produces intense and pulsed proton beams which are subsequently guided to the neutron TS. It consists of a series of components that increase the proton energy up to MeV energies and shape the proton beam as required for optimal transport and use. Figure 1-2 shows a schematic block diagram of its main components.

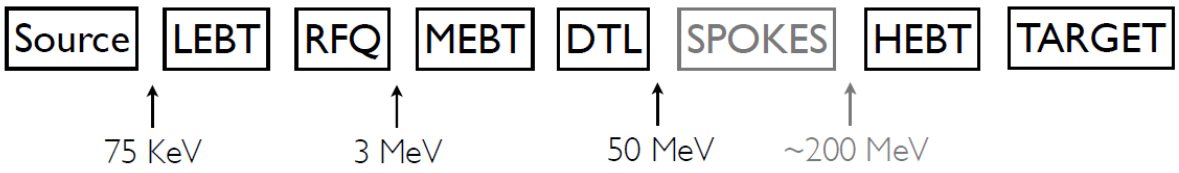

Figure 1-2: Schematic block diagram of the ESSB LINAC [10].

In an initial stage, protons are extracted from a plasma chamber at the ion source. Two types of interchangeable ion sources producing either H^+ cations or H^- anions are envisaged,

although operation at any given time will be restricted to one type of source. In the case of the H^+ source, protons exit the ion source at an energy of 75 keV, and are guided through the low-energy beam transport (LEBT) section for injection into a radio frequency quadrupole (RFQ). At the RFQ, protons are grouped and further compressed into *bunches* and accelerated up to 3 MeV. At this point, the medium-energy beam transport (MEBT) unit takes the beam to the drift-tube LINAC (DTL), where the beam is finally accelerated up to 50 MeV. Future upgrades of the facility include acceleration up to 200 MeV by means of additional spoke cavities and a high-energy beam transport (HEBT) section [10]. Table 1-1 lists final proton-beam parameters as reported in the latest LINAC design report [11].

Table 1-1: ESSB proton-beam Parameters.

Species	H^+
Particle Energy	$50 - 60$ MeV
Peak Current	75 mA
Average Current	$2 - 5$ mA
Repetition Rate	$20 - 50$ Hz

1.2.2 TARGET STATION

The ESSB TS hosts a target for neutron production and its auxiliary components. The neutron target [12] consists of a rotating wheel (aluminium alloy 6061 T6) with beryllium plates, as shown in Figure 1-3. Following a comparative study of potential materials for the target plates, beryllium was chosen on the basis of its optimal ratio between neutron yield and average neutron energy – 0.065 neutrons per incident proton at an average energy of 7.76 MeV [8]. This target assembly is cooled with water injected into the target wheel at a flow rate of 26 l/s in order to dissipate a total power load during operation of 112.5 kW [13]

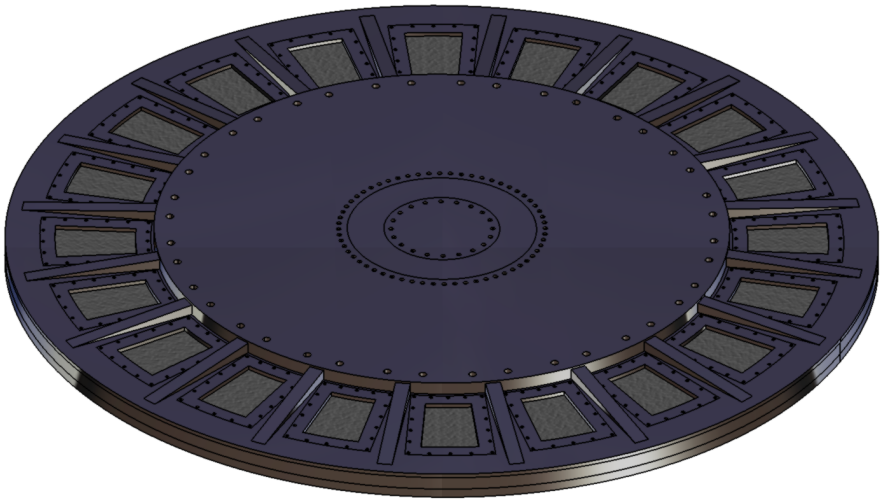

Figure 1-3: ESSB rotating target wheel [12].

The current design of the target wheel includes a total of twenty beryllium plates. Given a proton-pulse repetition rate of 20 Hz, each plate would therefore see an effective frequency of 1 Hz. Account made of other design parameters, the total beam power into the target is 112.5 kW.

The rotating target is located inside a target vessel (TV). This vessel is made of steel and encloses moderators, reflector, shielding, a target-positioning unit, as well as proton and neutron tubes. The TV is shown in Figure 1-4. It acts as a radiation shield, confines possible radioactive products, and contains the necessary equipment to drive the cooling and mechanical rotation of the neutron target.

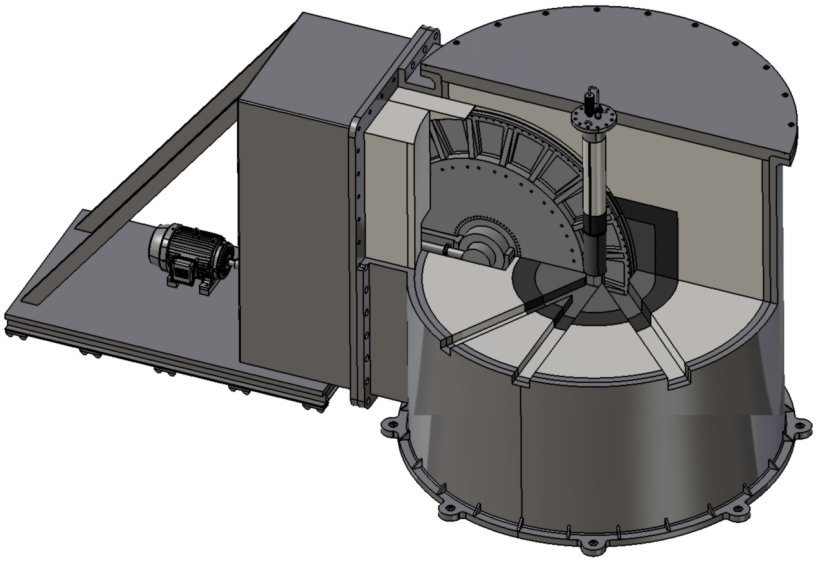

Figure 1-4: ESSB target vessel [12].

The TS is a large concrete structure hosting the TV, as well as neutron and proton tubes. Its purpose is to shield radiation coming from the TV and to allow for sufficient space for the operation and maintenance of the target, moderators, and reflector. An overview of the TS is shown in Figure 1-5.

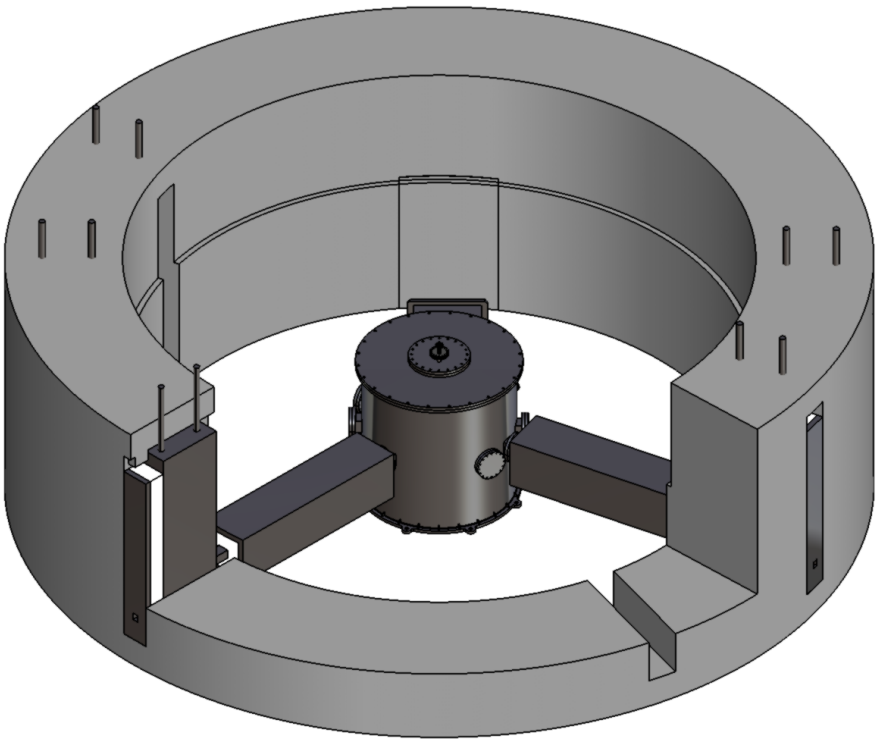

Figure 1-5: Overview of ESSB target station [12].

2 NEUTRON MODERATION

This chapter examines neutron moderation in the ESSB target station without any further adjustments to the beam that might be required in neutron-scattering instruments, i.e., chopping, focusing, collimation, and so on. All neutrons are the result of a (direct) nuclear reaction between beryllium in the target and proton pulses with an energy of 50 MeV and peak currents up to 75 mA. These proton pulses can be produced between 0.1 ms (at a repetition frequency of 50 Hz) and 1.5 ms (at 20 Hz). Within these two extremes of operation, the cooling system can safely withstand the associated heat load on the rotating target.

Figure 2-1 shows a two-dimensional cut of the neutron-source model described in more detail in Ref. [14] . In this model, neutrons are produced by a **nuclear stripping reaction** on the beryllium target due to the impact of protons at an energy of 50 MeV. The Be(p,n) reaction is the most efficient process for neutron production with protons at these energies [15] . For the efficient production of cold neutrons, methane at 22 K has been chosen as moderating medium. Both beryllium target and moderator are also surrounded by a beryllium reflector. As the name implies, this component of the target station reflects neutrons back into the moderator in order to increase cold-neutron yields. We shall see later on that this secondary re-injection process can be detrimental to the time structure of moderated neutrons and a compromise must therefore be struck between flux and time widths. Other components shown in the figure include premoderators, grooves, and energy filters, described in more detail below.

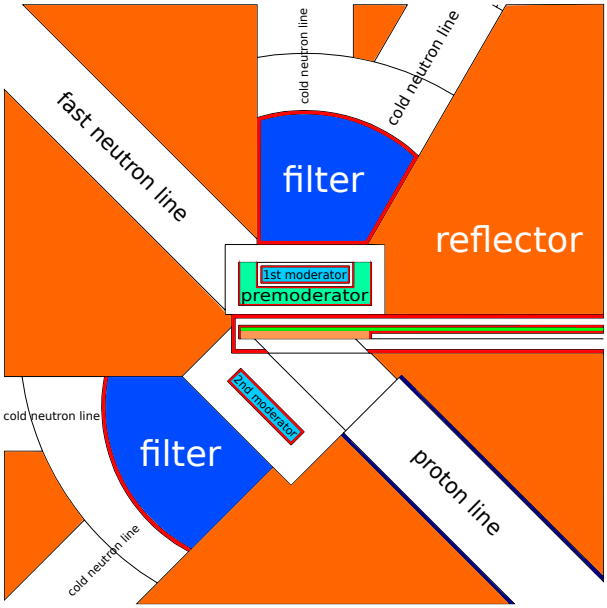

Figure 2-1: Two-dimensional view of the ESSB TMR assembly (advanced moderator configuration).

As opposed to spallation processes, it is important to note that neutrons emerging from a stripping reaction retain a good fraction of the momentum and direction of the incoming proton beam [16] . To capitalise on this feature, the ESSB model shown in Figure 2-1 has a fast-neutron line collinear with the proton beam in addition to thermal/cold ports. In this situation, a SLAB configuration for the moderators results in a significant reduction of high-energy neutron backgrounds of no practical use in conventional neutron-scattering instruments. This report will be devoted to an analysis of cold-neutron fluxes emerging from these moderator faces. The **baseline configuration** consists of a methane moderator, whereas the **advanced configuration** includes the possibility of grooved moderator faces, as well as the use of a water premoderator and a beryllium filter placed in front of the moderator face at 77 K, as described in detail in Refs. [1] and [17]. In either case, the MCNPX code from Los Alamos [18] was used calculate the neutronic response of these various Target-Moderator-Reflector (TMR) geometries, followed by an analysis of spectral and temporal properties using the BILBAO_source McStas component (see APPENDIX A, pag. 69).

2.1 Time-integrated flux

The time-integrated flux, i.e., the total number of neutrons emerging from a given moderator as a function of the wavelength regardless of its underlying time structure, is shown in Figure 2-2. This figure shows this quantity (**per pulse**) for several cases, including only one methane moderator, two methane moderators, and the addition of a water premoderator (Figure 2-3). To facilitate a first comparison, no beryllium filters have been considered in these calculations.

The use of a second moderator reduces the flux at the face of the first one. Such a reduction arises from the presence of a gap in the reflector, needed to host the second moderator. In spite of this flux reduction, the addition of a second moderator gives the possibility of accommodating a higher number of neutron beamlines around the ESSB TMR. It is also to be noted that the use of a water premoderator results in a relatively modest (∼10%) gain in time-integrated flux at thermal and cold neutron wavelengths.

Figure 2-4 reports the time-integrated flux per pulse for the baseline configuration (two methane moderators) compared to the advanced configuration (grooved moderator faces and beryllium filter) [17]. The primary effect of the beryllium filter is to reflect high-energy neutrons back into the TMR assembly as well as further moderate the epithermal tail. Hence the advanced configuration can reduce high-energy backgrounds and produce 20% more cold neutrons (above 0.35 Å) than the baseline configuration. As shown later on, the prominent peak around 1.5 Å in the advanced configuration will only be useful for coarse-resolution applications where the time distribution is not a relevant parameter. The low response of the Be-filter between 2 and 4 Å gives rise to a valley where the flux is reduced to 50% relative to baseline values. Nevertheless these effects can give rise to an increase in flux of ca. 60% above 4 Å 60% relative to the baseline configuration.

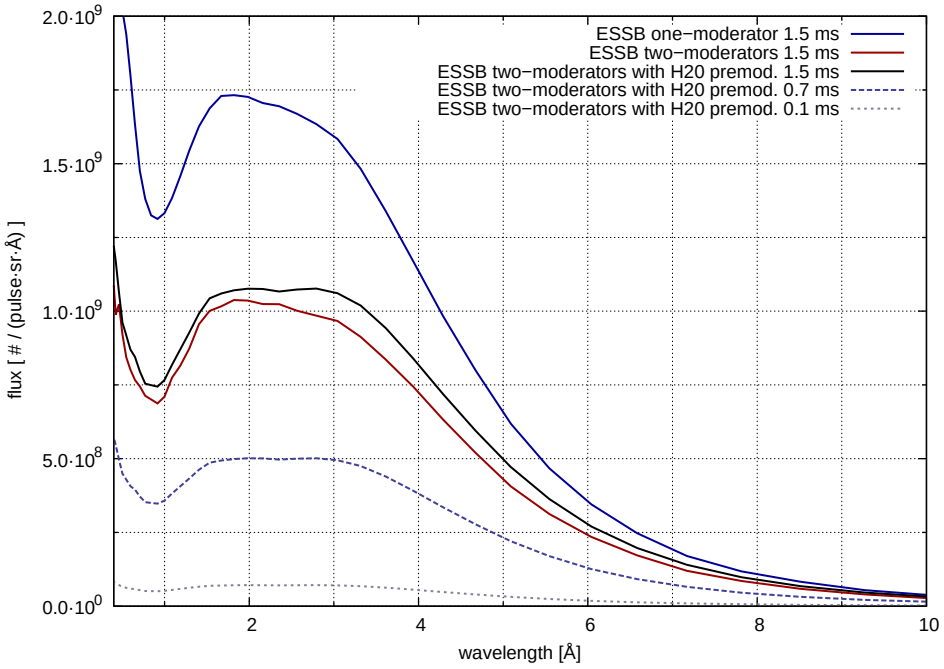

Figure 2-2: Time-integrated flux per pulse for configurations without filter.

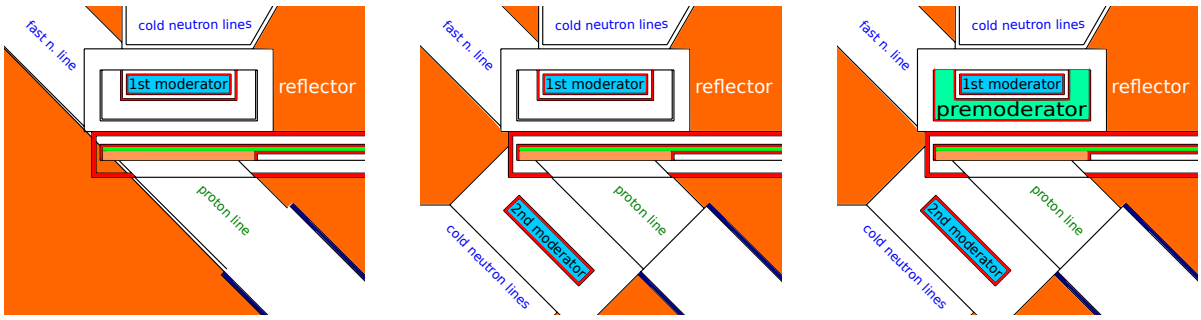

Figure 2-3: Two-dimensional cuts of TMR geometries discussed in the accompanying text: one moderator (left), two moderators (middle), and addition of a water premoderator (right).

To place the above numbers in the context of other developments in target design and performance, Figure 2-5 provides a comparison with the hydrogen and grooved moderators on ISIS Target Station 2 (ISIS-TS2). This figure shows that a single long pulse of cold neutrons (1.5 ms above 0.35 Å) from the ESSB baseline/advanced configuration could produce between 20 and 30% of the neutronic output of a single ISIS-TS2 pulse. Likewise, between 1 and 2 Å, the ESSB advanced configuration could produce a similar time-integrated flux than ISIS-TS2. Between 2 and 4 Å, the ESSB baseline configuration can only reach up to 20% of ISIS-TS2. ESSB moderators perform quite well above 4 Å, where the neutron yield in both ESSB and TS2-ISIS decreases monotonically. These results shown that the ESSB advanced configuration could produce as much as 50% of the ISIS-TS2 hydrogen-moderator time-integrated flux above 6 Å.

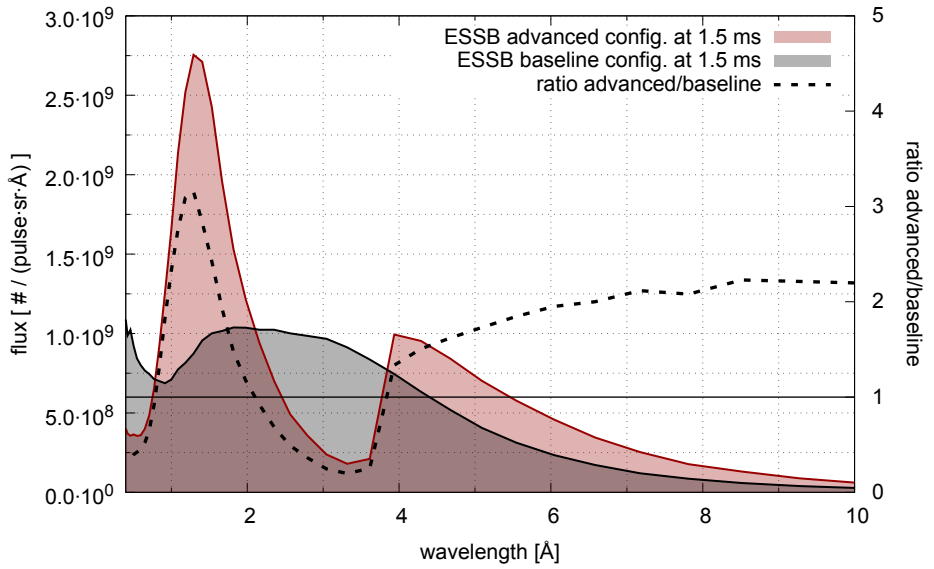

Figure 2-4: Time-integrated flux per pulse for baseline and advanced configurations.

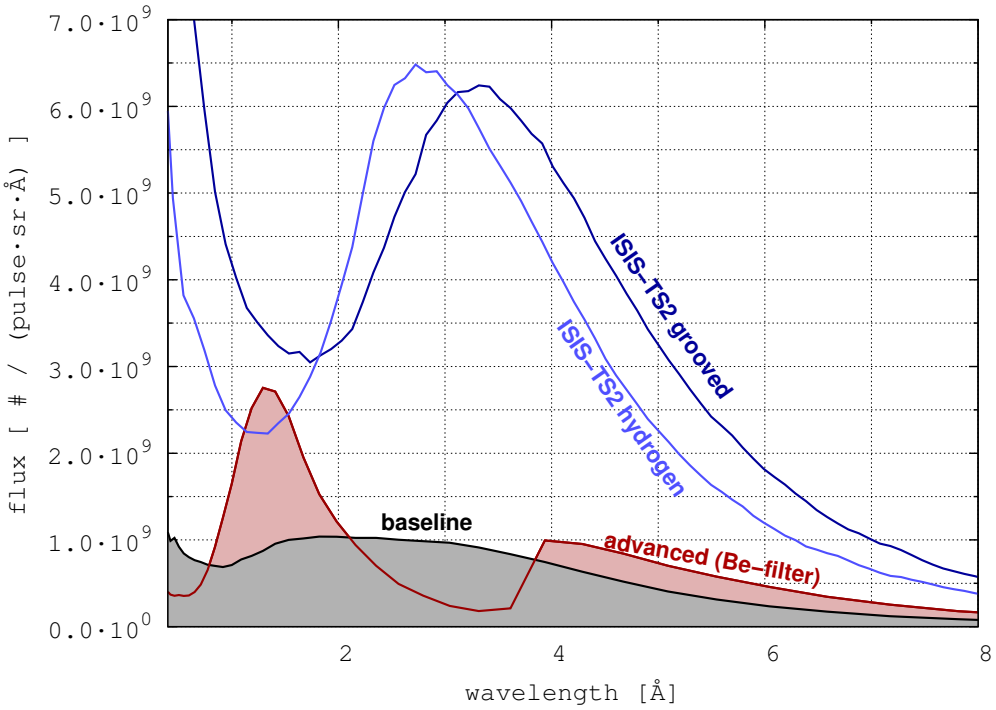

Figure 2-5: Time-integrated flux per pulse for ESSB baseline and advanced configurations compared to ISIS-TS2 (grooved and hydrogen faces).

The different operational modes of the ESSB accelerator, i.e., the length and repetition rate of the proton pulses reaching the neutron target, determines the time-integrated flux **per second** (not per pulse) at the moderator face. As already discussed above, the ESSB accelerator can operate between two well-defined limits, namely, in short-pulse (0.1 ms at 50 Hz) and long-

pulse modes (1.5 ms at 20 Hz), hereinafter denoted as SPM and LPM, respectively. Figure 2-6 shows the time-integrated flux per second for ESSB-SPM and LPM compared with ISIS-TS2, the latter using ub-μsec proton pulses. At a first glance, this figure shows again how LPM could deliver six times more neutrons per second than SPM regardless of time structure. Compared to ISIS-TS2 (running at 10 Hz), the LPM (running at 20 Hz) could improve its ratio of time-integrated flux "per second" relative to "per pulse" by a factor of two (20 Hz /10 Hz), although at the price of a reduced dynamic range since at 20 Hz neutron pulses will be closer to each other in the time domain. Table 2-1 summarises the ratios of time-integrated flux per second for several wavelength intervals using the LPM baseline configuration as reference.

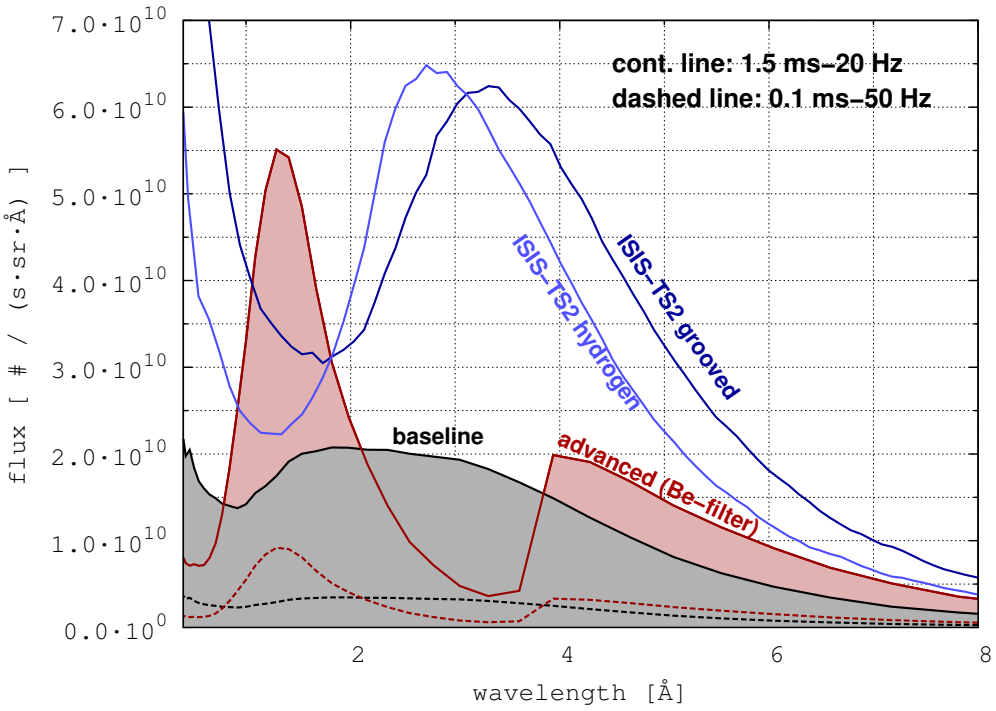

Figure 2-6: Time integrated flux per second for ESSB baseline and advanced configurations compared to ISIS-TS2 grooved and hydrogen moderators.

Table 2-1: Time-integrated flux per second referenced to the ESSB-LPM baseline configuration.

	1-2 Å	2-3 Å	3-4 Å	4-5 Å	5-6 Å	6-7 Å	7-8 Å
ISIS-TS2 grooved @ 10 Hz	x1.69	x2.09	x3.09	x3.40	x3.48	x3.29	x3.26
ISIS-TS2 hydrogen @ 10 Hz	x1.32	x2.62	x2.78	x2.52	x2.36	x2.16	x2.15
Advanced config. 1.5 ms 20 Hz	x2.20	x0.58	x0.40	x1.37	x1.58	x1.75	x1.83
Advanced config. 0.1 ms 50 Hz	x0.37	x0.10	x0.07	x0.23	x0.26	x0.29	x0.30
Baseline conf. 1.5 ms 20 Hz	**x1.0**	**x1.0**	**x1.0**	**x1.0**	**x1.0**	**x1.0**	**x1.0**
Baseline conf. 0.1 ms 50 Hz	x0.17	x0.17	x0.17	x0.17	x0.17	x0.17	x0.17

To sum up, a single ESSB pulse can produce up to ca. 20-30% of an ISIS-TS2 pulse. Account made of the source repetition rate, the time-integrated cold-neutron flux per second from ESSB approaches that of ISIS-TS2 at certain wavelengths. Nevertheless, this rather favourable comparision can only be achieved in LPM and, therefore, its realm of applicability would be highly dependent on application.

2.2 Time structure

The time-integrated flux provides a convenient metric to assess total cold-neutron production, envisaged to be useful in applications requiring little or no wavelength resolution using TOF techniques (i.e., running ESSB as a steady-state neutron source). It is nonetheless well known that the inherent lower neutron yield from accelerator-driven pulsed sources relative to steady fission reactors can be offset by orders of magnitude via judicious exploitation of the inherent time structure of the former, as discussed in depth in Refs. [19], [20] and [21]. These considerations require going beyond a simple analysis of the total time-integrated flux and are of particular relevance when one considers applications requiring medium and high wavelength resolution. From the outset, we recognize that the following features of ESSB may actually weaken the rather optimistic comparison presented in the previous section, namely:

- ESSB pulses can be considerably broader than those available on ISIS-TS2, and
- ESSB pulses will have longer Neutron-Pulse Falling edge (NPF) or tail and, therefore, a worse ratio Useful Neutrons (UN)/non-Useful Neutrons (nUN) in a number of applications. For the purposes of the present discussion, we will take the Neutron-Pulse Rising edge (NPR) as a measure of UN. This simple estimator is of particular relevance to the time response of LPM.

A more appropriate way to measure the potential use of ESSB for high-resolution applications and hence to compare it directly with ISIS-TS2 could involve considering the neutron flux around the most-probable (peak) value. Figure 2-7 shows the peak fluxes for ESSB and ISIS-TS2 (note the logarithmic scale on this figure). It can be seen that ISIS-TS2 provides around two-order-of-magnitude higher peak fluxes than ESSB, because the latter are inherently too spread out in the time domain. The largest differences in peak flux can be observed around 1 Å, where the moderator response is fast (microseconds) and, hence, ISIS-TS2 pulses will be much brighter compared to ESSB (dominated by an already broad proton pulse). For ESSB, the situation becomes more favourable for neutron wavelengths above 2-3 Å, as intrinsic moderation times increase to hundreds of microseconds in both cases. Between 2 Å and 4 Å, we also note that the ESSB baseline configuration can provide higher peak fluxes than the advanced configuration.

Figure 2-8 extends the comparison presented above to account for source repetition rate, so as to compare peak-flux ratios per second (as opposed to per pulse) relative to the ESSB baseline configuration in LPM. As in the previous case, ESSB peaks fluxes are still significantly below those characteristic of ISIS-TS2 for neutron wavelengths below 1 Å. This ratio improves quite significantly at longer wavelengths as the ISIS pulses also tend to spread out owing to longer

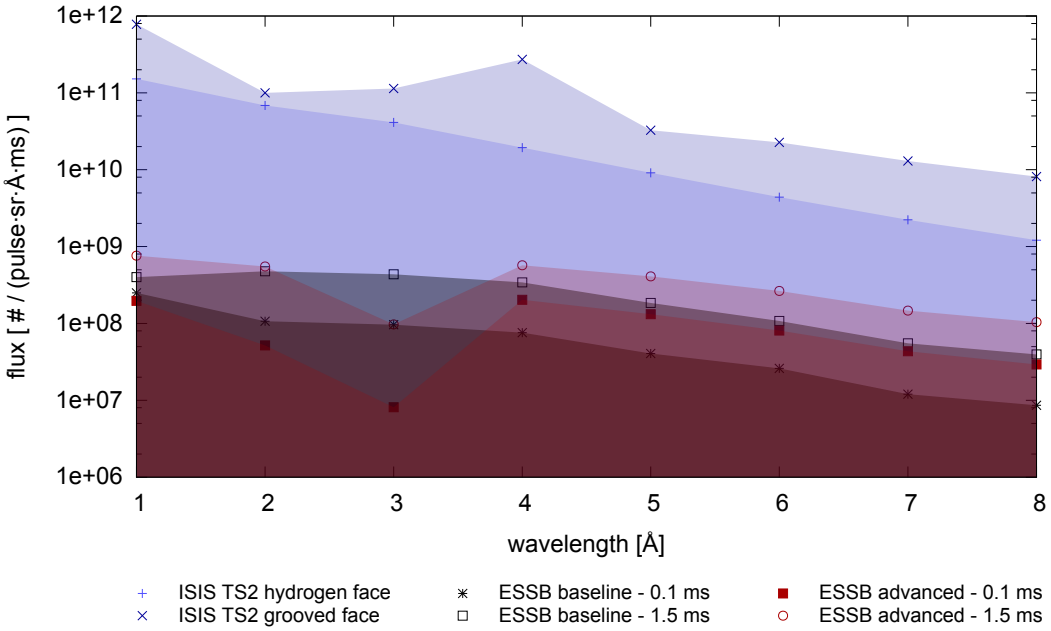

Figure 2-7: Comparison of peak neutron flux per pulse: ESSB baseline and advanced configurations versus ISIS-TS2 moderators.

(intrinsic) moderation times. At 8 Å, the ESSB-LPM advanced configuration becomes six times lower the ISIS-TS2 hydrogen moderator. Furthermore, LPM provides a higher peak flux per second than SPM, in spite of the higher repetition rate of the latter. Another point of favour of LPM resides in its intrinsically wider dynamic range given its lower repetition rate. These advantages must, however, be tensioned against other instrumental requirements and constraints such as spectral resolution, overall length of the beamline, etc. Overall, the above results begin to suggest that ESSB provides competitive capabilities in LPM and SPM for wavelengths above ca. 3 Å.

At this juncture, we can examine the UN flux that ESSB could provide for a given wavelength band. Figure 2-9 illustrates the important distinction between UN and total neutron fluxes for typical ESSB-LPM operation. In well-established pulsed-neutron instrument concepts (see Refs. [19] and [21]), the selected time width of UN is directly related to the ultimate spectral resolution. Hence, if we can adjust the time width, it is possible to adjust the resulting spectral resolution. Figure 2-10 shows the time-integrated flux of UN adjusted to time widths of 0.6, 0.2, and 0.08 ms for LPM, i.e., ESSB tuned for medium- and high-resolution applicactions. It must be noted, however, that the values shown in this figure correspond to the best-case scenario, where a fast chopper placed next to the moderator (technically difficult) would cut the pulses perfectly. We will treat more realistic scenarios later on in this chapter.

Hence the potential use of ESSB for neutron-scattering applications will be on the order of 100 times less than ISIS-TS2 at thermal and epithermal wavelengths. Above 4-5 Å, this figure

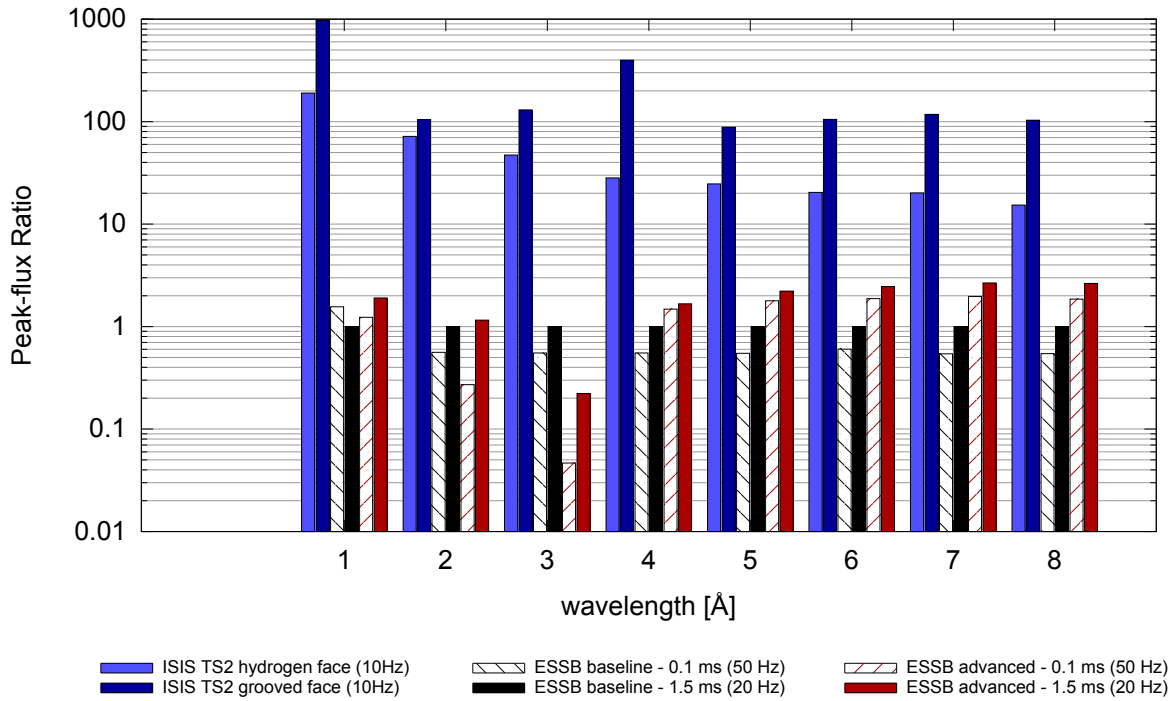

Figure 2-8: Comparison of peak-flux ratios per second for ESSB and ISIS-TS2 referenced to the ESSB-LPM baseline configuration (1.5 ms, 20 Hz).

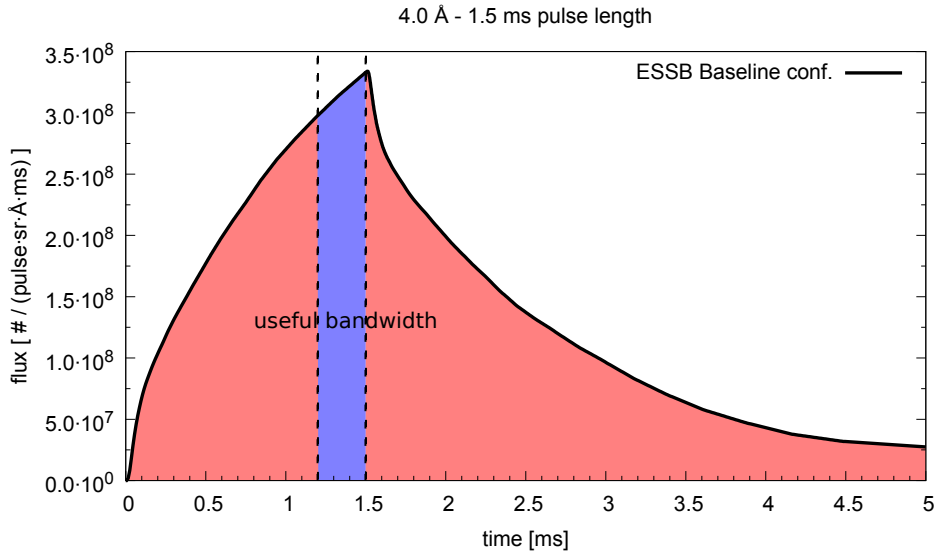

Figure 2-9: Example of the temporal range dictating the UN bandwidth for a particular application, e.g., chopper spectroscopy.

is significantly more favourable with a ca. ten-fold relative increase in performance, placing ESSB a reasonable factor of ca. 7 below ISIS-TS2.

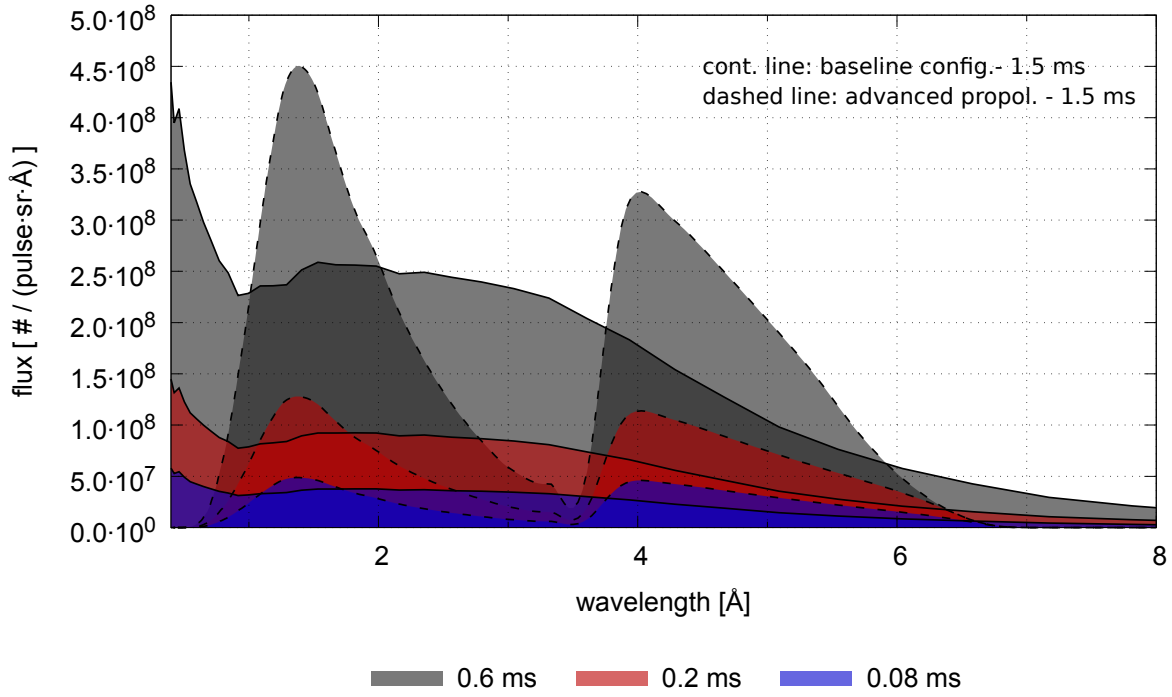

Figure 2-10: Time-integrated flux of UN for customized time widths as a function of wavelength.

2.3 Intrinsic time response

The intrinsic time response of the TMR (including target, reflector, premoderador, moderator, and filters in the advanced configuration) is important for a number of reasons and, in particular, because:

- It corresponds to the neutronic output from an infinitely sharp proton pulse and, therefore, it serves to define a characteristic timescale for the creation of a particular band of neutron wavelengths. As such, it can be strongly dependent on this quantity and can be a major contribution to the ultimate spectral resolution of the outgoing neutron beam.
- It may be responsible for the emergence of long NPFs in the time structure. For ESSB, this can be an important contributionn, leading to long NPFs due to the inherent coupling between moderator and reflector.
- Together with the length of the proton pulse, it determines the shape of the neutron pulse, particularly in SPM – for LPM, the temporal response is largely dominated by the duration of the proton pulse alone.

If the length of the proton pulse is much shorter than the moderator response time, then the neutron pulse will be dominated by the latter. Such is the case of ISIS-TS2, where the synchrotron delivers two sub-microsecond proton pulses whose duration is much shorter than the moderator response for cold neutrons – intrinsic neutron time widths become comparable

to the proton-pulse duration only for epithermal neutrons (>1 eV). At the other extreme, if the proton pulse is much longer, the neutron pulse will be dominated by the proton pulse (ESSB-LPM with proton pulses of duration up to 1.5 ms). For ESSB-SPM the length of the moderator response and the proton pulse are similar and, therefore, does not conform to either limiting case presented above.

Figure 2-11, and Figures B.1-1 to B.1-8 in APPENDIX B, pag. 76 show the intrisic moderator response of ESSB and ISIS-TS2 over the neutron-wavelength range 1-8 Å. These data show that the response of the ESSB baseline configuration is relatively similar to the ISIS-TS2 ones (the temperatures of the moderators are similar). Significant departures are observed for the ESSB advanced configuration from 2 to 3 Å, a region where the effect of the beryllium filter is to induce a further broadening of the intrinsic response leading to much-longer temporal NPFs.

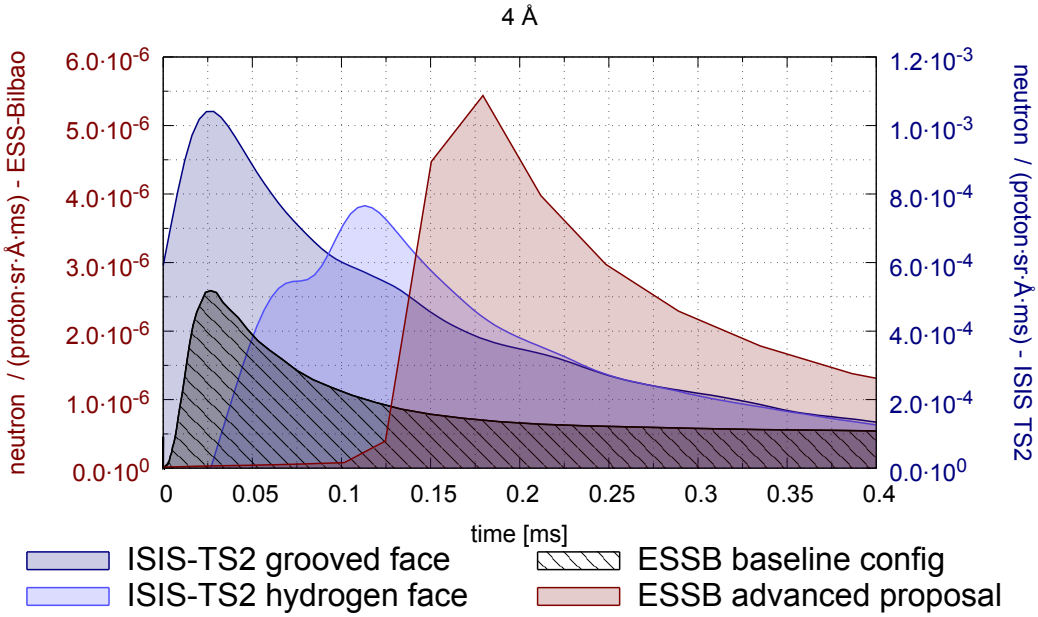

Figure 2-11: Intrinsic moderator response: ESSB vs ISIS-TS2 at 4 Å

These figures also show a net displacement of the response for the ESSB advanced configuration because of the extra time required for neutrons to emerge from the filter face further downstream relative to the moderator. We also note that neutron production per proton at ESSB will be around 250 times less than those characteristic of ISIS-TS2. This difference arises from the higher neutron yield of spallation reactions at 800 MeV (≈16 n/p) over a stripping reaction at 50 MeV (≈1/15 n/p). ESSB seeks to improve its total neutron production by using a higher average proton current (2.25 mA for ESSB vs 0.2 mA for ISIS).

In closing this section, we note that the ESSB TMR response tends to produce long NPFs due to the coupling between moderator and reflector. Nevertheless the width of the ESSB baseline configuration is found to be similar than ISIS-TS2, particularly at the longer wavelengths,

with both moderator temperatures being around the same value. The intrinsic response of the ESSB advanced configuration is significantly broader at certain wavelengths owing to the presence of the beryllium filter after the moderator.

2.4 A closer look at the neutron pulses

At this stage, a closer examination of the neutron-pulse line shape in the time domain becomes necessary in order to assess the cumulative effect associated with the temporal properties of the proton pulse and the subsequent TMR response. The final neutron pulse is the result of the convolution of these two contributions, as schematically shown in Figure 2-12.

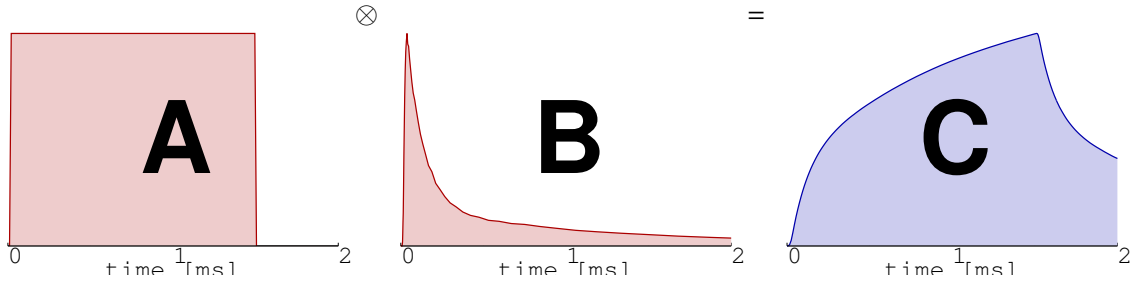

Figure 2-12: Convolution between the ESSB proton pulse (A) and the TMR response of the ESSB baseline configuration (B). For illustrative purposes, A is assumed to be a square pulse.

Figures 2-13 and C.1-1-C.1-8 in APPENDIX C, pag. 81 compare the neutron pulses for the baseline and advanced configurations of ESSB-SPM versus ISIS-TS2. In the range 1-3 Å, the length of the ESSB pulses will be longer than on ISIS-TS2 because at these wavelengths the moderator response (which dominates on ISIS-TS2), is significantly faster than the width of the proton pulse for ESSB-SPM (0.1 ms, cf. Figure 2-11). Up to 3-4 Å, the neutron pulses of ESSB-SPM will be dominated by the proton pulse, while above 4 Å both contributions become comparable. In spite of the coupling of the moderator-reflector assembly, this is also one of the reasons why ESS-SPM is still characterized by longer NPFs than ISIS-TS2 (which are only governed by the moderator response). These data also show a small time displacement of pulse peak positions for the ESSB-SPM advanced configurations, as already discussed in connection with the intrinsic moderator response in Section 2.3, pag. 17 .

As a complement to the above results, Figure 2-14 and Figures C.2-1- C.2-8 show similar data for ESSB-LPM. In this case, the temporal line shape of neutron pulses is clearly dominated by the proton pulse. Hence, the proton pulse alone dictates the intrinsic wavelength resolution of these neutron pulses, and further tailoring of this property requires the use of additional components downstream.

To gain a global perspective of the time response of ESSB, Figure 2-15 and Figures C.1-9, C.1-10 and C.2-10 show two-dimensional maps of the wavelength-dependent temporal responses in LPM and SPM. These figures highlight the preponderance of NPFs in the ESSB advanced configuration, particularly around 1 Å. Figure C.2-10 (like showed by Figure C.2-4) shows how the advanced configuration has lower NPFs around 4Å, indicating a more efficient neutron

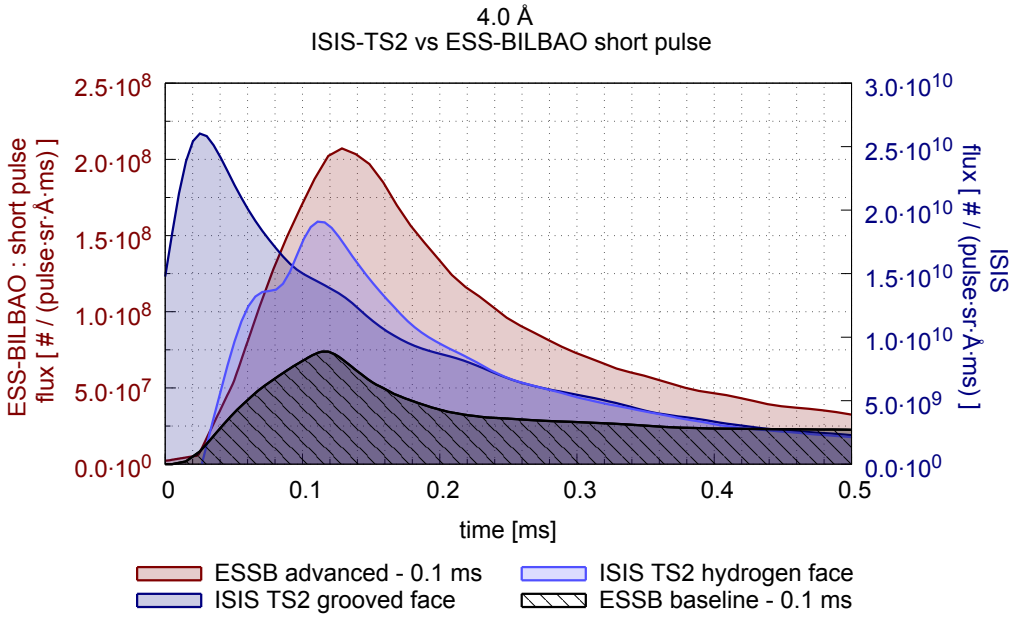

Figure 2-13: Neutron pulses at 4 Å for ESSB-SPM compared to ISIS-TS2.

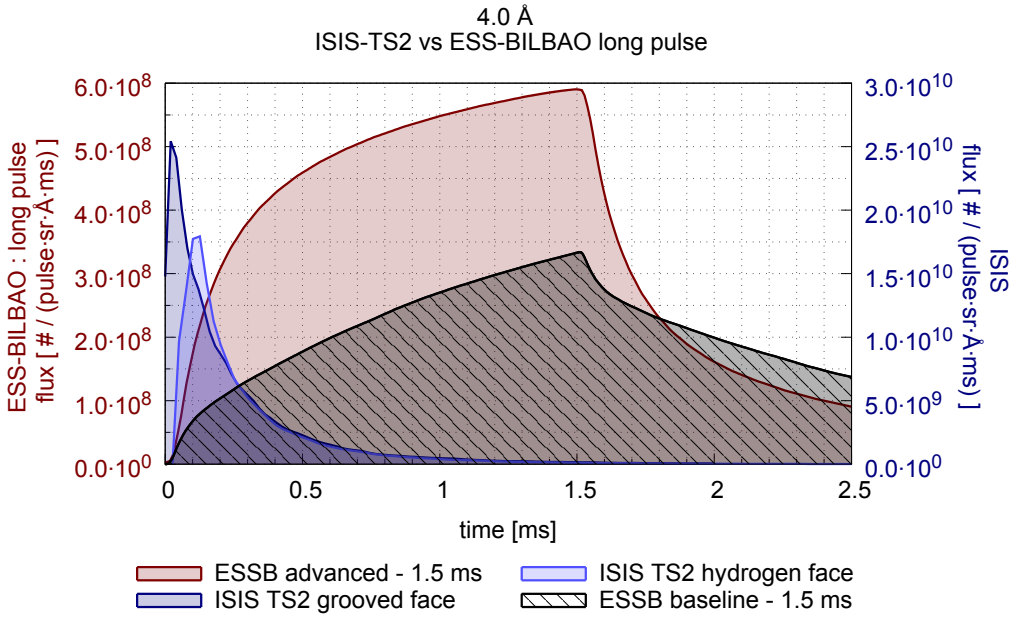

Figure 2-14: Neutron pulses at 4 Å for ESSB-LPM compared to ISIS-TS2.

production comparaed with the baseline configuration. Thus ESSB-LPM will be dominated by the accelerator proton pulse, while the effects of accelerator and moderator response need to be taken into account explicitly for ESSB-SPM.

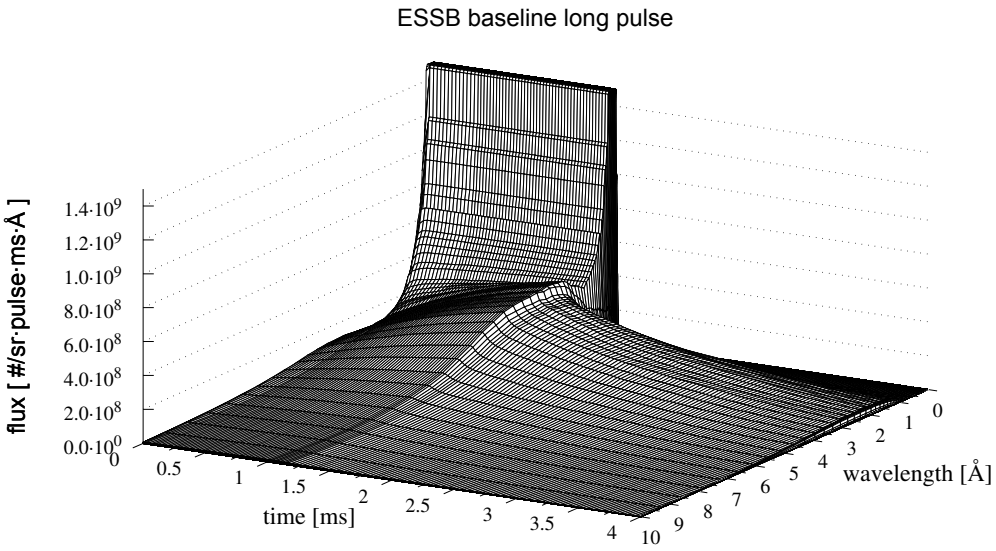

Figure 2-15: Neutron pulses for the ESSB-LPM baseline configuration.

2.4.1 CENTRAL-MOMENT ANALYSIS

A general analysis of pulse shapes (for every wavelength) is an interesting exercise in its own right in order to examine how line shapes can be related to the optimal use of the neutronic response. Important parameters to consider include spectral resolution, dynamic range, and total flux. All of them depend on the overall number of neutrons at a wavelength, its time width, as well as the ratio of pulse peak to tail, etc.

In this context, a central-moment analysis of the pulse time distributions constitutes a model-independent mathematical framework to characterise neutron line shapes [22]. The expression for the n^{th}-order central moment (M_n) is given by Eq. (1) below.

$$M_n = \int_0^\infty (t-\mu)^n \cdot f(t)dx \tag{1}$$

where,

M_n, is the n^{th} moment in units of milliseconds raised to the power of n.
t, is the time of every point of the pulse, in milliseconds.
μ, is the most-probable value of the time for a given point, in milliseconds.
$f(t)$, is the probability density function for every point of the pulse.

We note that this definition makes use of the peak time (μ), instead of the mean value (M_1), so as explore the relationship between time-dependent neutron flux before and after the maximum of the distribution. Also, to facilitate comparison between these moments, we can also define a corresponding **reduced** n^{th}-order moment as [23]

$$M_n^r = sgn(M_n)|M_n|^{1/n} \tag{2}$$

where $sgn(M_n)$ is the signum function of M_n defined as $sgn(M_n) = M_n/|M_n|$, necessary to account for both positive and negative values of the odd moments. With this definition, all reduced central moments share the same units (milliseconds in our case).

In the present analysis, we have considered up to the 4^{th}-order moment. These quantities carry the following information about the underlying probability density function:

- the 0^{th} moment (**integral**) corresponds to the time-integrated flux, already presented and analyzed in Section 2.1, pag. 10 ,
- the 1^{st} moment is a measure of the number of neutrons before and after the most-probable value, embodied in a net deviation of the mean value from the most-probable value μ
- the 2^{nd} moment (**deviation**) is related to the pulse width (spectral resolution),
- the 3^{rd} moment (**skewness**) characterizes the degree of asymmetry relative to the most-probable value. If positive, then the NPF dominates over the leading edge of the distribution, and
- the 4^{th} (**kurtosis**) provides a measure of the relative peakedness or flatness of a distribution.

Figure 2-16 shows the most probable values and central moments for the ESSB baseline and advanced configurations.

The **most-probable times** for the ESSB-LPM baseline configuration, case **a)** in Fig. 2-16, undergo a small increase above 0.1 ms (the length of the proton pulse) as a function of wavelength. This behaviour is caused by the similar widths of the moderator response and the proton pulse in SPM. This effect is not considerable for LPM (cf. **b)** in the same figure), because these pulses reach their maximum values when the neutron pulse is close to saturation. The advanced configuration displays a similar behaviour, in addition to the presence of an extra time lag inside the beryllium fiter (see also discussion in Section 2.3, pag. 17).

At the lower wavelengths, the neutron pulses tend to follow the proton pulse and, hence, the 1^{st} moments are negative, i.e., most neutrons will be in the NPR). As the wavelength increases, the moderation process becomes progressively slower, up up milliseconds. These trends indicate that there will be more neutrons on the NPF than in the NPR for the SPM because the inertia of the moderator response wins over that of the proton pulse. For LPM the amount of neutrons in the NPR and in the NPF tends to be similar. Neverthess, the mean functions have maxima at certain wavelengths, around 2 Å (baseline) and 1-3.5 Å (advanced), where the ratio NPR/NPF will be the lowest. These findings serve to highlight the least efficient wavelength ranges as far as time structure is concerned (cf. Fig. 2-17. These cases

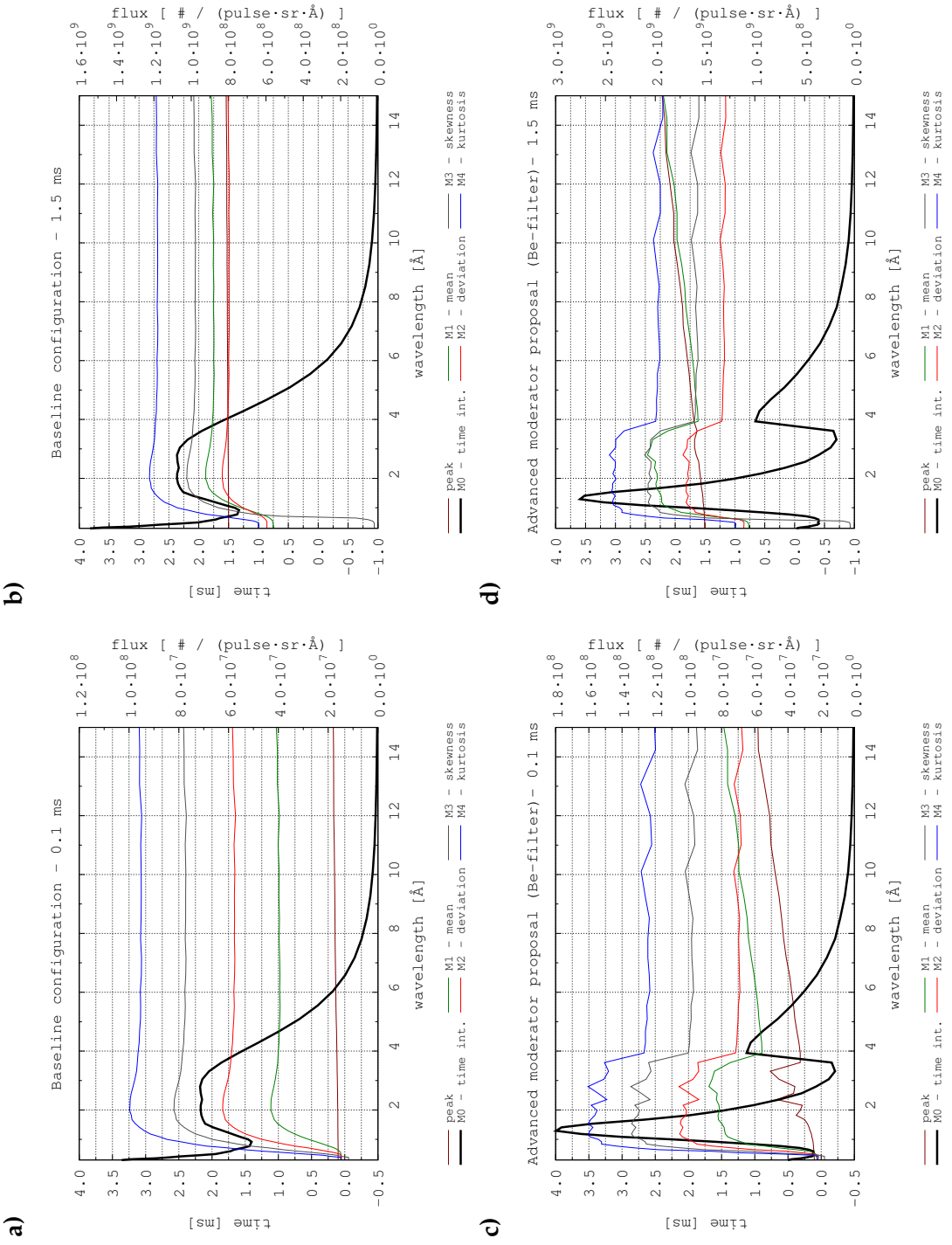

Figure 2-16: Reduced moments for the ESSB baseline and advanced configurations (SPM and LPM operation).

coincide with the peak in the moderated flux, as well as conform with the received wisdom

that maximization of neutron flux tends to occur at the expense of peak fidelity in the time domain.

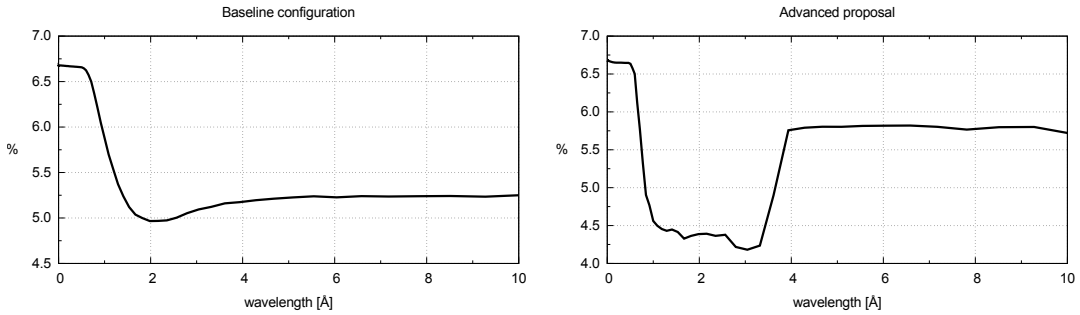

Figure 2-17: Ratio of time-integrated flux of UN within a reference bandwidth of 0.1 ms and total neutron flux of a pulse as function of wavelength (ESSB-LPM).

Up to 1-1.5 Å, the 2^{nd} moments grow quickly from the half of the proton pulse width to a constant value around 1.5 ms for both SPM and LPM. This feature indicates the relative importance of the NPF, specifically for SPM, as these times are well above the width of the proton pulse (0.1 ms). The advanced configuration, **c)** and **d)**, shows a plateau where the width of the pulses will be too wide due to the aforementioned effects associated with the presence of the beryllium filter. This plateau can be problematic for applications requiring better-than-coarse resolution over this wavelength range.

At very low wavelengths, the **skewness** becomes negative indicating that the NPR is more intense than the NPF at longer times. This situation quickly turns itseof around because ESSB tends to produce long NPFs due to the strong coupling between moderator and reflector. Likewise, the **kurtosis** starts off being quite small, hence the time distrubution is centered around the peak (i.e., the neutron pulse follows the proton pulse). This parameter also increases with wavelength, reflecting an increasingly flatter distribution.

The analysis carried out in this section shows that the use of central moments (referenced to most-probable values) can be a useful tool to characterise neutron-pulse line shapes in the time domain. Pulses from the ESSB baseline configuration tend to follow the natural evolution corresponding to a moderator at a certain (cold) temperature, i.e., short and well-defined pulses at low wavelengths, and longer at the longer ones. ESSB-SPM is characterized by a similar response of the moderator and the proton pulse (0.1 ms). Line shapes for the advanced configuration display some peculiarities owing to the presence of the beryllium filter.

2.4.2 ROBUST LINE-SHAPE ESTIMATORS

In the course of our investigations, we have noticed that the NPF (mathematically, $\{f(x)\}, \forall x > \mu$) can be fitted by an expression of the form $f(x > \mu) = t^{-\alpha}$. In those cases where $\alpha < n$, Eq. (1) describing the central moments relative to the most-probable value will be divergent, thereby limiting the realm of applicability of our previous analysis to central moments M_n

such that $n < \alpha$. In this situation, it is then necessary to resort to another set of (more robust) parameters to characterise the neutron line shapes in the time domain.

In addition to the total integral over time (time-integrated flux) and the TOF of the most-probable value, we may define the following wavelength-dependent quantities:

- a full-width-at-half-maximum (FWHM), and
- some appropriate measure of the degree of asymmetry of the pulse around the most-probable value.

To quantify deviations from a perfectly symmetric pulse around its peak value, we can define a width and a line shape asymmetry parameter (Width Asymmetry Parameter (WAP) and Line shape Asymmetry Parameter (LAP), respectively) as follows

$$WAP(\lambda) = \frac{HWHM_{right}(\lambda)}{HWHM_{left}(\lambda)} - 1 \tag{3}$$

$$LAP(\lambda) = \frac{\int_0^{\infty} \Phi(t,\lambda)dt}{2 \cdot \int_0^{t_{max}} \Phi(t,\lambda)dt} - 1 \tag{4}$$

In the definition of the LAP, we have explicitly assumed that the NPR represents the ideal waveform on either side of the most-probable value. For a fat-tailed pulse, these asymmetry parameters will be positive. Figure 2-18 shows these estimators for ESSB-LPM/SPM (baseline and advanced configurations), along with a series of representative pulses at selected wavelengths. For ESSB-LPM, it is noteworthy that the asymmetry parameters are negative, indicative of a very different regime to that typically encountered in short-pulse spallation. This asymmetry is more marked in close proximity to the most-probable value, i.e., a large fraction of the neutron flux arrives before the maximum. Moreover, these asymmetry parameters are fairly constant above 2/4 Å in the baseline/advanced configuration. For the advanced configuration, neutrons in the range 1.5-3.5 Å are significantly broader and the asymmetry is reversed. ESSB-SPM represents a very different situation. For the baseline configuration, FWHMs increase monotonically with neutron wavelength and the observed asymmetry parameters are more in line with the presence of moderation processes characterized by similar timescales to the duration of the proton pulse. For the advanced configuration, neutrons are inherently fat-tailed across the wavelength range. As in the LPM case, the region where the beryllium filter is most effective leads to an order-of-magnitude increase in pulse widths and asymmetry parameters, yet the overall line shape remains qualitatively similar to that seen at other wavelengths.

From this analysis, it is reassuring to see how the overall temporal response of both ESSB-LPM and SPM may be parametrized and understood quantitatively via recourse to a handful of (easily accessible) line shape parameters. We anticipate that such an approach may also be of use in the analysis of other practical scenarios.

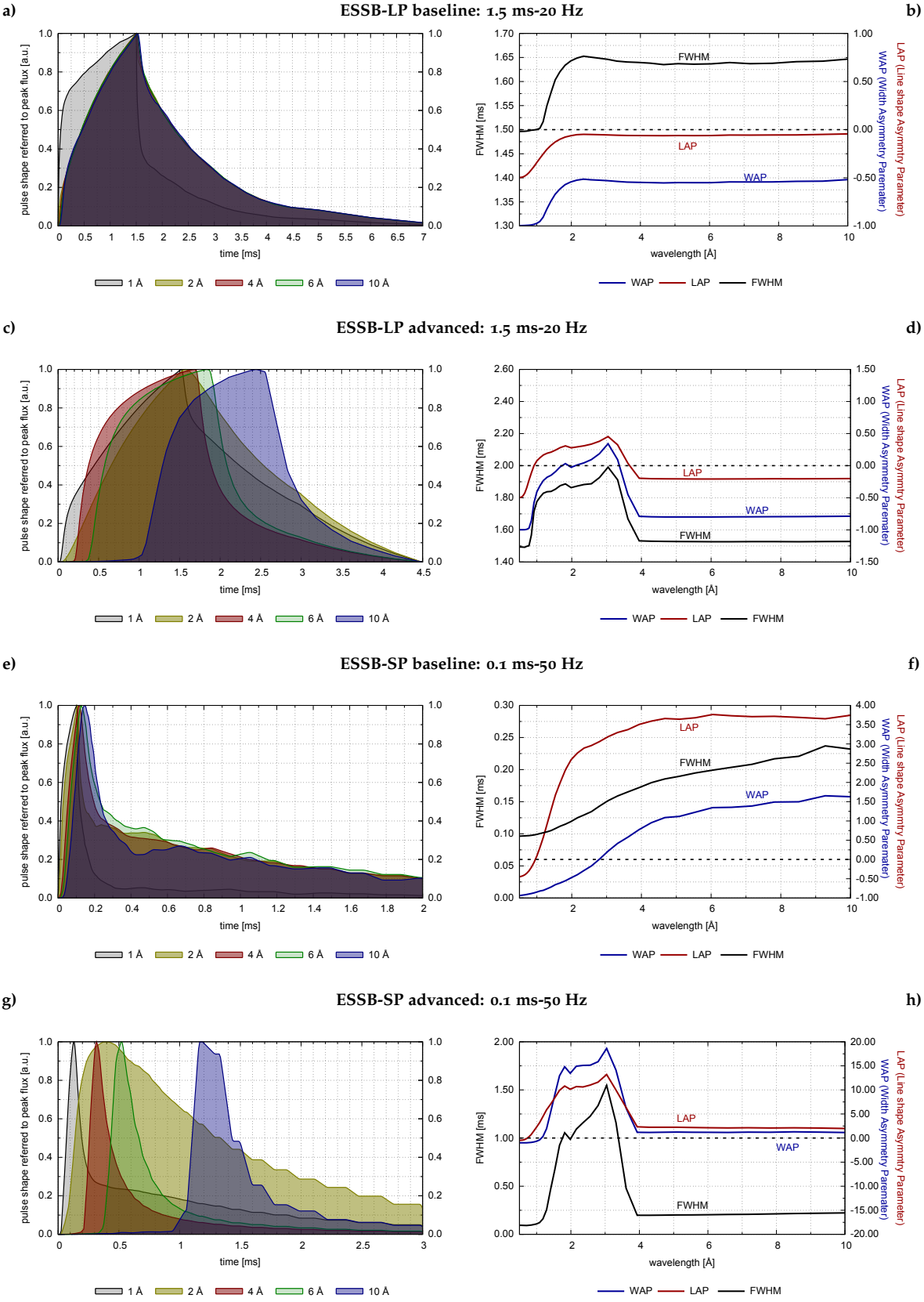

Figure 2-18: Right: Pulse line-shape estimators for ESSB (baseline and advanced configurations). Left: neutron pulses.

2.5 Conclusions

This section has looked in some detail at the neutronic output from ESSB, both in terms of its spectral and temporal characteristics. From these results, the following concluding remarks are in order:

- The **ESSB accelerator** can operate the so-called SPM and LPM, delivering proton pulses of duration 0.1 ms (at 50 Hz) or 1.5 ms (at 20 Hz). ESSB-LPM provides six times more neutrons per second than ESS-SPM.
- ESSB-LPM can deliver between 20 and 30% of the total cold-neutron flux per pulse available at large-scale facilities like ISIS-TS2. The unfavourable time distribution of these pulses, however, is likely to limit applications to those requiring rather coarse resolution.
- ESSB-SPM can produce a similar time distribution to ISIS-TS2 (similar moderator responses), but it would be limited to 5% of the cold neutron flux per pulse available on the latter.
- ESSB pulse line shapes (i.e., neutrons emerging after the pulse peak) show prominent and long NPFs in the time domain due to the high coupling between the target, reflector, and moderator/beryllium reflector assemblies.
- LPM neutron pulses could deliver higher values of **UN** than SPM via the use of additional wavelength-selecting components, e.g., fast choppers in close proximity to the source.
- Depending on resolution requirements, the **ESSB advanced configuration** could provide a higher neutron output than the baseline configuration at certain wavelengths.

3 NEUTRONS FOR SCATTERING TECHNIQUES

In the previous chapter, we have examined the ESSB neutronic output following the creation and subsequent moderation of neutrons within the TMR assembly. In this analysis, we did not consider additional ways of optimizing the neutron flux for applications in neutron scattering. The present chapter extends our previous discussion by providing an assessment of the main parameters associated with the efficient utilization of ESSB for condensed-matter research, including those that are key for an optimised use of the available neutron flux. To provide a realistic assessment of future capabilities at ESSB, we shall limit our discussion to well-established and thoroughly tested instrument concepts at pulsed (mostly spallation) neutron sources over the past three decades, e.g., IPNS, ISIS and, more recently, SNS and J-PARC.

Without much doubt, neutron-scattering techniques are (and will continue to be in the foreseeable future) inherently flux-limited. As such, the primary requirement involves the efficient transport of as many useful neutrons as possible to the sample. Such a requirement is a necessary one because

- neutron-matter interactions are much weaker than those characteristic of other particles such as electrons or photons. This apparent disadvantage can be turned into an opportunity, for example, in the study of physical properties well within the bulk of the specimen (buried interfaces, engineering components, etc).
- and neutron-scattering experiments require the construction of dedicated (large-scale) facilities - i.e., unlike X-ray synchrotrons, there is no laboratory equivalent to a neutron source.

As succintly put by R. Pynn in his (superbly written) *Neutron Primer*: "The combination of a weak interaction and low fluxes make neutron scattering a signal-limited technique, which is practiced only because it provides information on the structure and dynamics of materials that cannot be obtained by other means." [24].

In view of the above, the primary objective behind target and moderator optimization must first consider the maximisation of neutron flux over a certain (useful) energy range. It is precisely in this spirit that the ESSB baseline and advanced configurations have been optimised, as described in the previous chapter. From the point of view of an optimal use of neutrons by the condensed-matter scientist, the situation is sensibly more intricate. For pulsed-neutron sources, it has been recognized from the early days [19] that the use of time-of-flight techniques represents a natural way to separate neutron wavelengths thanks to the linear relationship between these two quantities. In this situation, the distance away from the source becomes an additional variable to consider whereby spectral resolution (proportional to distance) may be traded against total flux and available dynamic range at the sample position. For instruments using a broad range of incident wavelengths simultaneously (the natural choice at a pulsed neutron source), the line shape of neutron pulses in the time do-

main also becomes an important factor for instrument design. The present chapter attempts to put the above considerations on a firmer ground by mapping scientific requirements onto quantitative considerations relating to total available flux, dynamic range, and underlying pulse widths and line shapes in the time domain.

3.1 The background

In addition to the (sometimes) inevitable temporal overlap between different wavelengths in the thermal and cold ranges, the nuclear processes leading to neutron produccion in the MeV range lead to the presence of a considerable number of neutrons at epithermal and higher energies. This high-energy contribution is not a useful one in a number of applications, notable exceptions being techniques such as neutron Compton scattering. Therefore, it may be classed as an unwanted background signal.

Moreover, these high-energy backgrounds can be responsible for radiation damage of instrument components (e.g., detectors) or the specimen under investigation itself. Also, it can interfere with the neutron-scattering response at thermal and cold energies, leading to further (and sometimes unsurmountable) complications in the analysis of experimental data. Unlike steady-state sources, the inherent time dependence of neutron production in the target station constitutes and often-overlooked advantage, as the presence of high-energy neutrons will be primarily concentrated during the early times (microseconds) following the interaction of a given proton with the neutron-producing target. In this situation, primary high-energy backgrounds may be filtered in the time domain via the use of velocity-selection devices and time-of-flight methods. Dealing with secondary backgrounds arising from the interaction (and possible slow-down) of high-energy particles with the various components of the target monolith or instrument is a far more intricate task. Traditionally, suppressing this secondary backgrounds has been much of an experimental art, requiring systematic (and time-consuming) efforts on the part of instrument developers and scientists at neutron facilities. The advent of sufficiently accurate computer codes to simulate these processes has facilitated greatly this task, and allows for a detailed assessment of possible sources of backgrounds prior to the actual construction and commissioning of new instruments.

For the purposes of this report and envisaged applications of ESSB for condensed-matter studies, we define the 'background' as neutrons below a wavelength of 0.35 Å. As described earlier in Chapter 2, pag. 9 , neutrons emerging from the Be(p,n) stripping reaction will maintain most of the original proton-beam momentum, so even a SLAB moderator configuration can lead to a considerable suppresion of high-energy neutrons on beamlines viewing directly the moderator face, as illustrated previously in Figure 2-1.

Figure 3-1 shows the cumulative distribution function of the neutron energy sprectra of the ESSB baseline and advanced configurations (see also discussion in Chapter 2, pag. 9 and Refs. [1] ,[17]). These data show that around 85% of all neutrons in the ESSB baseline configuration will contribute to the high-energy background as defined above. For the ESSB advanced configuration, the addition of the beryllium filter brings this number down to ca. 32%. For comparison, the equivalent figure for ISIS-TS2 is ca. 50%.

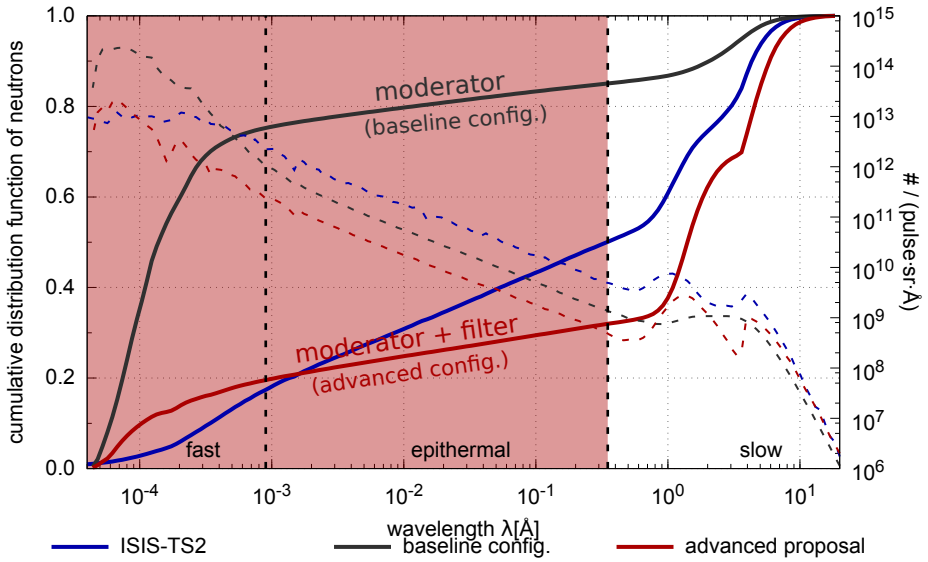

Figure 3-1: Left axis (solid lines): cumulative distribution function of neutron spectra for ESSB (baseline and advanced configurations) and ISIS-TS2. The dashed lines (right axis) show the associated time-integrated spectra.

To sum up, the ESSB baseline configuration produces sensibly higher backgrounds than ISIS-TS2. Nevertheless this ratio can be improved by factors of up to 2-3 with the beryllium filter in the advanced configuration, displaying the highest performance in terms of the production of thermal and cold neutrons (60% of the neutrons are above 1Å).

3.2 Background suppression

The most straightforward way to block high-energy particles and radiation damage downstream from the TMR assembly is via the use of a so-called T_0-chopper. In addition, bent neutron guides with a specific wavelength cutoff (directly related to their radius of curvature) can also be used to prevent a direct view of the moderator face at the sample position. Whereas the use of a T_0-chopper may be regarded as a generic solution to background suppression, the wavelength response of a bent neutron guide is application-specific, which tends to favour the transmission of the colder part of the neutron spectrum. To keep this discussion as general as possible at this stage, we therefore analyse in some detail the main characteristics of the T_0-chopper. For a good and up-to-date discussion of the merits and strengths of curved neutron guides vs. T_0-choppers, the reader is referred to Ref. [25].

In its simplest incarnation, a T_0-chopper consists of a robust rotating disk which blocks neutrons hitting its blades (see Figure 3-2). To block high-energy backgrounds, blade thicknesses are primarily dictated by the mean-free path of the unwanted radiation. Quantitative estimates of this important design parameter are given in APPENDIX D, pag. 94 , indicating typical thicknesses of tens of centimeters.

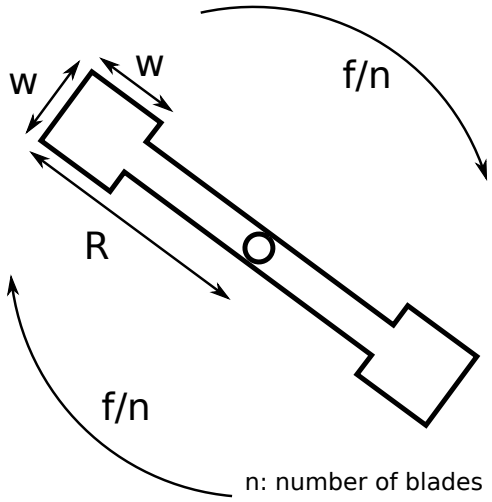

Figure 3-2: Schematic diagram of a two-blade T_0-chopper. For further details, see the text.

In the present analysis, we assume an ideal T_0-chopper, that is, all neutrons hitting the blades will be stopped and will reach the sample position during the time of measurement. Within this approximation, the only relevant parameters are the aperture-to-radius ratio (W/R), its operating frequency (f), the number of blades (n), and the distance to the moderator face (L).

It is important to note that deviations from the ideal conditions assumed above for the operation of the T_0-chopper can be quite relevant for the design and optimization of neutron instrumentation. In pulsed neutron sources, much-slower neutrons of the background associated with previous pulses reach the T_0-chopper at the same time as faster neutrons associated with the tail of the moderated-neutron pulse. In this situation, both background and useful neutrons will be inevitably blocked altogether, thereby reducing the effective flux of the latter for subsequent use. The time-distance diagram in Figure 3-3(top) shows how the background (red area) of the LPM (i.e. 0-0.35 Å) is perfectly blocked by a T_0-chopper at 5 m, although at the expense of some useful flux (green area below the chopper). Figure **??**(bottom) shows the same case for SPM. The reduction in neutron flux over the range of useful neutron wavelengths will be lower for SPM, i.e., over the range from 0.35 Å to 0.43 Å.

Given these two competing effects, a compromise must be struck between the number of transmitted neutrons and the concomitant reduction of background levels, a situation which may be circumvented altogether via the use of curved neutron guides. These considerations are particularly relevant when the length of the proton pulse greatly exceeds the intrinsic time response of the TMR assembly, as illustrated in Fig.3-4. In line with previous examples, this figure shows the effect of a T_0-chooper placed at 5 m from the moderator face for LPM. the shadowed area represents the time window of the chopper (2 ms), and the goal is to block all wavelengths in the background (red), i.e., every neutron of wavelength below 1.5 Å. Inevitably, wavelengths between 0.35 and 1.58 Å are also blocked (green) because they reach the

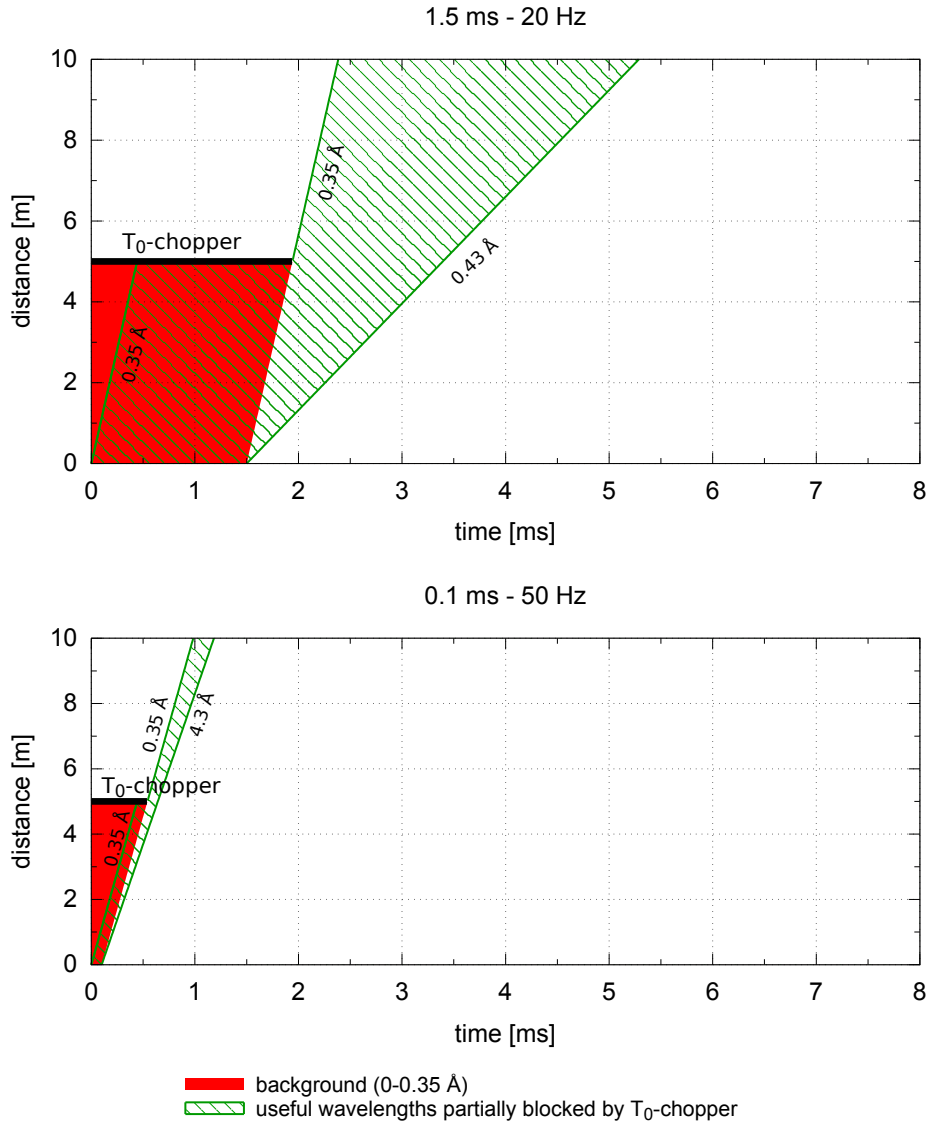

Figure 3-3: Time-distance diagram of the LPM(top) and SPM(bottom) with an ideal T_0-chopper at 5 m. The red area corresponds to the background and the green area to those neutron wavelengths partially blocked by the T_0-chopper. Zero time along the abcissa corresponds to the time of arrival of the leading edge of the proton pulse.

T_0-chopper blades at within its duration. The remaining (blue) wavelengths are transmitted through the T_0-chopper.

Quantitatively speaking, the range of useful neutron wavelengths that are inevitably blocked by a T_0-chopper can be written as

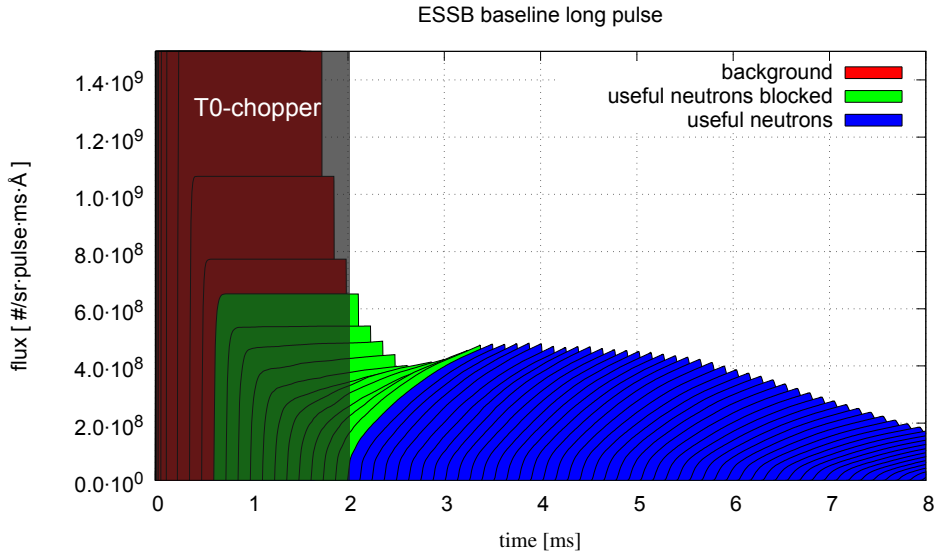

Figure 3-4: Time-of-flight profiles for ESSB-LPM (baseline configuration) with a T_0-chopper at 5 m. The different colours correspond to backgrounds below 0.35 Å (red), useful neutrons blocked over the range 0.35-1.5 Å (green), and transmitted neutrons to the sample position (blue).

$$\lambda_u - \lambda_b = \frac{3.96 \cdot \Delta t_{window}[ms]}{L[m]} \quad , \quad \forall \lambda_b \leq \lambda_u \tag{5}$$

where,

λ_u, *is the maximum wavelength blocked by the* T_0*-chopper, in Å.*
λ_b, *is the maximum wavelength of the background, Å.*
Δt_{window}, *is the duration (time window) of the* T_0*-chopper, in milliseconds.*
L, *is the distance between source and* T_0*-chopper, in meters.*

Equation (5) can be used to calculate the fraction of useful wavelengths that will be partially blocked by the T_0-chopper, i.e., all wavelengths between λ_b (the lowest neutron energy in the background) and λ_u (the lowest neutron energy of useful neutrons blocked by the T_0-chopper). From this expression, it appears as if the range of blocked wavelenghts decreases as the distance L increases. This inverse relation, however, is applicable to the response for a single neutron pulse, as increasing L will also block the slower neutrons from previous pulses because the T_0-chopper will need to block the beam during a longer period of time. As illustration, we take 18 Å to be the longest wavelength of interest and 0.35 Å to be the shortest one. For a T_0-chopper rotating at the same frequency as the source, slow (and still useful) neutrons from the trailing edge of the pulse will have up flight time from source to T_0-chopper of (20-0.1)/(50-1.5) ms for SPM/LPM, respectively. Hence, the maximum T_0-chopper distance becomes 4.4 m for SPM and 10.7 m for LPM.

The previous chapter showed that high-energy particles (the background) mimick the proton pulse (a square pulse with no additional lag). Hence, for this contribution Δt_{window} in Eq. (5) can be equated to the length of the proton pulse. Under these circumstances, placing the T_0-

chopper at 4.4 m from the moderator fulfills the aforementioned bandwidth requirements. To guarantee ease of maintenance, this component should be placed outside of the target area (at least 5 m from the moderator) as shown in Figure 3-5. At this distance, the longest accessible wavelength is reduced to 15.8 Å for SPM (50 Hz) and 38.4 Å for LPM (20 Hz).

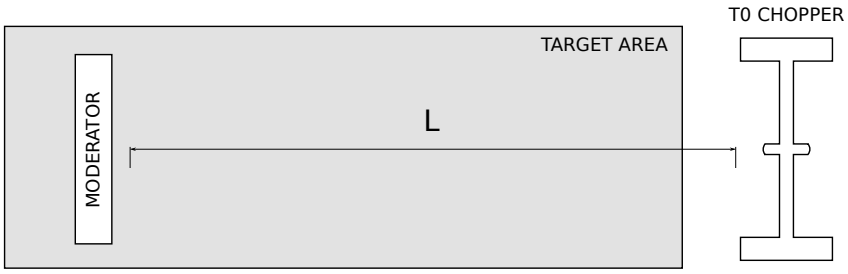

Figure 3-5: Schematic diagram of a T_0-chopper placed outside the target area.

Table 3-1 summarizes all of these condiderations for three T_0-chopper distances, namely, 1.5, 5, and 10 m in LPM and SPM. The distance from the moderator to the T_0-chopper should be selected depending on the requirements of a particular instrument. In practical terms, distances will have to be greater than the 5 m defining the target area. This minimum distance will be assumed in our subsequent analysis. In this table, $\Delta\lambda_{useful_B}$ represents the wavelength range of useful neutrons partially blocked by the T_0-chopper as given by Eq. 5, whereas $\Delta\lambda_{useful}$ is the wavelength range of neutrons fully transmitted through the T_0-chopper.

Table 3-1: Range of useful neutrons transmitted by a T_0-chopperat different distances and accelerator operational modes.

Case	Distance	Freq.	FWHM	$\Delta\lambda_{useful_B}$	$\Delta\lambda_{useful}$	Maintenance
A	1.50 m	20 Hz	1.5 ms	0.35-4.31 Å	4.31-131.3 Å	hard
B	1.50 m	50 Hz	0.1 ms	0.35-0.61 Å	0.61-52.80 Å	hard
C	5.00 m	20 Hz	1.5 ms	0.35-1.54 Å	1.54-39.60 Å	easy
D	5.00 m	50 Hz	0.1 ms	0.35-0.43 Å	0.43-15.84 Å	easy
E	10.0 m	20 Hz	1.5 ms	0.35-0.94 Å	0.94-19.80 Å	easy
F	10.0 m	50 Hz	0.1 ms	0.35-0.39 Å	0.39-7.920 Å	easy

The T_0-chopper should block the beam during length of the proton pulse (from 0.1 to 1.5 ms) plus the TOF of the slowest neutrons associated with the background. Mathematically, we can then write this time as $\lambda_b \cdot L/3.96 + FWHW$ where $FWHM$ is the width of the proton pulse. Furthermore, the opening and closing of such a chopper must be synchronised and phased relative to the operation of the proton accelerator. These conditions can be expressed as

$$\frac{w}{2\pi R/n} = \left(\frac{\lambda_b}{3.96} \cdot L + \text{FWHM}\right) \cdot \frac{f}{10^3} \tag{6}$$

where,

w is the width (in centimeters) of the T_0-chopper. This value is taken to be equal to that of the moderator face.
R is the radius of the T_0-chopper, in centimeters.
n is the number of T_0-chopper blades.
λ_b is the maximum wavelength of the background, in Å.
L is the distance of the T_0-chopper from TMR, in meters.
$FWHM$ is the width (in milliseconds) of the neutron pulse, taken to be equal to the length of the proton pulse for background.
f is the frequency of the neutron source, in Hz.

According to this expression, the use of n blades will allow rotation at lower frequencies to ensure best mechanical stability. However, we also note that a higher number of blades will require a higher radius R. Table 3-2 illustrates typical parameters for n=1,2 in LPM and SPM to block wavelenghts up to 0.35 Å over an area equal to the ESSB moderator face (12x12 cm). We do note, however, that these beam-size parameters should be revisited to accommodate for other beam-transport requirements from moderator to sample position. If mechanical-design constraints are not an issue, the most compact solution involves the use of a double blade.

Table 3-2: Geometrical and theoretical parameters for a T_0-chopper placed at 5 m from the source.

Case	L	f_{source}	$f_{T0-chopper}$	FWHM	w	n	λ_b	R
C1	5.0 m	20 Hz	20 Hz	1.5 ms	12 cm	1	0.35 Å	49.17 cm
D1	5.0 m	50 Hz	50 Hz	0.1 ms	12 cm	1	0.35 Å	70.48 cm
C2	5.0 m	20 Hz	10 Hz	1.5 ms	12 cm	2	0.35 Å	98.35 cm
D2	5.0 m	50 Hz	25 Hz	0.1 ms	12 cm	2	0.35 Å	140.97 cm

We also note that once a given T_0-chopper design has been chosen, its rotational frequency may be changed so as to match that of the source, while all other geometrical parameters (w, R, L, n) remain fixed. Different repetition rates will translate into different ranges of frequencies that may be blocked by the chopper. Equation (7) shows the relationship between the maximum wavelength that can be avoided at different source frequencies. For example, if the T_0-chopper is designed to block wavelengths below 0.35 Å for LPM, this cutoff becomes 0.54 Å for SPM.

$$\lambda_{b-2} = \lambda_{b-1} \cdot \frac{f_1}{f_2} + \left(\text{FWHM}_1 \cdot \frac{f_1}{f_2} - \text{FWHM}_2\right) \cdot \frac{3.96}{L} \tag{7}$$

The analysis presented in this section has shown that a T_0-chopper can be a useful device to block high-energy neutrons, although other possibilities such as the use of curve-neutron

guides could also be contemplated. For ESSB, placing this component at 5 m from the source appears to be a reasonable option.

3.3 Spectral resolution

Within the width of the proton pulse, neutrons of different energies emerge from the moderator (roughly) at the same time. As they travel away from the source, this initial pulse will spread out in time and energy by virtue of the inverse relationship between neutron velocity and wavelength. As a result, the pulse front at a given distance from the source will contain a larger(smaller) fraction of fast(slow) neutrons – just as in the case of optical photons travelling through a medium with a frequency-dependent refractive index. If sufficient discrimination between neutron wavelengths (or 'colours') is possible, then a measurement of TOF from source to detector becomes the most convenient way to infer the neutron wavelength (or energy). These simple considerations constitute the basis to initiate a more detailed discussion of spectral (wavelength) resolution.

In the above context, the distance from the source becomes a central parameter. Figure 3-6 illustrates these ideas, showing how tighter pulses lead to a better spectral resolution at a given distance from the source. For two given proton-pulse operational modes, the ratio of maximum attainable spectral resolutions will be inversely proportional to the requisite distances. For LPM and SLM, this condition implies that LPM (1.5 ms) will require distances fifteen times longer than SPM (0.1 ms), with a concomitant reduction in flux unless neutron-transport is further optimised (e.g., use of neutron guides over long distances). These requirements for LPM vs SPM therefore need to be tensioned against other important factors such

as physical limitations associated with the overall dimensions of the facility or budgetary constraints.

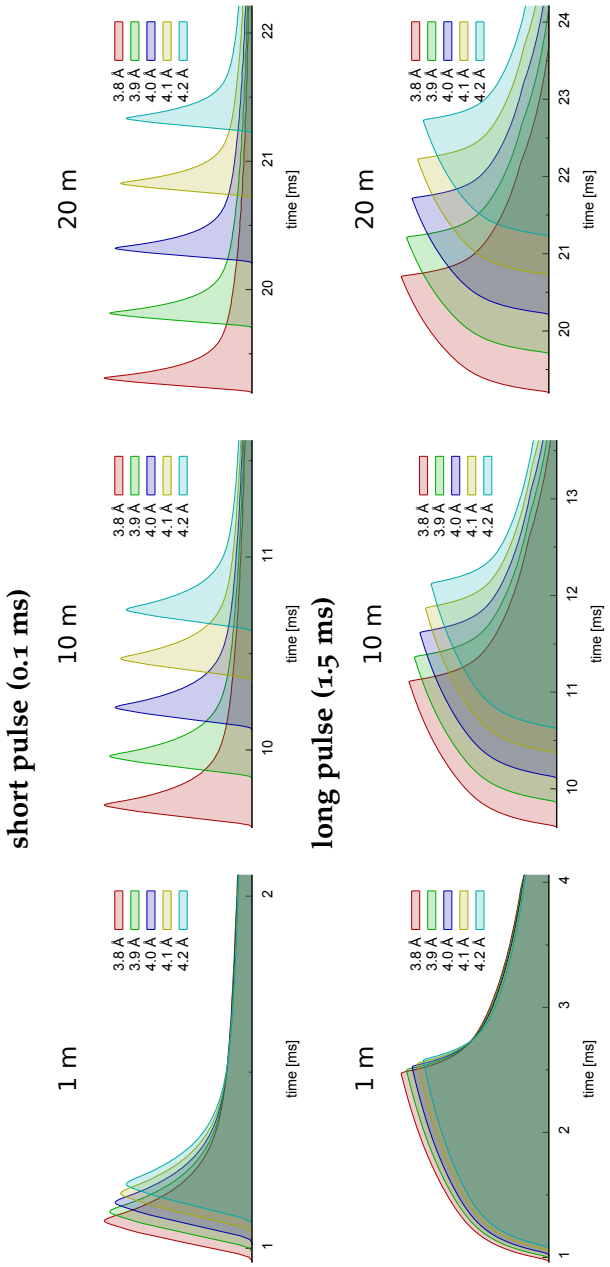

Figure 3-6: Spectral discrimination at several distances using TOF methods for the ESSB baseline configuration. Top: -SPM. Bottom: ESSB-LPM.

These semi-quantitative considerations are graphically illustrated in Fig. 3-6, where it is seen that a distance of 10 m would be sufficient to discriminate nearby neutron wavelengths around 4 Å in SPM. A similar spectral discrimination would require distances well in ex-

cess of 100 m in LPM using well-established pulsed-neutron techniques. We also note that a discussion of spectral resolution using wavelength (as opposed to energy) is a more natural choice owing to the linear relationship between this parameter and TOF for a given distance – i.e., the spectral flux is shape-invariant under a transformation from TOF to wavelength. Likewise, the time widths associated with moderation processes inside the target are wavelength dependent and, therefore, it is convenient to think of the overall neutron output as consisting of a collection of neutron packets of different wavelengths subjected to an intrinsically wavelength-dependent time broadening. This time broadening increases monotonically with wavelength, a dependence that conforms to physical intuition as the attainment of colder wavelengths requires (on average) a higher number of collisions with the moderating medium. Quantitatively, the spectral resolution can be written as

$$R(\lambda) = \frac{3.96}{\lambda[\text{Å}]} \cdot \frac{\Delta t[ms]}{L[m]} \tag{8}$$

where,

R, is the spectral resolution, dimensionless.
λ, is the neutron wavelength, in Å.
Δt, is the pulse width for wavelength λ, in milliseconds.
L, is the distance from the moderator, in meters.

Figures 3-7a) and 3-7b) show the spectral resolution for a series of distances, all of them fulfiling space constraints for the ESSB facility layout. ESSB-LPM can attain a low spectral resolution, so its applications are necessarily limited to coarse and low-resolution instruments, such as SANS, reflectometry, imaging, transmission or spin-echo techniques. With ESSB-SPM, the spectral resolution can be over an order of magnitude higher, thereby enabling its use for medium-resolution applications including diffraction and spectroscopy. In this respect, ESSB-SPM represents a more versatile option in spite of the requisite reduction in incident flux.

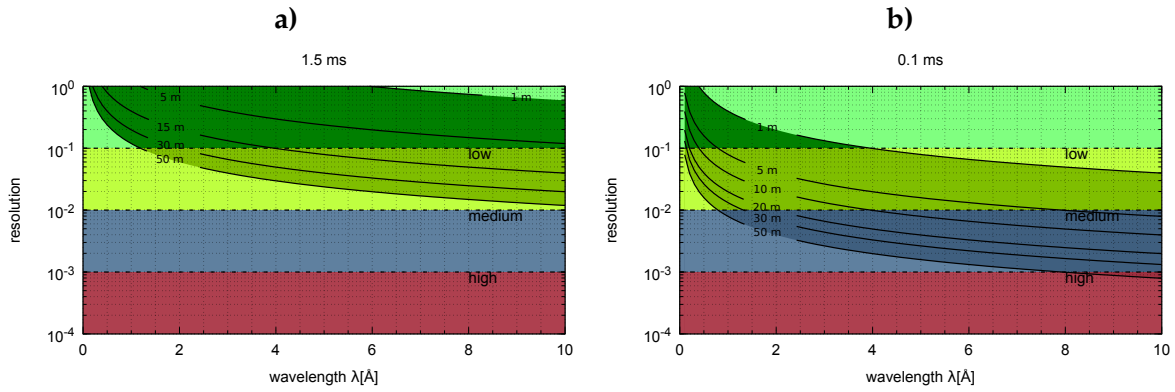

Figure 3-7: Spectral resolution as a function of wavelength at several distances from the source: Left/right: ESSB LPM/SPM.

3.4 Dynamic range

The dynamic range corrresponds to the band of useful neutron wavelengths available to the experimenter for neutron-scattering measurements. Unlike steady-state sources, pulsed neutron sources are unique in that it becomes possible to exploit a wide dynamic range within each neutron pulse using TOF techniques. This 'multiplexing advantage' can lead to order-of-magnitude increases in detected count rate and also explains why the *peak* neutron flux is a more appropriate figure of merit to assess instrument performance, as opposed to analogous time-averaged quantities [19]. The dynamic range is both dependent on the distance to the source (as the spectral resolution) as well as the repetition rate of the source, as shown by Eq. (9). Figure 3-8 shows time-distance diagrams for two consecutive LPM pulses. At 20 m, there frame-overlap between a given wavelength and longer wavelengths will happen, as described by Equation 9, a complication that may be avoided via judicious use of bandwidth as well as frame-overlap choppers.

$$\Delta\lambda[\text{Å}] = \left(\frac{10^3}{f[Hz]} - FWHM[ms]\right) \cdot \frac{3.96}{L[m]} \tag{9}$$

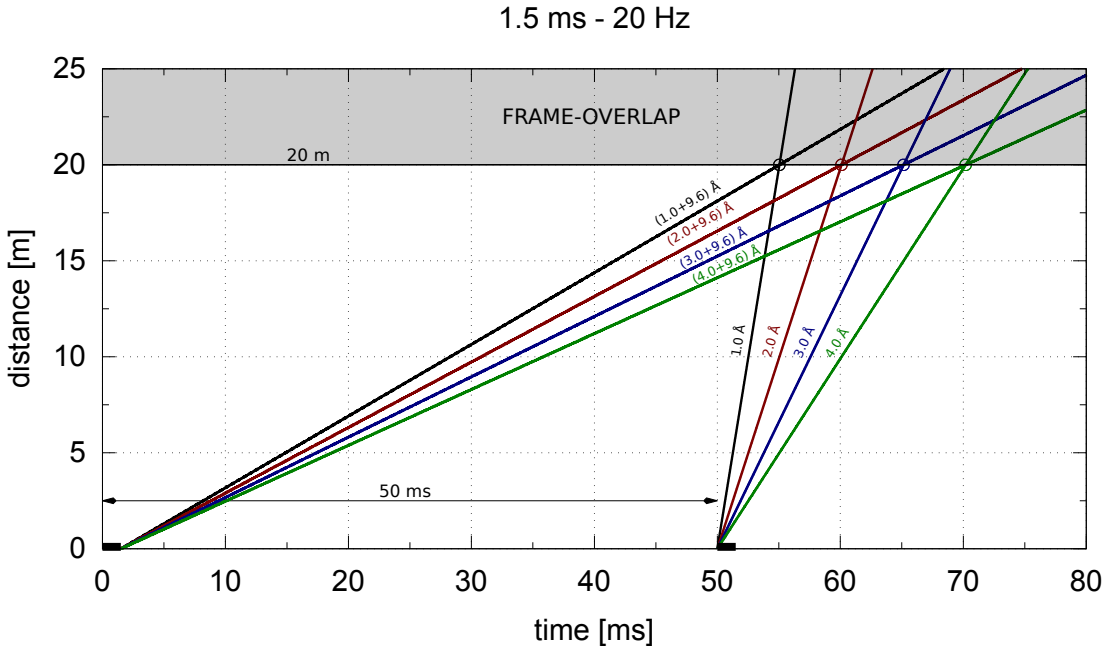

Figure 3-8: Time-distance diagram for two consecutive pulses in LPM illustrating frame-overlap for several wavelengths at 20 m.

According to this expression, the dynamic range decreases with both distance and repetition rate. These purely mathematical relationships must also be put in the context of the range of available wavelengths available from a given moderator, which is many circumstances also

dictate the lowest and highest available neutron wavelengths at a given position relative to the source. As any instrument development is necessarily driven by specific scientific requirements (i.e., range of required neutron wavelengths at the sample position), the choice of an appropriate moderator constitutes the first step in deciding the type of instrument that will be most suited for a particular application. This choice in turn largely determines the total available dynamic range of incident neutron wavelengths. Given a source repetition frequency, Eq. (9) can be then used to determine the *maximum* distance at which it is possible to access these wavelengths before the next neutron pulse arrives. We emphasize that this maximum distance might not be the ideal one for certain applications where total available flux (requiring shorter primary paths) is more important than resolution (requiring longer distances). This is the case, for example, of direct-geometry spectrometers where the use of a fast chopper relatively close to the source will select a given incident energy, thereby decoupling the characteristics of the source from those of the incident spectrometer. In this particular case, short distances are typically preferred because they provide a significant increase in flux, particularly at thermal and epithermal energies where neutron guides are no longer as efficient as for cold wavelengths. By virtue of Eq. (8), this maximum distance also fixes the best-possible resolution without any further compromise in the range of available bandwidth. Thus, we see that both dynamic range and resolution are inextricably linked to each other, a relationship that will be explored in more detail in the next section. The sequential procedure described above has underpinned most instrument design and optimization at pulsed neutron sources to date, whereby the requirements associated with a particular scientific application impose important constraints on the choice of moderator, source frequency, and instrument length based on the required dynamic range, resolution, and flux.

To facilitate the present discussion, Figure 3-9 shows a typical time-distance diagram corresponding to ESSB-SPM (50 Hz). In this figure, 18 Å-neutrons will overlap 0.35 Å-neutrons from the next pulse at a distance of 4.4 m. Figure 3-10 shows how the lower repetition rate of ESSB-LPM (20 Hz) will meet this condition at a longer distance of 10.7 m, a figure simply dictated by the ratio of repetition frequencies of ESSB-SPM vs. ESSB-LPM.

The optimal dynamic range ultimately depends on the application at hand. To illustrate this (very important) consideration, Figure 3-11 shows the time-distance diagram for two different instruments classes at ISIS-TS2, namely, a small-angle instrument (SANS2D) and a neutron diffractometer (WISH).

Figure 3-12 shows the dependence of dynamic range with distance. The T_0-chopper allows for the transmission of neutron wavelengths over the range 0.35-18 Å. We recall from our previous discussion that these two wavelengths (coming from sequential pulses) will cross each other in the time domain at 4.4 m for ESSB-SPM (50 Hz). Beyond this distance, the dynamic range will necessarily decrease as showed by the red line (ratio of available dynamic range relative to the initial range defined by the T_0-chopper). Once the useful dynamic range for the experiment is chosen, there is, therefore, a maximum distance beyond which such a requirement is no longer met. Figure 3-13 shows the same analysis for ESSB-LPM, where for a similar dynamic range than the short pulse, the associated distance is longer. We emphasize

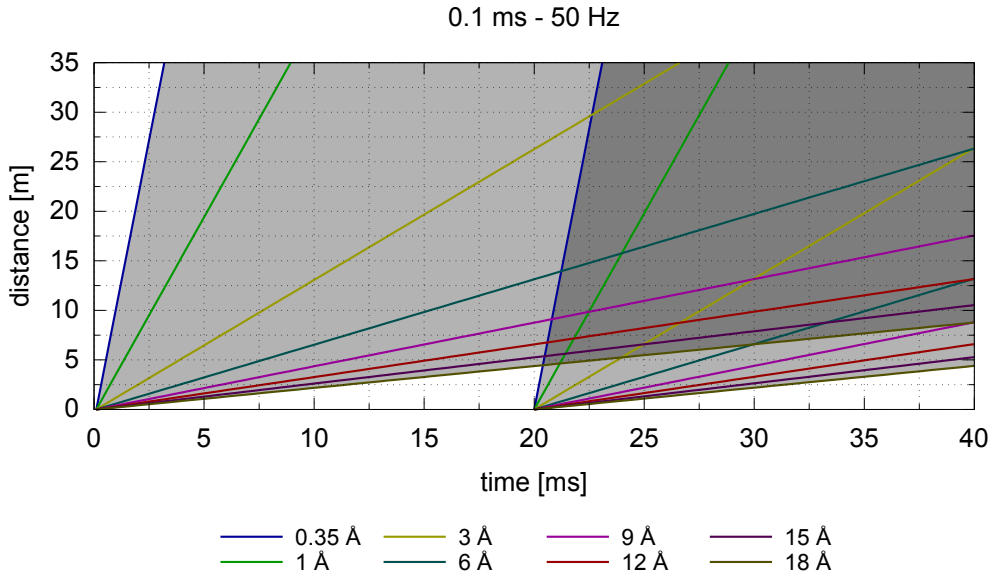

Figure 3-9: Time-distance diagram for ESSB-SPM.

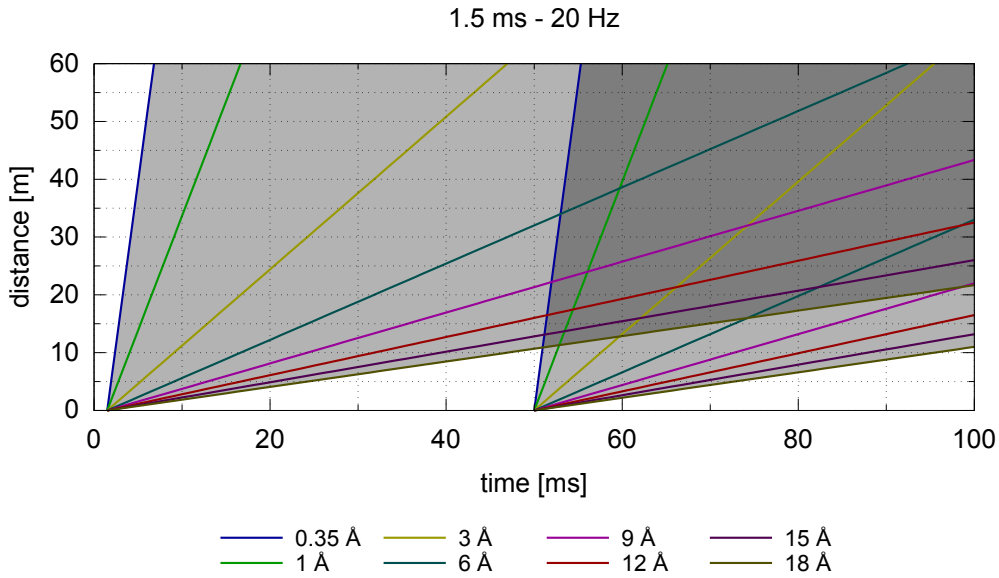

Figure 3-10: Time-distance diagram for ESSB-LPM.

at this stage that these considerations are *only* dictated by the repetition rate of the source for a given moderator. From this discussion, it becomes clear that ESSB-LPM can provide a broader dynamic range than ESSB-SPM in the thermal- and cold-neutron regimes. Such a distinction, for example, has driven the construction of ISIS-TS2 (operating at 10 Hz), relative to the original ISIS-TS1 (operating at 50 Hz).

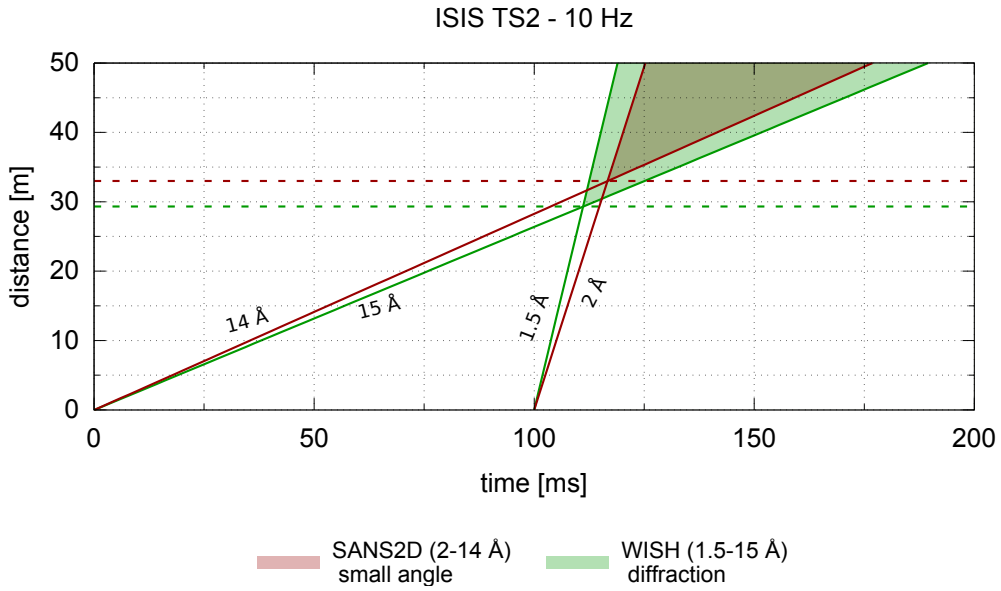

Figure 3-11: Time-space diagram for some instruments on ISIS-TS2.

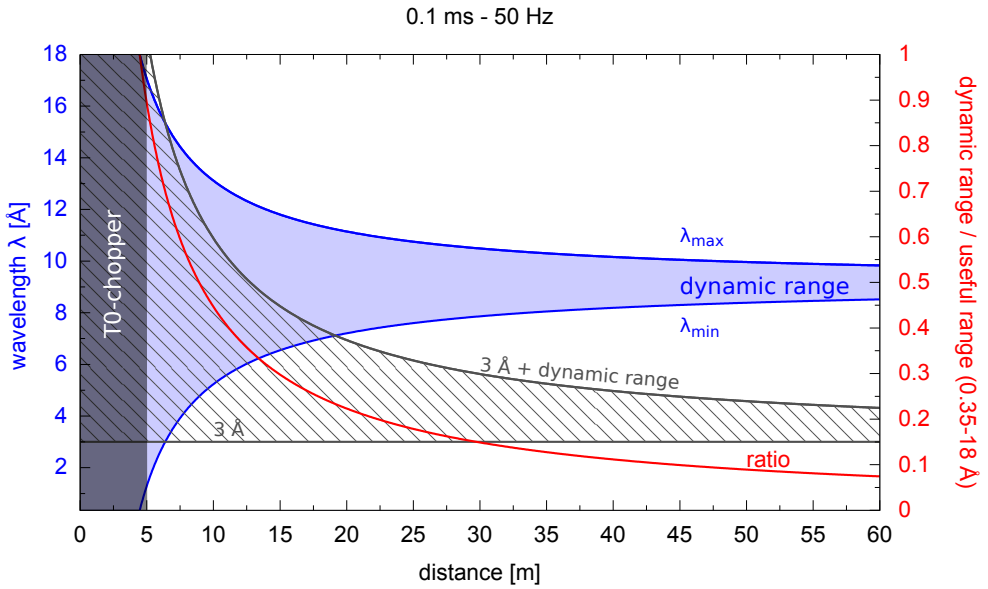

Figure 3-12: Available dynamic range as a function of distance for SPM. The blue area represents an equal reduction in the upper and lower wavelength limits of the range. The gray area represents a reduction only in the upper limit. The right axis corresponds to the ratio between final and original dynamic ranges.

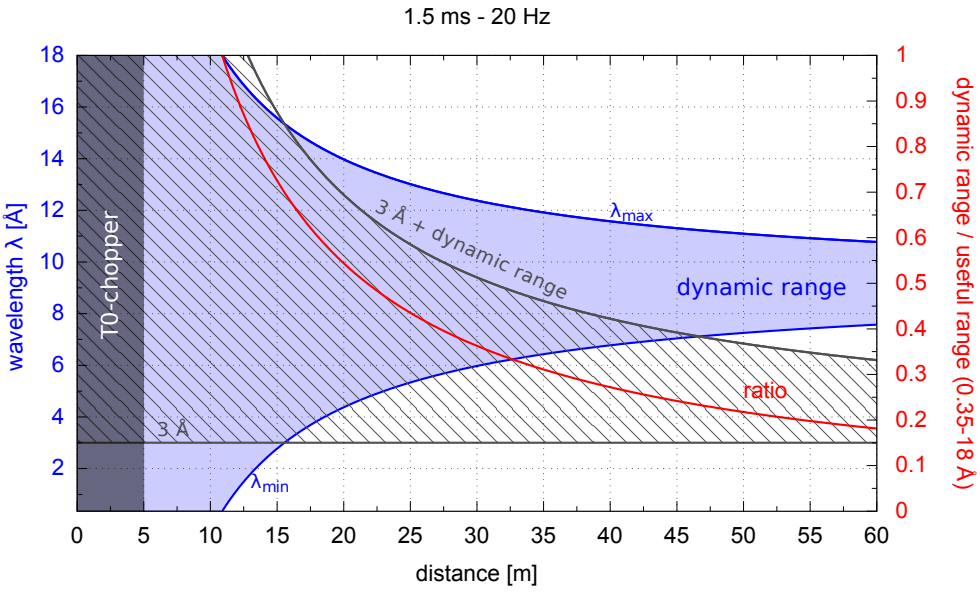

Figure 3-13: Available dynamic range as a function of distance for LPM. The blue area represents an equal reduction in the upper and lower wavelength limits of the range. The gray area represents a reduction only in the upper limit. The right axis corresponds to the ratio between final and original dynamic ranges.

3.5 Resolution vs. dynamic range

The range of neutron wavelengths required for a particular application can be used to set the distance between source and sample position, and we have already seen that a lower source repetition frequency (ESSB-LPM) presents some obvious advantages in this regard. Fixing the distance on the basis of dynamic range alone has nonetheless consequences in terms of spectral resolution. It is therefore of interest to consider these two variables together, along with other constraints associated with the layout of ESSB.

Figures 3-14 and 3-15 show how low, medium, and high resolution requirements relate to the available dynamic range (distance from the source) as a function of neutron wavelength. In this comparison, we have adhered to the definitions proposed by Schober et al. in their general analysis of pulsed-neutron instrumentation [26] In these figures, the ordinate axis on the right shows the maximum distance associated with a given dynamic range (left ordinate axis). At this distance, both dynamic range and resolution are maximal. These figure shows quite clearly that a consideration of both dynamic range and resolution requirements places ESSB-SPM in a more favourable position than ESSB-LPM. ESSB-LPM is, in essence, a coarse-to-low-resolution pulsed neutron source, and medium resolution can only be attained at distances well beyond 30 m at the cost of severe limitations in available dynamic range. ESSB-SPM, on the other hand, can deliver low, medium, as well as high-resolution within the layout constraints of ESSB. We do recall, however, that the improved resolution characteristics of ESSB-SPM come at the cost of a lower integrated flux relative to ESSB-LPM – a factor of ca. six taking into account both the total number of protons per pulse hitting the target, as well as the different repetition rates. Given current constraints associated with the ESSB facility layout, this decrease in flux might be a necessity for certain applications requiring a spectral resolution below a few percent.

3.6 Fast choppers in long-pulse mode

From our discussion above, SPM provides easier access to higher spectral resolution while keeping instrument distances from the source well within layout constraints. In this operational mode, however, we have also noted that there will be an associated (and quite significant) cut in neutron flux per second. In what follows, we explore ways whereby the spectral quality of LPM pulses may be improved further while keeping neutronic output as high as practicable.

Such a task may be accomplished via the use of a fast (or 'pulse-shaping') chopper to trade spectral resolution (and dynamic range) against flux [27] . To explore this possibility, we consider two counterotating choppers running at 400 Hz each, as schematically shown by Figure 3-16. Figure 3-17 shows a time-distance diagram for a LPM pulse cut by a 400 Hz fast-chopper at 5 m from the moderator face. Note that this configuration is not an optimized one because it presents shadow regions for certain wavelengths, e.g., 2.1-3.0 Å. Figure 3-18 shows the regions of spectral resolution attainable with such a device as a function of neutron wavelength and distance from the source. Operating at a frequency of 400 Hz , two counter-rotating blades will produce pulse widths of 0.07 ms over a 12 cm-window. It can be noticed

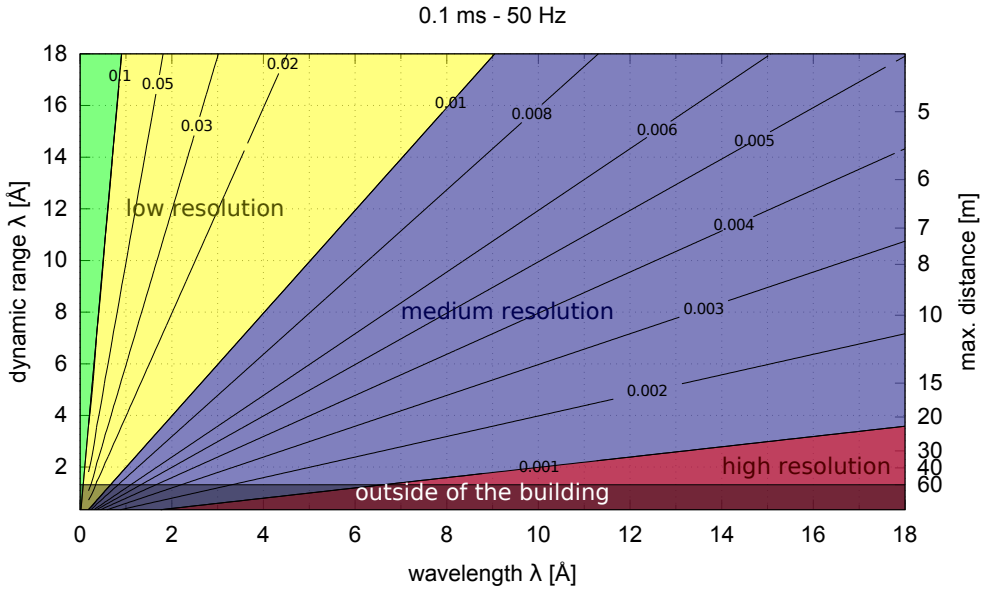

Figure 3-14: Regions of spectral resolution as a function of neutron wavelength and dynamic range for ESSB-SPM. For further details, see the text.

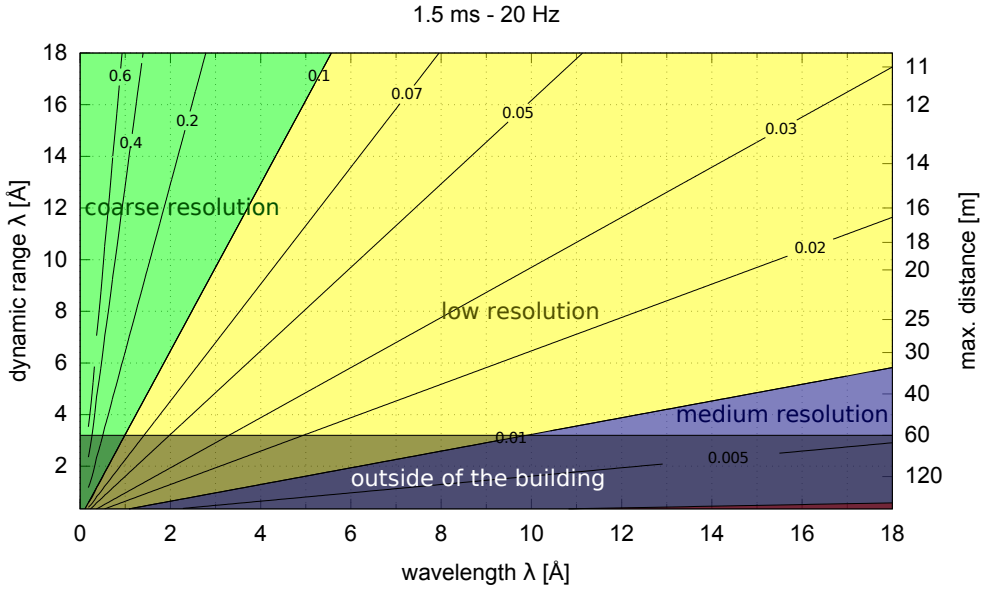

Figure 3-15: Regions of spectral resolution as a function of neutron wavelength and dynamic range for ESSB-LPM. For further details, see the text.

that for any dynamic range the resolution using this configuration can be much improved over that characteristic of ESSB-SPM. A net gain in the number of neutrons may also be achieved provided that the fast chopper is used in LPM pulses at the peak of the neutron pulse as shown by Figure 3-19. This figure represents the number of neutrons per second

as a function of time and shows how the 0.07 ms region transmitted by the fastchopper can have 30-40% more neutrons than the 0.1 ms region of SPM. This approach therefore appears to provide a convenient means of accessing medium- and high-resolution applications while operating in LPM. As an additional advantage, the use of a fast chopper in close proximity to the source would also redefine the time structure of the emerging pulse to be symmetric, thereby minimizing spectral congestion between adjacent neutron wavelengths.

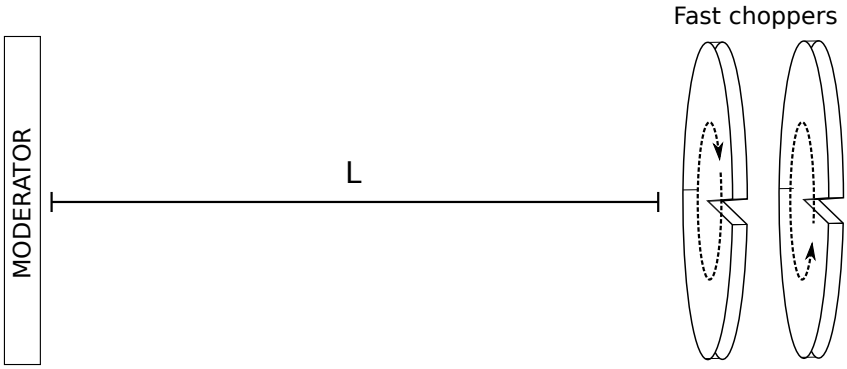

Figure 3-16: A schematic diagram of a set of two counter-rotating choppers.

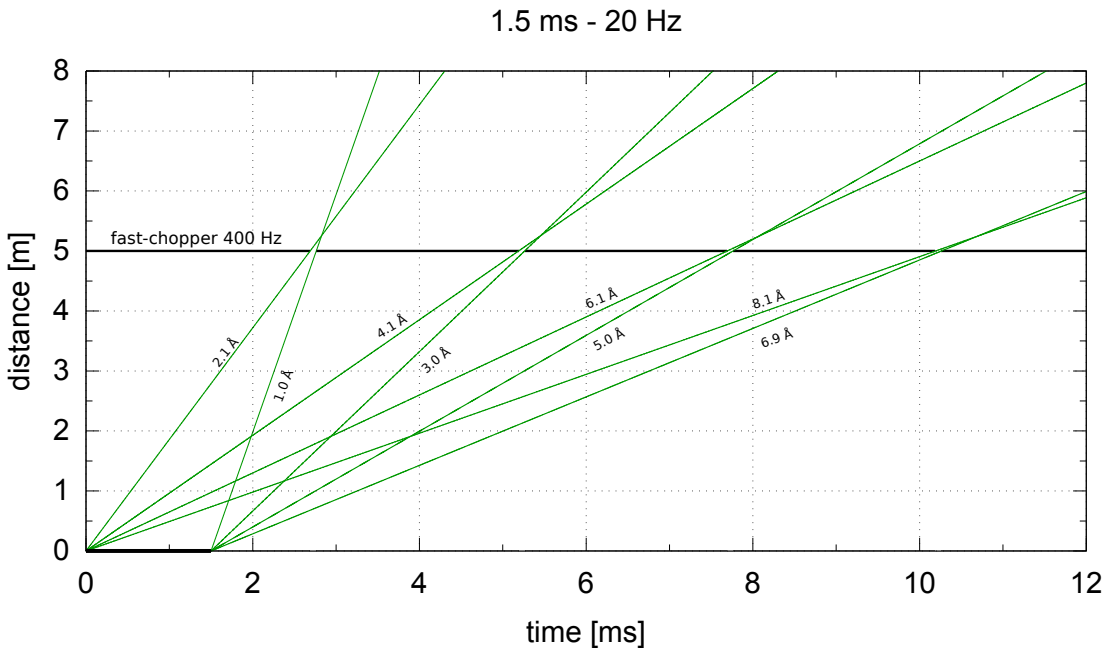

Figure 3-17: Time-space diagram of LPM with a 400 Hz-fast-chopper at 5 m. The chopper transmission time window is 0.07 ms.

The performance of a fast-chopper system is ultimately limited by its maximum attainable tangential velocity, and current engineering and materials limitations place an upper bound

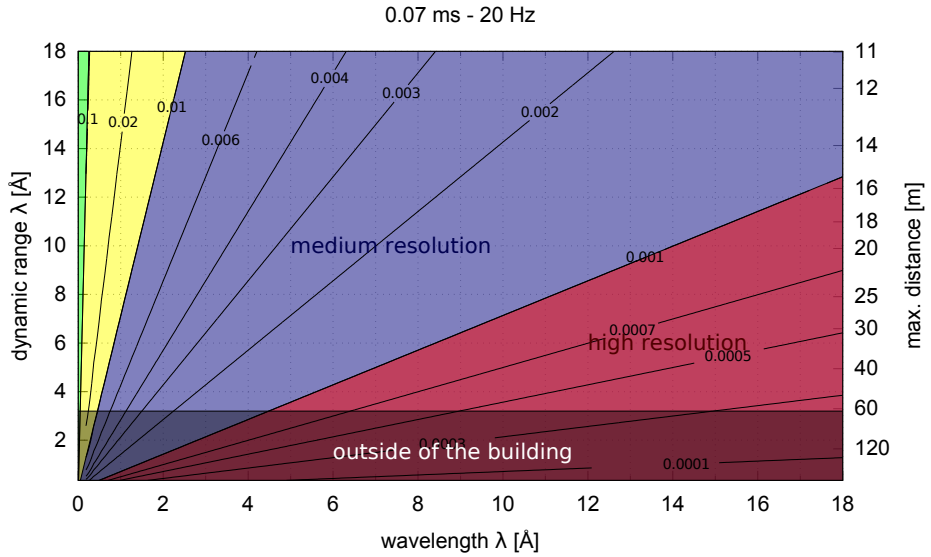

Figure 3-18: Regions of spectral resolution as function of neutron wavelength and dynamic range for ESS-LPM operating with two counter-rotating 400 Hz-choppers. For further details, see the text.

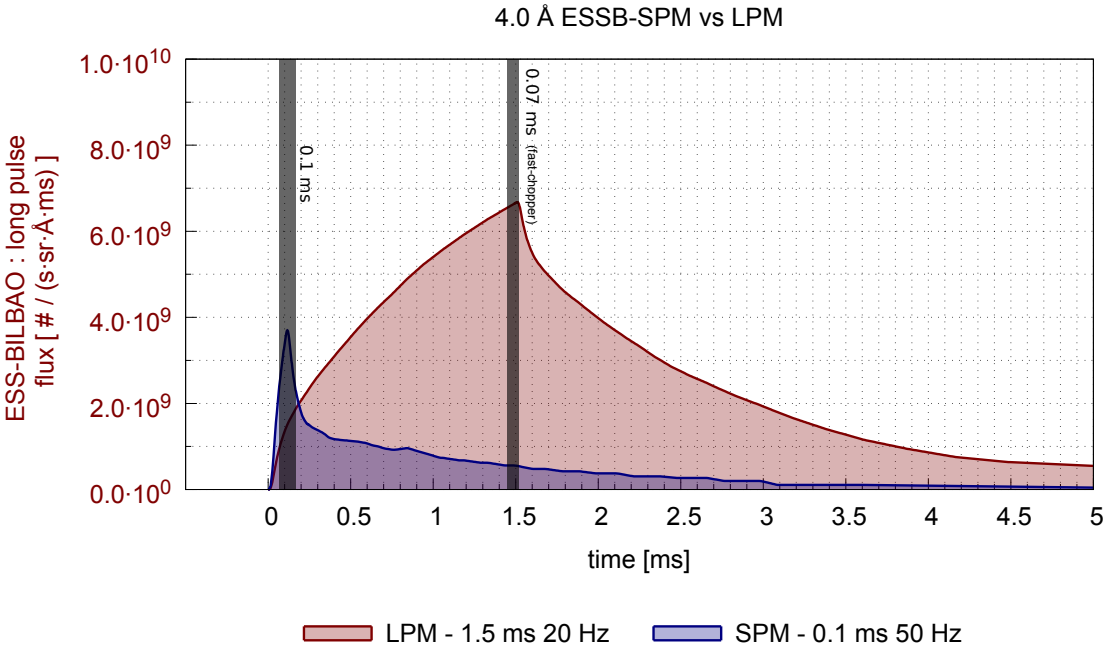

Figure 3-19: Comparison between ESSB-SPM and LPM for neutron pulses at 4 Å.

of ca. 24000 rpm for a disk diameter of 80 cm [28]. For a beam width of 12 cm, we therefore have a minimum time window of 0.14 ms, a figure that can still be reduced by a factor of two (0.07 ms) via the use of two counter-rotating disks.

To examine in more detail the consequences of using a fast chopper to redefine the time structure of the pulse, Figure 3-20 shows its response at a distance of 1.5 and 5 m from the moderator surface. At 1.5 m, pulses from different wavelengths still display a significant amount of temporal overlap and therefore the associated dynamic range will be considerably wider than the second case at 5 m. This longer distance, however, would place this chopper system outside the ESSB target area [1]).

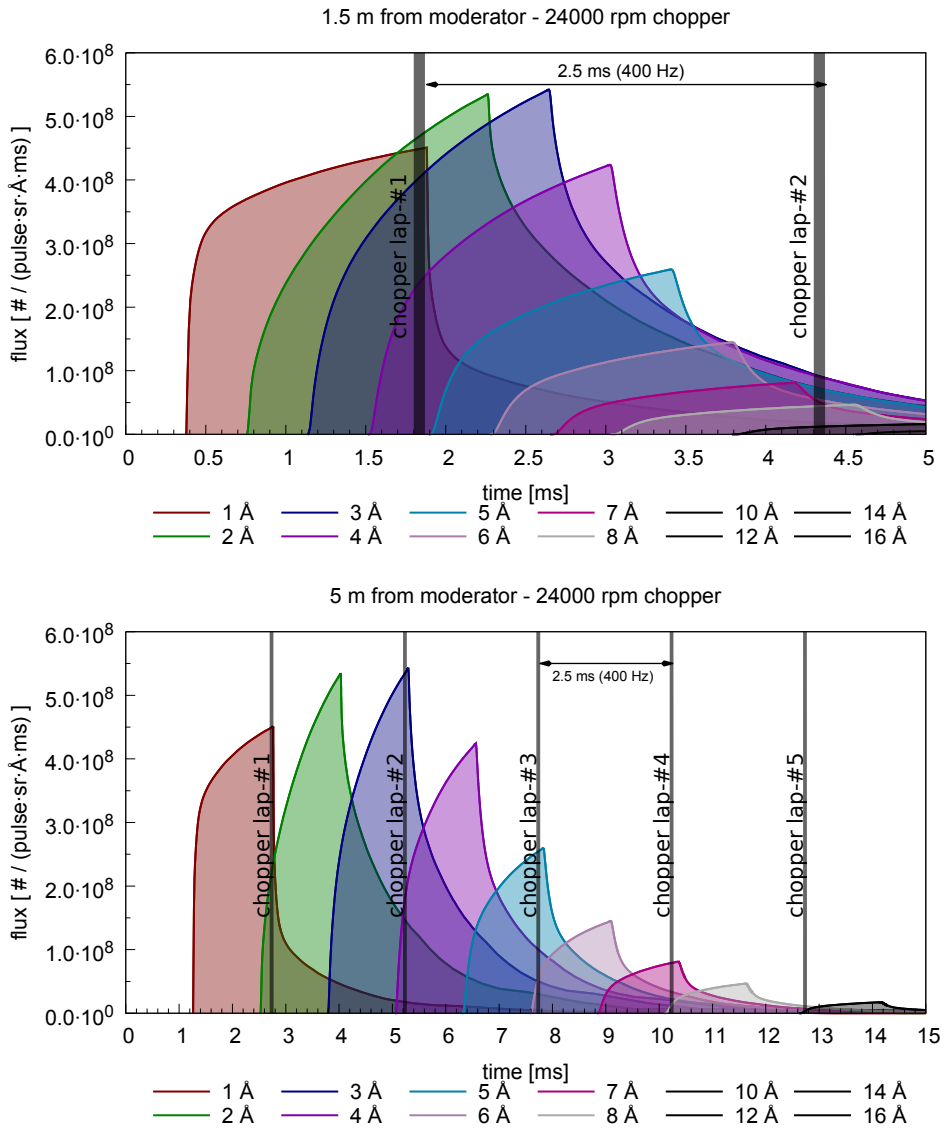

Figure 3-20: TOF profiles for a number of neutron wavelengths. Shadowed areas represent the time cuts produced by a fast chopper rotating at 400 Hz and a transmission time window of 0.07 ms, placed at 1.5 (top) and 5 m (bottom) from the moderator face.

Figure **??**(top) shows TOF profiles at 10 m after chopping the original LPM pulse by two 400-Hz counter-rotating choppers (0.07 ms) placed at 1.5 m from the moderator face (outside the

ESSB target vessel). Figure **??**(bottom) shows analogous data with the chopper located at 5 m (outside of the ESSB target-station area). As expected on the basis of our previous discussion, the available dynamic is considerably wider when a fast chopper system is placed in close proximity to the target.

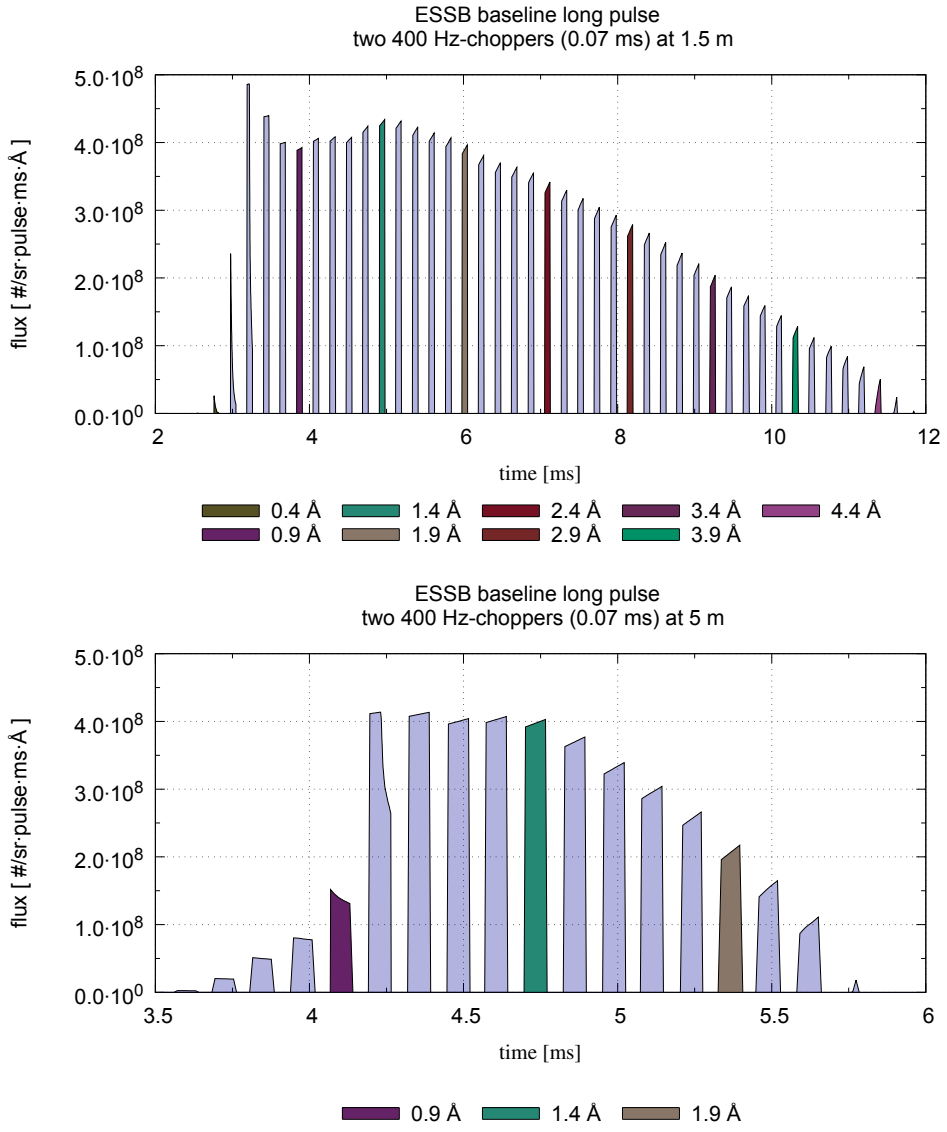

Figure 3-21: TOF profiles of a LPM neutron pulse cut by a fast-chopper located at 1.5 m (up) or 5 m (bottom) from the moderator face. At 1.5 m, the dynamic range transmitted by the chopper system will be about 3.5 Å, a figure which is reduced to 1.5 Å at 5 m. A square 0.07 ms transmission time window has been assumed.

To sum up, the use of fast-chopper systems in close proximity to the source represents an interesting option to improve spectral resolution, enabling routine access to medium and high resolution applications on ESSB-LPM. On the other hand, a broad dynamic range (greater than 1.5 Å) requires to place the chopper system as close as possible to the moderator face

in closer proximity to the target area (worse maintenance, radiation evironment). For certain wavelengths, a fast chopper in LPM could provide between 30-40% more neutrons than 0.1 ms pulses in SPM.

3.7 Conclusions

The analysis presented in this chapter has provided a number of important insights into the nature (and suppression) of high-energy backgrounds on ESSB, as well as its inherent characteristics in terms of available dynamic range and spectral resolution in both SPM and LPM. Such an exercise provides an overall view of the realm of applicability of ESSB in scientific applications using neutron-scattering techniques relative to other pulsed neutron sources around the world. At this juncture, we may conclude that:

- The suppression of high-energy backgrounds on ESSB will also reduce the neutron flux over a given dynamic range. A T_0-chopper placed outside the target area will be required to cope with these unwanted neutrons.
- Both source repetition rate and pulse width dictate the dynamic range and resolution of the neutron beam reaching the sample . Long pulses and high repetition rates produce higher neutron fluxes but worse resolution and dynamic range, respectively. On the other hand, short pulses ensure a higher resolution and a low repetition rate ensures a wider dynamic range.
- ESSB-SPM can deliver medium spectral resolution over a broad dynamic range using acceptable primary distances. Access to a higher resolution is also possible via the use of fast-chopper systems in close proximity to the source. Such a possibility is particularly enticing so as to extend the range of applications on ESSB-LPM. These choppers are best placed as close as possible to the moderator (inside the target area) in order to guarantee a broad dynamic range.

4 AN INSTRUMENT DEFINITION

This section applies the concepts introduced so far in order to establish a general framework for the analysis and selection of neutron instrumentation at ESSB. The first step in the selection of a particular type of neutron-instrument class is necessarily dictated by *what kind of science one wants to do*, then followed by the optimization of a particular instrument concept to deliver a given set of technical and scientific specifications associated with such a goal. On the basis of the results presented so far relating to the neutronic response and characteristics of ESSB, it is safe to conclude that ESSB will be able to deliver coarse resolution irrespective of whether it operates in LPM or SPM. In this context, a *small-angle neutron scattering* (SANS) instument represents a natural choice for further analysis, as this intrument class requires a moderate wavelength resolution to study large-scale structures down to nanometer lengthscales in a wide range of scientific disciplines including physics, chemistry, and biology [29] . In this sense, SANS represents the simplest technique requiring a certain level of wavelength resolution, as opposed to, for example, the implementation of a neutron-irradiation station for applications in materials science. In what follows, we outline how the scientific requirements associated with the use of ESSB for applications in SANS may be mapped onto the neutronic characteristics of the neutron source, as well as compare expected performance with that available at other neutron facilities across the globe. The guiding principles introduced in this chapter therefore constitute the starting point for the analysis of other (more elaborate) instrument classes such as high-resolution diffraction and spectroscopy, a task beyond the scope of this report.

4.1 SANS in brief

As an experimental technique, SANS is used to probe so-called large-scale structures, typically over the range 10-10000 Å. In conjunction with its X-ray analogue (commonly referred to as SAXS), it has been used extensively over the last few decades to probe the properties of supramolecular species and phenomena at the mesoscale including polymers, complex fluids, proteins, emulsions, or nanostructured materials [30].

As shown by Eq. 10, Bragg's law (10) defines the condition for the coherent scattering of neutrons in condensed matter. According to this law, the ability to probe structures larger than typical interatomic distances necessarily implies access to low values of neutron momentum transfer, quantitatively expressed in terms of the *scattering vector* $\vec{Q}$. This *scattering vector* corresponds to the difference between the incoming ($\vec{k}_i$) and the outgoing ($\vec{k}_f$) neutron *wave vectors*. Mathematically, we can write

$$|\vec{Q}| = |\vec{k}_i - \vec{k}_f| = n\left(\frac{2\pi}{d}\right) \tag{10}$$

where,

Q, *is the scattering vector, in* $\mathring{A}^{-1}$
n, *is an integer*
d, *is a characteristic distance (or d-spacing), in* $\mathring{A}$

For elastic scattering, Q can be expressed as a function of the incident neutron wavelength (λ) and the *Bragg angle* θ, as shown by Eq. (11). Hence low values of Q can be achieved via the use of long incident wavelengths and/or the use of detectors at low *scattering angles* ϕ given the relation $\phi = 2\theta$.

$$Q = \frac{4\pi sin\theta}{\lambda} \tag{11}$$

At accelerator-driven sources, neutron production at wavelengths of the same order of magnitude as mesoscopic length scales is not straightforward. In this situation, neutron detection at small angles (close to the transmitted beam) becomes a mandatory requirement such that the incident neutron wavelength leads to sufficiently small values of neutron momentum transfer to probe large characteristic distances d, as shown by Eq. (12)

$$d = \frac{\lambda}{2sin\theta} = \frac{2\pi}{Q} \tag{12}$$

When the *Bragg angle* is small, Expression (12) can be approximated by

$$d \approx \frac{\lambda}{2\theta} \tag{13}$$

where,

θ, *is the Bragg angle in radians, such that* $\phi = 2\theta$

For more details on the mathematical formalism underpinning SANS, the reader is referred to Ref. [31].

4.2 Source operational mode

As described in detail in previous chapters, ESSB can operate in either LPM or SPM. LPM delivers a higher neutron flux per second than SPM yet its inherent spectral resolution is compromised significantly, as shown by Figure 3-7. For SANS, we must account for both uncertainties in incident wavelength as well as scattered angle, where the small-angle approximation is made. Assuming that both resolution components add in quadrature (i.e.,

they are independent of each other and obey a normal distribution), the overall relative uncertainty in final momentum transfer is given by

$$\frac{\Delta Q}{Q} \approx \left(\left(\frac{\Delta \lambda}{\lambda} \right)^2 + \left(\frac{\Delta \theta}{\theta} \right)^2 \right)^{1/2} \tag{14}$$

Figure 4-1 reproduced from Ref. [32] shows that the ultimate angular resolution (the second term in Eq. 14) is a function of the geometry of the source, the sample size, and the detector size when using a so-called pinhole configuration. We note that in both Eq. 14 and Fig. 4-1, θ is now used to denote the scattering angle. We can then write

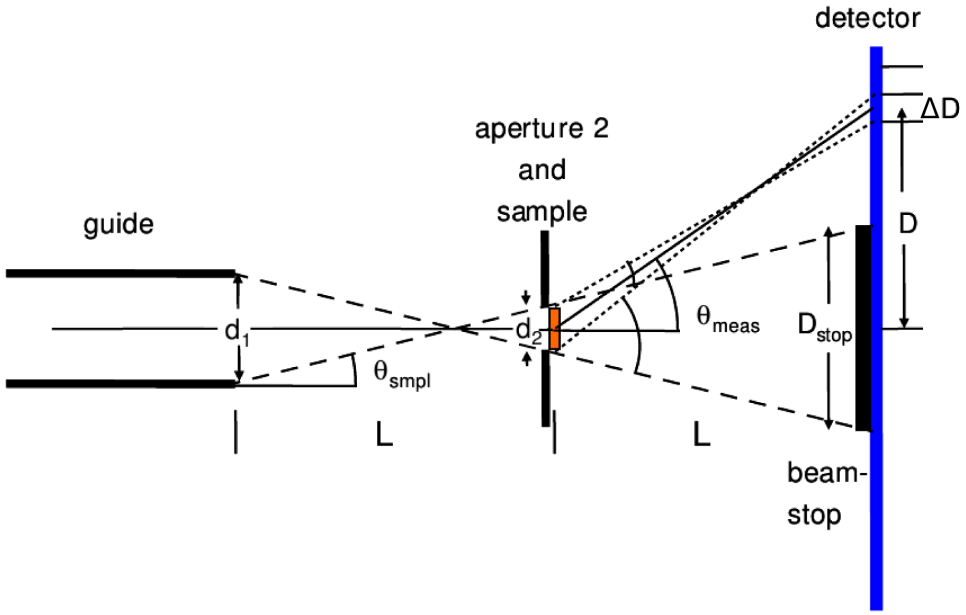

From K. Lieutenant [32]

Figure 4-1: Geometric parameters defining the angular resolution of a SANS instrument.

$$\frac{\Delta \theta}{\theta} \approx \frac{\left(\left(d_1 + d_2 \right)^2 + \left(d_2 + \Delta D \right)^2 \right)^{1/2}}{4D} \tag{15}$$

where,

d_1, *is the size of the aperture of the neutron guide exit*
d_2, *is the size of the sample*
D, *is the lateral position of the detector*
ΔD, *is size of the detector*

Typical values for Eq. (15) are $d_1 = 3\ cm$, $d_2 = 1\ cm$, $D = 2.5 - 50\ cm$ and $\Delta D = 1\ cm$, which give values for the angular resolution between 0.02 (at the corner of the detector) and 0.40

(close to the beam-stop). On the other hand Figure 3-7 show ESSB-LPM can deliver a spectral resolution ($\Delta\lambda/\lambda$) below 0.03 for wavelengths above 4 Å and flight paths longer than 50 m (for SPM the spectral resolution would be significantly lower). These values for the spectral (incident wavelength) and angular resolution show that the total resolution in terms of scattering vector resolution is dominated by the angular term, and such as value is fixed for a given instrument geometry. From the above considerations, it follows that the spectral resolution of the ESSB pulses does not dominate. LPM is then an appropriate operational mode to maximise neutron flux at the sample (Figure 2-6). Furthermore, a lower repetition rate on LPM provides an additional advantage in terms of available dynamic range as illustrated earlier in Fig. 3-10. Also, the use of bandwidth choppers can avoid neutron wavelengths below 4 Å, where the spectral resolution is degraded relative to the aforementioned (optimal) values. Moreover, the ESSB advanced configuration (making use of a beryllium filter) has been optimised above 4 Å, as shown by Figure 2-6, and would be able deliver about 60% higher flux than the baseline configuration above this wavelength.

To conclude this discussion, the coarse resolution requirements associated with the implementation of SANS calls for the operation of ESSB in LPM using the advanced configuration. This choice arises from the relative insensitivity of such an instrument to incident-wavelength resolution relative to angular resolution, a situation where total incident flux becomes the primary figure of merit.

4.3 A sketch of a SANS instrument at ESSB-LPM

For a SANS instrument, the primary goal is to reach low values of Q. For the wavelength range available at ESSB (and, similarly, at typical neutron sources), such a task requires implementing neutron detection in close proximity to the trasmitted neutron beam. A schematic diagram of a SANS instrument at ESSB-LPM is shown in Fig. 4-2. The primary instrument (i.e., prior to the sample) consists of a neutron-extraction system to transport neutrons away from the ESSB TMR assembly. A bent neutron prevents direct view of the moderator and serves to avoid gamma backgrounds from the beryllium target. The coating of the bender can be selected to transport a reasonably wide incident-wavelength range, i.e., $4 - 7.8$ Å. A maximum wavelength of 7.8 Å corresponds to the available dynamic range at 50 m starting at 4 Å (cf. Eq. 9).

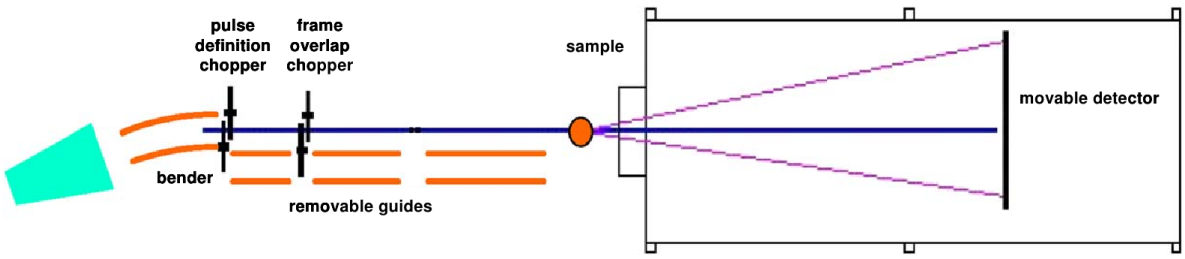

From K. Lieutenant [32]

Figure 4-2: Sketch of a SANS instrument at ESSB-LPM.

Neutrons extracted from the ESSB TMR assembly are contaminaited with neutrons from other wavelength bands, and bandwidth choppers are therefore necessary to avoid overlap with these unwanted wavelengths from the same or other neutron pulses. Figure 4-3 shows how the first chopper (at 5.5 m) defines the bandwidth 4-7.8 Å while the second one (at 9 m) avoids frame overlap between consecutive pulses.

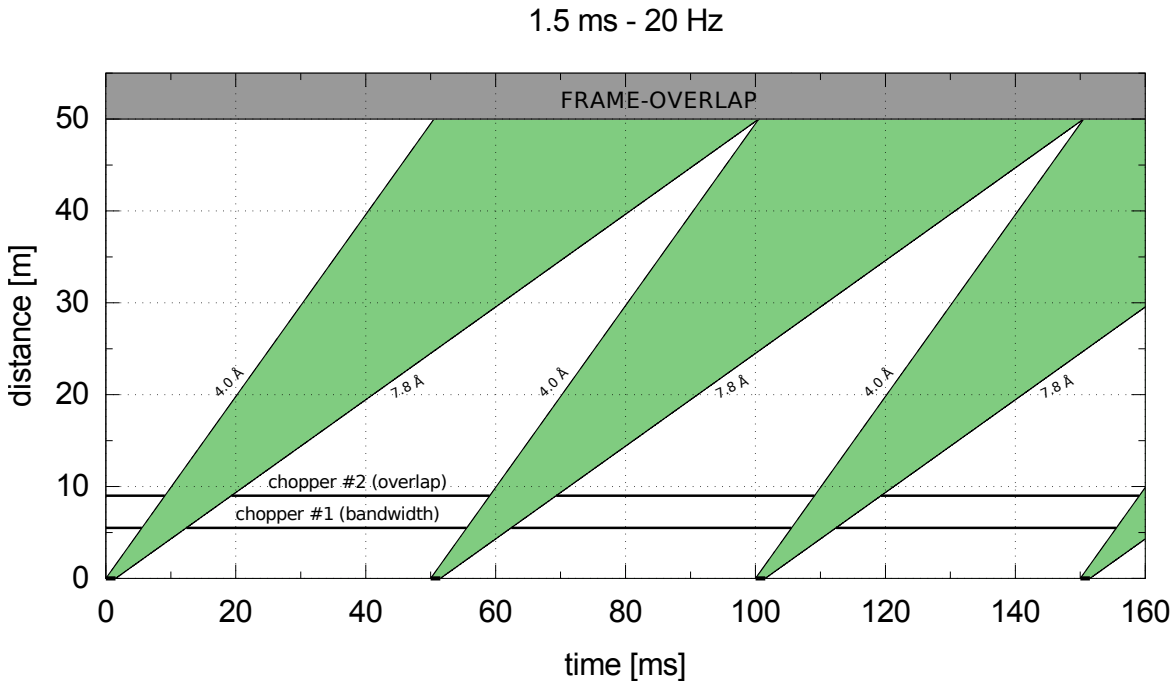

Figure 4-3: Time-distance diagram for the bandwidth (at 5.5 m) and frame-overlap choppers (at 9 m) defining a bandwidth of 4-7.8 Å for SANS.

The available Q-range, the count rate, and the resolution for any particular experiment can be further optimised via the use of movable and interchangeable neutron guides to vary the position of the *effective source* as well as the total flight path. This *effective source* corresponds to the point where neutrons emerge from the last neutron guide and, hence, it defines the final divergence of the neutron beam and the Q-resolution. The use of a movable detector in a evacuated tank (to avoid air scattering) would also add much-needed flexibility to the proposed instrument. Likewise, a pinhole geometry would be preferred over a collimation system in order to increase flexibility. Such a pinhole geometry optimizes the intensity at the detector, and leads to the collection of sharp SANS patters. This type of geometry requires that the free-flight path (the distance between the *effective source* and the sample) and the secondary path (the distance between the sample and the detector) are equal. Such a condition can be easily achieved with the movable detector.

Typical detector areas are 1 x 1 m^2 pixelated down to 1 x 1 cm^2. The center of the detector hosts a beam stop which avoids radiation damage of transmited neutrons. Potential materials for this beam-stop include ^{10}B or Cd. Diaphragms can be used in order to adjust the size of

the *effective source*, thereby offering an additional means of tuning Q-resolution. In closing this discussion, we note that the above has not taken into account any gravity effects associated with the transport of neutrons down to the sample position. At wavelengths as long as 7.8 Å, these effects can be significant given the long flight times from the TMR assembly to 50 m (ca. 98 *ms*). These effects can be compensated via the use of gravity-focusing devices consisting of fixed and moving apertures [24].

4.4 A more detailed specification

In SANS, the length of the instrument largely dictates the largest object that can be measured. The angular divergence of neutrons of the same wavelength leaving the *effective source* (that is, the exit point of last neutron guide before the sample) lead to a spread in distance before interaction with the sample. To still retain the requisite level of spatial coherence leading to interference phenomena, Pynn [33] has argued that the largest measurable object is related to purely geometrical parameters by

$$d = 10^{-2} \cdot \left(\frac{\lambda}{a}\right) L \tag{16}$$

where,

d, is the size of the largest measurable object, in µm,
λ, is the longest neutron wavelength, in Å,
a, is the size of the effective source exit aperture, in cm,
L, is the distance between the effective source exit and the sample, in m.

An incident wavelength of 4 Å corresponds to the optimal range for a ESSB-SANS instrument (advanced configuration), and the maximum distance allowed by the ESSB facility layout is 50 m from the moderator. Without frame overlap or loss of dynamic range, the maximum usable wavelengh would be 7.8 Å, as estimated from Eq. (9). Taking a minimum value for the aperture of the *effective neutron source* of $1\ cm$ (d_1 in Fig, 4-1), a pinhole geometry rather than a collimation system requires an *effective source*-to-sample distance $L = (50 - 5)/2 = 22.5\ m$, where 5 m corresponds to the dimensions of the target area. Taking into account all of these values, the largest object that the proposed ESSB-SANS could measuse would be 1.7 μm. Using Eq. (12) the lowest Q-value accessible on such instrument is $3.7 \cdot 10^{-4}$ Å^{-1} Such a value is of the same order as similar instruments (existing or proposed) at ESS ($3 \cdot 10^{-4}$ Å^{-1}), BIO-SANS ($9 \cdot 10^{-4}$ Å^{-1}) at SNS, or SANS2D ($2 \cdot 10^{-3}$ Å^{-1}) at ISIS. The *scattering angle* required to achive a Q as low as $3.7 \cdot 10^{-4}$ Å^{-1} using 7.8 Å neutrons corresponds to 0.026°, as shown by Eq. (11). Hence the outgoing neutron will need to reach a detector located at 22.5 m from the sample and at 1.03 cm orthogonal to the beam direction. All neutrons below this transverse distance are regarded as belonging to the transmitted beam. To block this unwanted contribution, a beam-stop of $2\ x\ 1.03 = 2.06\ cm$ can be placed in front of the SANS detector.

Referring back to Fig. 4-1 and Eq. (17), the optimal size of the sample (d_2) depends on the *effective source* aperture (d_1) as well as on the size of the beam-stop D_{stop}. Its optimal value is

about 0.5 *cm*, a suitable figure for most applications yet it can also be increased if resolution requirements can be relaxed.

$$D_{stop} = d_1 + 2d_2 \tag{17}$$

where,

d_1, *is the size of the effective neutron source aperture,*
d_2, *is the size of the sample,*
D_{stop}, *is the size of the beamstop*

The maximum Q-value should be enough to probe sizes of the order of about 15 Å. This requirement calls for a scattering vector of about 0.4 $Å^{-1}$. The best neutron wavelength to achieve it is 4 Å, a region where the ESSB-LPM advanced configuration delivers the highest neutron flux. The associated scattering angle (2θ) is 14.6°. Taking into account a common detector area of 1 x 1 m^2, the minimum distance between the sample and the detector should then be 1.92 m (the same distance from the *effective source* to sample). These values are summarised in 4-1. The Q-range accessible at ESSB-LPM is therefore comparable to that available in similar instruments at other (pulsed and steady) neutron sources around the world. Given the temporal characteristics of ESSB-LPM, it is however unlikely that the ESSB-SANS can extend its Q range to achieve medium-resolution diffraction, like EQ-SANS at SNS [34].

This section has established the feasibility of a SANS instrument at ESSB, i.e, covering a Q-range of $3.7 \cdot 10^{-4} - 0.4$ $Å^{-1}$ (1.7 $\mu m - 15$ Å). This Q range is comparable to those available at existing neutron sources and could very well serve a number of scientific requirements across nanometre and mesoscopic length scales. The main elements of this SANS instrument are described in the following sections.

Table 4-1: Operational extreme values for the SANS proposal.

Wavelength of incident neutron	Distance sample to detector	Scattering vector Q	Size of measurable object
4.0 Å	1.92 m	0.4 $Å^{-1}$	15 Å
7.8 Å	22.5 m	10^{-4} $Å^{-1}$	1.7 μm

4.4.1 NEUTRON EXTRACTION FROM TARGET AREA

Neutron extraction from the target area is an important (and potentially innovative) aspect given the relative compactness of the ESSB facility and the low proton energies used to drive neutron production. Such a process involves both the efficient transport of neutrons down to the sample position as well as the elimination of fast-neutron and gamma-ray backgrounds from the target. This task can be achieved via the use of a mechanical device like a T_0-chopper, described in Section 3.2, pag. 30 . Since a SANS instrument at ESSB only requires efficient neutron trasnport above 4 Å, neutron-optical solutions like the use of a bender system are

also a possibility. A bender system improves the transmission over a T_0-chopper for long wavelengths, as already demonstrated for EQ-SANS at SNS [35].

A possible bender system consists of a supermirror material enabling the efficient transmission of neutrons above 4 Å. It blocks neutrons below this wavelength as well as gamma backgrounds present if the instrument were to have a direct line of sight of the source. In order to attain maximum throughput, the current design of the ESSB moderator system allows the installation of guides up to 30 *cm* away from the moderator face. Given a target area radius ca. 5 *m*, the characteristic bender length (L_1 in Fig. 4-4) will be 4.7 *m*.

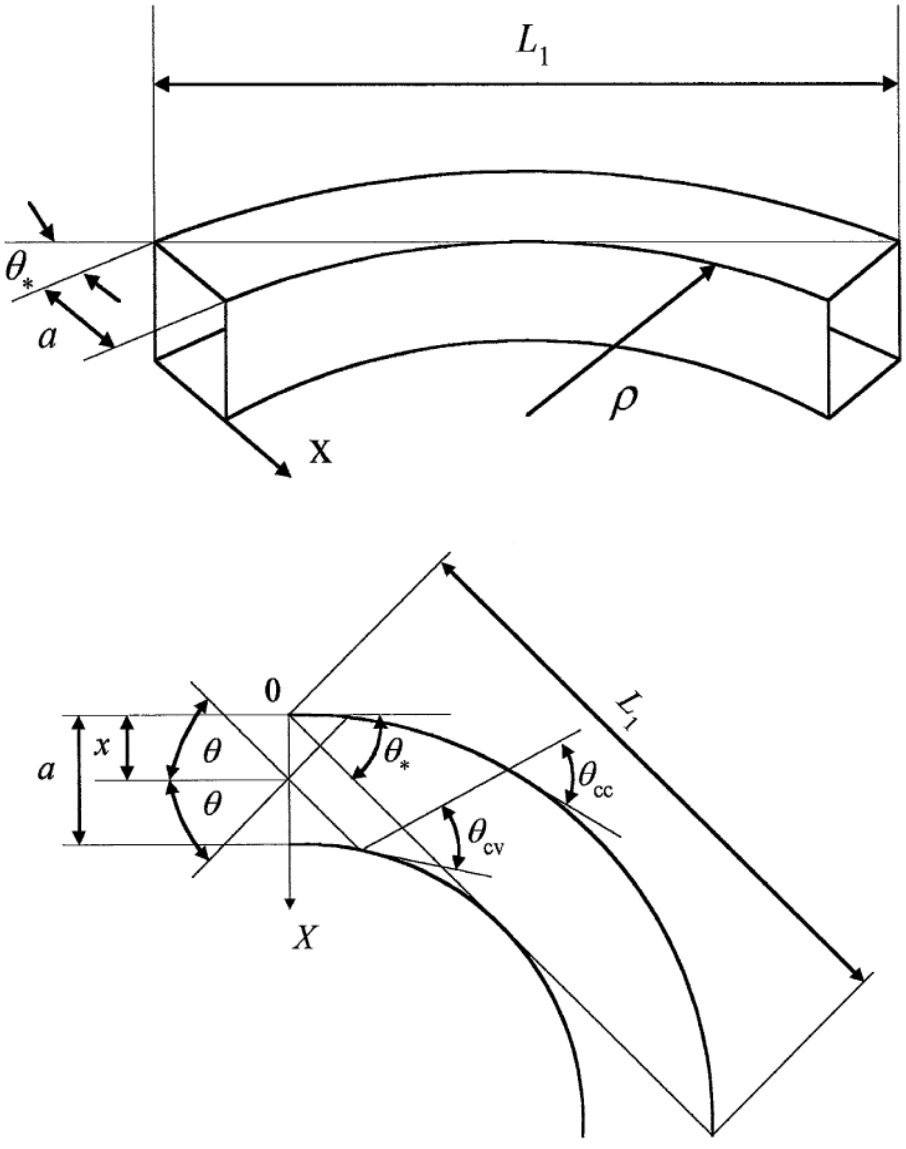

From A. Schebetov [36]

Figure 4-4: A schematic diagram of a neutron-guide bender system.

Given $a^2 = 4\ x\ 4\ cm^2$ for the bender cross section, trigonometric relations (within the small-angle approximation, cf. Fig. 4-4) imply a radius given by Eq. (18) so as to avoid direct view

of the moderator. For ESSB, such a radius is 69 m, and it is associated to a *characteristic angle* (θ_*) of 1.95°, corresponding to the maximum glancing angle described by Eq. (19).

$$\rho = \frac{L_1^2}{8a} \tag{18}$$

where,

ρ, *is the bender radius,*
L_1, *is the bender length,*
a, *is the bender cross section.*

$$\theta_* = \frac{4a}{L_1} \tag{19}$$

where,

θ_*, *is the characteristic angle.*

Following Shebetov [36] , we define the glancing angle of a divergent trajectory over the concave (Eq. 20) and the convex (Eq. 21) sides as

$$\theta_{cc} = \theta_* \sqrt{\left(\theta/\theta_*\right)^2 + x/a} \tag{20}$$

where,

x, *is the coordinate of the intersection point of the trajectory and the bender entrance,*
θ, *is the angle between the incident trajectory and the entrance normal.*

$$\theta_{cv} = \theta_* \sqrt{\left(\theta/\theta_*\right)^2 + x/a - 1} \tag{21}$$

Since $\theta_{cc} > \theta_{cv}$, a necessary condition for transport corresponds to a glancing angle (θ_{cc}) [in degrees] lower than $\theta_{cc} < 0.099 \cdot m \cdot \lambda$, where m is the supermirror-coating number (multiples of the response of natural Ni), and λ [in Å] is the minimum wavelength to be transported. Equation (20) then dictates the admittance angle θ_1 via Eq. (22), which is the maximum angle of the incoming neutron (relative to the normal of the bender entrance) that will be transported by a m-supermirror coating according to

$$\theta_1 = \theta_* \sqrt{\left(\frac{0.099 \cdot m \cdot \lambda}{\theta_*}\right)^2 - \frac{x}{a}} \tag{22}$$

At present, m-supermirror coatings up to 7 have been demonstrated. This m-number will allow to transport 4 Å neutrons wavelengths up to divergences of 2.77°. Taking into account this angle, a moderator-bender distance of 30 cm, a moderator size of 12 cm, and a bender entrance size of 4 cm, there will still be a significant loss in flux relative to the intensity at

the moderator surface. Alternatives to a high m-supermirror value could involve the use of channels inside the bender to reduce the *characteristic angle*.

In summary, neutron transport from the target area to the sample position could be achieved with a bender system to extract neutrons from the target station. Such a solution prevents direct view of the moderator and gamma radiation from the beryllium target. Its radius of curvature would have a radius of 69 m, with a cross section of 4 x 4 cm^2 and a length of 4.7 m. A supermirror coating of $m = 7$ for the bender would maximize neutron transport around 4 Å with a maximum divergence of 5.5°.

4.4.2 BANDWIDTH

The bender system introduced earlier is optimized to transport neutrons above 4 Å, yet shorter wavelengths between 0.05 and 4 Å will be also transmitted through this device. To avoid these, bandwidth choppers are needed to define our wavelength range between 4 and 7.8 Å.

These bandwidth choppers are set to rotate at the frequency of ESSB-LPM, i.e. 20 Hz. The first one will be located just outside of the Target Station at a distance of 5.5 m from the moderator face. In order to To transmit a bandwidth between 4 and 7.8 Å, these choppers need to be open between 5.55 and 12.39 ms (Figure 4-3). Note that time zero is defined to correspond to the emergence of the first neutron from the moderator for every pulse. Due to the length of the LPM pulse, some neutrons between 3.9 and 7.96 AA will pass through the first chopper. To avoid frame overlap, a second chopper is needed. It should be located at a certain distance from the first one, e.g. 3.5 m to let the beam pass through between 9.09 and 19.23 ms. At 50 m, the wavelength resolution will be between 0.03 and 0.015 as Figure 3-7 shows.

4.4.3 BEAM DIVERGENCE AND INSTRUMENT CONFIGURATIONS

Beam divergence is an important parameter to consider when examining neutron transport from the bender system down to the sample position. The maximum glancing angle of a neutron hitting the sample is given for the shortest flight path, i.e 1.92 m (minimum distance between *effective source* and sample). From Fig. 4-1, this maximum glancing angle is given by $\theta_{smpl} = atan\big(1/2(d_1 + d_2)/1.92\ m\big) = 0.22°$. Neutrons reaching the sample for any other *effective source*-sample distance will therefore emerge at lower angles. Natural nickel transports 4 Å neutrons at angles below 0.465° so such a choice is a reasonable one. Note that Section 4.4.1, pag. 58 estimated a maximum glancing angle for 4 Å 2.77°. This value indicates that guide coatings for the bender of m=7 are not really necessary

As anticipated earlier, a flexible instrument at ESSB would require removable neutron guides and a movable detector in a evacuated tank. A possible design would host three different configurations. The first requires no guide after the bender. In this case, the *effective source* would be the exit of the bender and would corresponds to a total free flight path of 45 m (equal distance of 22.5 m for primary and secondary paths, as dictated by the adopted pinhole configuration). The second one would correspond to the shortest free flight path, i.e. 1.92 m leading to a guide length of $22.5 - 1.92 = 20.58$ m and a secondary path of 1.92 m (movable

detector). The third one would be an intermediate case of 11.25 m of neutron guide followed by an equal length after the sample. With an incoming wavelength range of $4 - 7.8$ Å, these three configurations lead to a Q-range of 3.7 10^{-4} Å^{-1} $-$ 0.035 Å^{-1} (22.5 m free-flight path), 7.4 10^{-4} Å^{-1} $-$ 0.07 Å^{-1} (11.25 m) and 4.32 10^{-3} Å^{-1} $-$ 0.4 Å^{-1} (1.92 m). The Q-resolution would vary between 0.005 and 0.26.

4.5 Conclusions

This chapter has presented the concept of a possible SANS at ESSB. As no high-resolution is required for this technique, LPM is an appropriate choice leading to an intrinsically higher count rate than SPM. Its main components and operational parameters are:

- A wavelength range of $4 - 7.8$ Å.
- The use of bandwidth and frame-overlap choppers. The first one sits at 5.5 m from the moderator face, to be followed 3.5 m donwstream,
- A bender system to extract neutrons from the target area. It avoids direct line of sight of the source and it is optimised to transport neutrons of wavelengths above 4 Å.
- A pinhole configuration with three possible geometries to access different Q ranges.

5 OUTLOOK

In this report, we have examined in some detail the ESSB facility, from neutron production and moderation, all the way to utilisation. Two operational limits, namely SPM and LPM, have been considered in depth, corresponding to proton pulse widths/frequencies of 0.1 ms/50 Hz and 1.5 ms/20 Hz, respectively. ESSB-LPM delivers a higher flux than SPM, yet at the expense of spectral resolution. Spectral resolution at ESSB-LPM can be recovered via the use of fast choppers, which could be of relevance for high-resolution applications.

The performance of ESSB has also been compared with ISIS-TS2. In terms of sheer neutronic output, ESSB-LPM delivers between 20 and 30% of the total cold-neutron flux per pulse relative to ISIS-TS2, yet at the cost of a lower spectral resolution limiting applications to those requiring a rather coarse definition of the incident neutron spectrum. In the cold-neutron range, ESSB-SPM produces a similar time distribution than ISIS-TS2, yet at the cost of available flux (ca. 2% of ISIS-TS2 per pulse or 11% per second). One of the key features of ESSB is the option to change both pulse length and repetition rate during operation. Long pulses and high repetition rates produce higher neutron fluxes and enhanced dynamic range but worse resolution. On the other hand, short pulses ensure a much better resolution. We have also considered the main parameters associated with the design of a SANS instrument using ESSB-LPM. Taking into account the accessible spectral and dynamic range, as well as space constraints within the facility, the available Q-range would be between $3.7 \cdot 10^{-4}$ and 0.4 Å^{-1}, of the same order as other facilities around the globe.

With the above figures in mind, we conclude that ESSB would represent a timely and much-needed addition to the current landscape of neutron sources in Europe. Characterised by a neutron yield intermediate between large- (e.g., ISIS-TS2) and small-scale (e.g., LENS) accelerator-driven sources, it provides hitherto inexistent opportunities in neutron science at both regional and national levels.

References

[1] ESS-Bilbao. Technical design report: Ess-bilbao target station. Technical report, ESS-Bilbao, may 2013. F.J. Bermejo and F. Sordo, editors. Available at http://essbilbao.org:8080/ESSBilbao/en/copy_of_LAN_TDR.pdf. Quoted in pages 1, 4, 10, 29 and 48.

[2] J.P. de Vicente. A preliminary approach to neutron-instrument selection at ess-bilbao. Master's thesis, Universidad Politecnica de Madrid, 2013. Quoted in page 1.

[3] F. Sordo, F. Fernandez-Alonso, S. Terron, M. Magan, A. Ghiglino, F. Martinez, F.J. Bermejo, and J.M. Perlado. Baseline design of a low energy neutron source at ess-bilbao. Physics Procedia, (in press, 2013). Quoted in page 1.

[4] F.J. Bermejo, F. Fernandez-Alonso, F. Sordo, and A. Rivera. Inspecciones no destructivas mediante haces de neutrones. Nuclear España, (in press, 2013). Quoted in page 1.

[5] F. Sordo et al. Design Studies at the ESS-Bilbao Neutronic Applications Laboratory. Invited talk presented at the VI Reunión Bienal de la Sociedad Española de Técnicas Neutrónicas, June 24-27th 2012, Segovia, Spain. Quoted in page 1.

[6] F. Fernandez-Alonso et al. Neutron Science at ESS-Bilbao: A First Assessment of Requirements. Invited talk presented at the 3rd Meeting of the Union for Compact Accelerator-driven Neutron Sources UCANS-III, July 31st - August 3rd 2012, Bilbao, Spain. Quoted in page 1.

[7] The european spallation source, 2012. http://ess-scandinavia.eu/. Quoted in page 4.

[8] F. Sordo, A. Ghiglino, M. Magan, F. Martinez, S. Terron, R. Vivanco, and J.P. De Vicente. Proyecto del laboratorio de aplicationes neutrónicas de ess-bilbao. Technical report, ESS-Bilbao, January 2012. Quoted in pages 4 and 6.

[9] C.M. Lavalle. The Neutronic Design and Performance of the Indiana University Cyclotron Facilty (IUCF) Low Energy Neutron Source (LENS). PhD thesis, Indiana Universtity, 2007. Quoted in page 4.

[10] I. Bustinduy. The ESSB front-end, an injector for light ion accelerator, Conference at UCANS III, jul 2012. Quoted in pages 5 and 6.

[11] F.J. Bermejo I. Bustinduy. The ess bilbao accelerator. Proceedings of the Union for Compact Accelerator-driven Neutron Sources, UCANS III, Bilbao, Spain, July 31-August 3, 2012. Proceedings of the Union for Compact Accelerator-driven Neutron Sources, UCANS III, Bilbao, Spain. Quoted in page 6.

[12] ESS-Bilbao Target Station Status, Conference at UCANS III, aug 2012. Quoted in pages 6, 7 and 8.

[13] S. Terron, F. Sordo, M. Magán, A. Ghiglino, F. Martinez, J.P. De Vicente, R. Vivanco, K. Thomsen, J.M. Perlado, F.J. Bermejo, and A. Abanades. Conceptual design of the beryllium rotating target for the ess-bilbao facility. Nuclear Instruments and Methods in Physics Research Section A: Accelerators, Spectrometers, Detectors and Associated Equipment, 724(0):34–40, 2013. Quoted in page 6.

[14] F. Sordo, S. Terrón, M. Magán, G. Muhrer, A. Ghiglino, F. Martínez, J.P. De Vicente, R. Vivanco, J.M. Perlado, and F.J. Bermejo. Neutronic design for ess-bilbao neutron source. Nuclear Instruments and Methods in Physics Research Section A: Accelerators, Spectrometers, Detectors and Associated Equipment, 707(0):1–8, 2013. Quoted in page 9.

[15] I. Tilquin, P. Froment, M. Cogneau, Th. Delbar, J. Vervier, and G. Ryckewaert. Experimental measurements of neutron fluxes produced by proton beams (23–80 mev) on be and pb targets. Nuclear Instruments and Methods in Physics Research Section A: Accelerators, Spectrometers, Detectors and Associated Equipment, 545(1-2):339–343, 2005. Quoted in page 9.

[16] F.J. Bermejo and F. Sordo. Chapter 2 - neutron sources. In F. Fernandez-Alonso and D.L. Price, editors, Neutron Scattering – Fundamentals, volume 44 of Experimental Methods in the Physical Sciences, pages 137–243. Academic Press, 2013. Quoted in page 10.

[17] R. Vivanco. Análisis de diseño y optimización neutrónica del moderador frío de ess-bilbao. Technical report, ESS-Bilbao - Instituo de Fusion Nuclear UPM, 2013. Quoted in pages 10 and 29.

[18] D.B. Pelowitz, editor. MCNPX User's Manual, Version 2.7.0. Los Alamos National Laboratory Report, LA-CP-11-00438. April 2011. Quoted in pages 10 and 70.

[19] C.G. Windsor. Pulsed neutron scattering. Taylor & Francis, 1981. Quoted in pages 14, 15, 28 and 39.

[20] D. L. Price and F. Fernandez-Alonso. Chapter 1 - an introduction to neutron scattering. In F. Fernandez-Alonso and D.L. Price, editors, Neutron Scattering – Fundamentals, volume 44 of Experimental Methods in the Physical Sciences, pages 1–136. Academic Press, 2013. Quoted in page 14.

[21] M. Arai. Chapter 3 - experimental techniques. In F. Fernandez-Alonso and D.L. Price, editors, Neutron Scattering – Fundamentals, volume 44 of Experimental Methods in the Physical Sciences, pages 245–320. Academic Press, 2013. Quoted in pages 14 and 15.

[22] W.H. Press; S.A. Teukolsky; W.T. Vetterling; B.P. Flannery. Numerical Recipes in C. Cambridge University Press, 1992. Quoted in page 21.

[23] F. Fernandez-Alonso, F.J. Bermejo, I. Bustinduy, M. A. Adams, and J. W. Taylor. Spin dynamics in liquid and rotationally disordered solid oxygen. Phys. Rev. B, 78:104303, Sep 2008. Quoted in page 21.

[24] R. Pynn. Neutron scattering - a primer. Summer School on the Fundamentals of Neutron Scattering. Quoted in pages 28 and 57.

[25] Documentation for EQ-SANS. http://neutrons.ornl.gov/eqsans/documentation/. Quoted in page 30.

[26] H. Schober, E. Farhi, F. Mezei, P. Allenspach, K. Andersen, P.M. Bentley, P. Christiansen, B. Cubitt, R.K. Heenan, J. Kulda, P. Langan, K. Lefmann, K. Lieutenant, M. Monkenbusch, P. Willendrup, J. Šaroun, P. Tindemans, and G. Zsigmond. Tailored instrumentation for long-pulse neutron spallation sources. Nuclear Instruments and Methods in Physics Research Section A: Accelerators, Spectrometers, Detectors and Associated Equipment, 589(1):34 – 46, 2008. Quoted in page 44.

[27] F. Demmel, V. Garcia Sakai, MTF Telling, and F. Fernandez-Alonso. FIRES : a novel backscattering spectrometer for ISIS. Technical report, RAL-ISIS, RAL Technical Reports RAL-TR-2010-005. 2010., 2010. Quoted in page 44.

[28] Aernnova engineering, editor. Neutron shielding of a carbon epoxy chopper disc with high strength boron fibers, 2012. Quoted in page 47.

[29] J. Penfold and I.M. Tucker. Chapter 5 - large-scale structures. In F. Fernandez-Alonso and D.L. Price, editors, Neutron Scattering - Fundamentals, volume 44 of Experimental Methods in the Physical Sciences, pages 353 – 413. Academic Press, 2013. Quoted in page 52.

[30] B. Hammouda. Probing Nanoscale structures - The SANS toolbox. National Institute of Standards and Technology, national institute of standards and technology edition, December 2010. Quoted in page 52.

[31] F. Fernandez-Alonso and D.L. Price, editors. Neutron Scattering - Fundamentals, volume 44 of Experimental Methods in the Physical Sciences. Elsevier Academic Press, 2013. http://www.sciencedirect.com/science/bookseries/10794042/44/supp/C. Quoted in page 53.

[32] K. Lieutenant, T. Gutberlet, A. Wiedenmann, and F. Mezei. Monte-carlo simulations of small angle neutron scattering instruments at european spallation source. Nuclear Instruments and Methods in Physics Research Section A: Accelerators, Spectrometers, Detectors and Associated Equipment, 553(3):592–603, 2005. Quoted in pages 54 and 55.

[33] R. Pynn. Neutron Scattering - Lecture 5: Small Angle Scattering. NIST Center for Neutron Research, 2013. Quoted in page 57.

[34] J.K. Zhao, C.Y. Gao, and D. Liu. The extended Q-range small-angle neutron scattering diffractometer at the SNS. Journal of Applied Crystallography, 43(5 Part 1):1068–1077, Oct 2010. Quoted in page 58.

[35] J. Zhao. Conceptual design and performance analysis of the extended q-range, high intensity, high precision small angle diffractometer. Technical report, SNS, Oak Ridge, May 2000. Quoted in page 59.

[36] A. Schebetov, A. Kovalev, B. Peskov, N. Pleshanov, V. Pusenkov, P. Schubert-Bischoff, G. Shmelev, Z. Soroko, V. Syromyatnikov, V Ul'yanov, and A. Zaitsev. Multi-channel neutron guides of pnpi: results of neutron and x-ray reflectometry tests. Nuclear Instruments and Methods in Physics Research Section A: Accelerators, Spectrometers, Detectors and Associated Equipment, 432(2-3):214–226, 1999. Quoted in pages 59 and 60.

[37] K. Lefmann and K. Nielsen. Mcstas, a general software package for neutron ray-tracing simulations. Neutron News, 10(3):20–23, 1999. Quoted in page 70.

[38] E. Klinkby, B. Lauritzen, E. Nonbøl, P. Kjær Willendrup, U. Filges, M. Wohlmuther, and F.X. Gallmeier. Interfacing mcnpx and mcstas for simulation of neutron transport. Nuclear Instruments and Methods in Physics Research Section A: Accelerators, Spectrometers, Detectors and Associated Equipment, 700(0):106–110, 2013. Quoted in page 70.

[39] S. Itoh, K. Ueno, R. Ohkubo, H. Sagehashi, Y. Funahashi, and T. Yokoo. {To} chopper developed at {KEK}. Nuclear Instruments and Methods in Physics Research Section A: Accelerators, Spectrometers, Detectors and Associated Equipment, 661(1):86–92, 2012. Quoted in page 95.

[40] J.J. Yugo, E.D. Blakeman, R.A. Lillie, and J.O. Johnson. Three-dimensonal shielding simulations and activation calculations of the sns neutron beam lines to, eo and bandwidth choppers. Technical report, Oak Ridge National Laboratory, 2008. Quoted in page 96.

[41] Preliminary shielding design of low energy shutter at ESS-Bilbao, Union of Compact Accelerator-Driven Neutron Sources (UCANS) III, 2013. J.P. De Vicente et al. Quoted in page 96.

[42] M. Narita and K. Narita. Average number of collisions necessary for slowing down of neutrons. Jounal of Nuclear Science and Technology, 26:819–825, September 1989. Quoted in page 96.

PART 2: SUPPLEMENTARY INFORMATION

APPENDIX A

THE ESSB MCSTAS COMPONENT

A.1 GENERAL DESCRIPTION

The total flux and underlying time distribution of neutrons emerging from a pulsed neutron source ultimately depend on the TMR configuration and on the properties of the proton pulse from the accelerator. Neutron production can be simulated accurately by codes like MCNPX [18] . Moderation processes lead to the production of thermal and cold neutrons, with characteristic wavelengths commensurate with interatomic distances, which become quite sentitive to the structure and dynamics of the material and ultimately lead to particle-interference phenomena between the incoming and outgoing neutron waves. Likewise, neutron reflection from surfaces and interfaces in the TMR assembly can be important for an accurate description of neutronic response. Beyond the moderator (described by well-characterized kernels), MCNPX has not been used traditionally to describe these phenomena associated with the cold-neutron response, thus the need for to integrate this code with other approaches to neutron-transport simulations.

McStas [37] is a well-established code that can take into account these phenomena as neutrons are transported away from the target area, i.e, wave reflection and transport in supermirrors. It is also a popular code amongst neutron-scattering practitioners and instrument developers because it incorporates a large number of components to predict neutronic performance away from the source. Moreover, McStas provides a number of *source components* for pulsed-neutron sources. In the context of ESSB, an accurate description of the baseline and advanced configurations requires the translation of MCNPX output into a form that can be used within the McStas package. Such a task may be achieved in a number of ways, some of which are still under development [38] . In our case, we have chosen to create a McStas ESSB source component (hereafter BILBAO_source) to read the MCNPX output and to transform it into the appropriate input for McStas. Below, we describe efforts to date to build an accurate and at the same time versatile BILBAO_source component in McStas.

A.1.1 Input

The inputs of the BILBAO_source component include the MCNPX tally output file (both energy and time tally) and some other parameters as shown in Table A.1-1. Those parameters marked with an asterisk are mandatory, otherwise default values have been listed. Although not mandatory, the use of the same moderator width and height as the one used for MCNPX is recommended. Neutrons emerge in all directions from the moderator. To increase the performance of the simulations, it becomes necessary to use focusing elements that consider only those neutrons able to reach the next component. As amply demonstrated throughout this report, sometimes it is useful to simulate a particular energy or time range instead of the whole spectrum. These ranges can be conveniently selected from the component inputs. The time distribution of protons from the accelerator is assumed to be a uniform square pulse, yet it is relatively straightforward to modify this input to model other (more complex) pulse shapes.

Table A.1-1: Inputs of the BILBAO_source component. For further details, see the main text.

input	value	units	description
double width	*	cm	width of the moderator face
double height	*	cm	height of the moderator face
double xw	*	cm	width of the focusing rectangle
double yh	*	cm	height of the focusing rectangle
int target index	+1		component whose position is used as focusing distance
double dist	0.0	cm	distance of the focusing element (alternative to the use of target_index)
double Emin	min.avail.	meV	minimum neutron energy
double Emax	max.avail.	meV	maximum neutron energy
double Lmin	min.avail.	Å	minimum neutron wavelength
double Lmax	max.avail.	Å	maximum neutron wavelength
double tmin	min.avail.	s	minimum time
double tmax	max.avail.	s	maximum time
int shape	0		shape of the incident proton pulse (only square pulse available at present)
double FWHM	1.5	ms	full-width-at-half-maximum of the proton pulse
double current	75.0	mA	peak current of the proton pulse
double protonEnergy	50.0	MeV	proton energy
char* source_file	*		mcnpx outp file (MCNPX tally should have total bins)
int tally	105		number of the MCNPX tally to read
double distTally	10.0	m	distance of the MCNPX point detector (useful to estimate values per steradian in the MCNPX FU card from SNS)
double* lambdas	*	Å	array of wavelengths to plot in output file

A.1.2 Output

As primary output, the BILBAO_source component generates a continuous neutron TOF distribution useful for subsequent McStas simulations. In addition, a number of text (*.dat) files in column format contain the proton-pulse distribution, the intrinsic moderator response, the neutron pulses, some central moments, the FWHM of the pulses, or the time distributions over a pre-defined wavelength range. In no particular order, the specific output files are:

- *protonSignal.dat* stores information on the proton pulse.
- *moderatorResponse.dat* and *moderatorResponse3D.dat* store the intrinsic moderator response.
- *neutronPulse.dat* and *neutronPulse3D.dat* store the convolved neutron source.
- *moments.dat* stores a statistical analysis.

- *fastChopper.dat* stores the energy-time distribution emerging from a fast chopper.
- And *lambdas.dat* stores the time distribution over a range of wavelengths specified by the variable *lambdas*.

The reader is referred to the main text of this report for a more detailed explanation and illustration of these quantities.

A.1.3 How it works

The BILBAO_source component follows a similar methodology to that implemented in the SNS_source component, as schematically illustrated in Figure A.1-1. First, it reads a neutron time-energy distribution from a MCNPX tally corresponding to the intrinsic moderator response per proton, i.e., the time-energy distribution of neutrons emerging from the moderator face as a result of the interaction of a single proton with the target. This response is a function of both wavelength and time. As such, it needs to be convolved with the temporal characteristics of the impinging proton pulse. The net result is a discrete neutron pulse at a particular wavelength and time. This discrete response is interpolated (in two dimensions) by the BILBAO_source component so as to generate a continuous pulse (a requirement of the McStas package).

Relative to similar implementations for other neutron sources, the following peculiarities of the BILBAO_source component should be noted:

- An automatic convolution procedure based on user-defined input parameters. For short-pulse spallation, a robust convolution tool is not critical because proton-pulse widths are less than a μsec, a value well below typical intrinsic moderator responses. We note that even in this favourable case, a quantitative description of the temporal response of epithermal neutrons will nonetheless require proper account of the structure of the proton pulse.
- The use of Hermite and bicubic interpolation algorithms in some cases, a feature of particular importance a few μsec around the peak of the pulses in order to obtain a good estimate of peak shapes. In other cases, we resort to linear interpolation.
- Parallel execution, where the component manages data flow across individual cores.
- The possibility to use customised wavelength and time ranges to improve simulation speed and performance.
- A detailed analysis of neutron line shapes in the time domain. These data include the central moments of the neutron pulses as described in the main text (time-integrated flux, mean, deviation, skewness, and kurtosis). In addition, we include the most probable value of these time distributions as well as half-width-at-half-maximums (HWHMs), and FWHMs, WAPs, and LAPs as a function of wavelength.

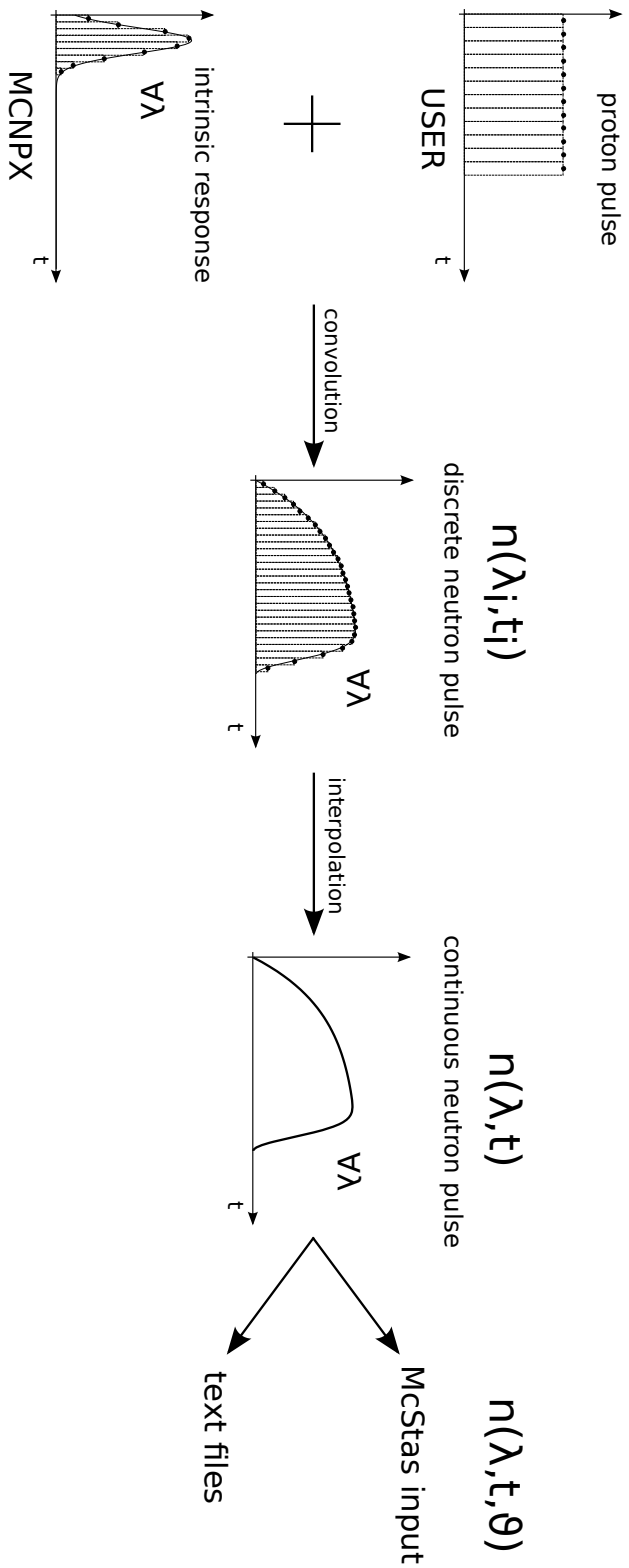

Figure A.1-1: Schematic diagram of the BILBAO_source component. For more details, see the text.

- Output files containing the proton signal, the intrinsic moderator response, the TOF distribution, and a line shape analysis of time structure and fast-chopper cuts. These files allow for straightforward 3D visualization on widely available software packages like Gnuplot.
- The component can be readily extended to describe proton beams beyond a square pulse.

A.2 THE SOURCE CODE

The McStas source code of the BILBAO_source component can be downloaded from

https://docs.google.com/file/d/0B6loJORHvdLbeWdfb0xwMXdSbWc/edit?usp=sharing

APPENDIX B

THE ESSB MODERATOR RESPONSE

B.1 INTRINSIC MODERATOR RESPONSE

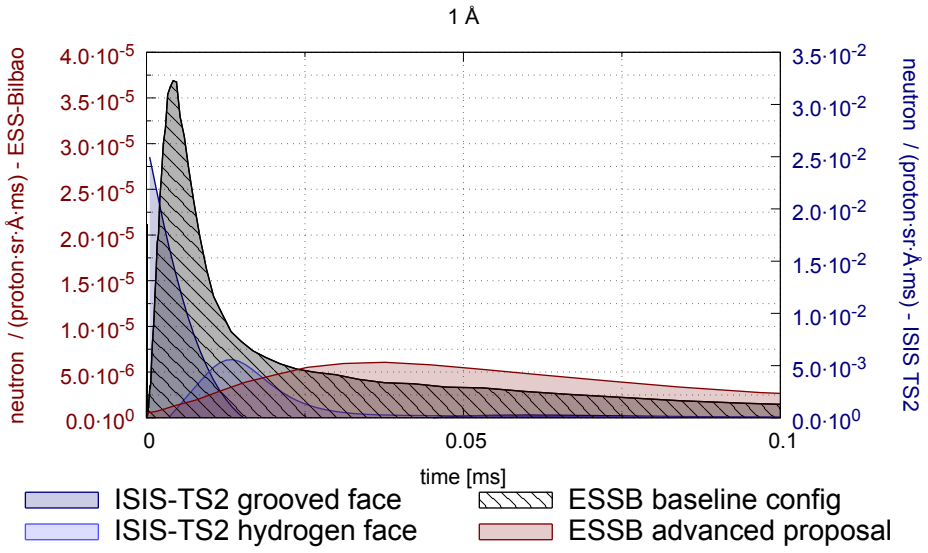

Figure B.1-1: Intrinsic moderator response: ESSB vs ISIS-TS2 at 1 Å.

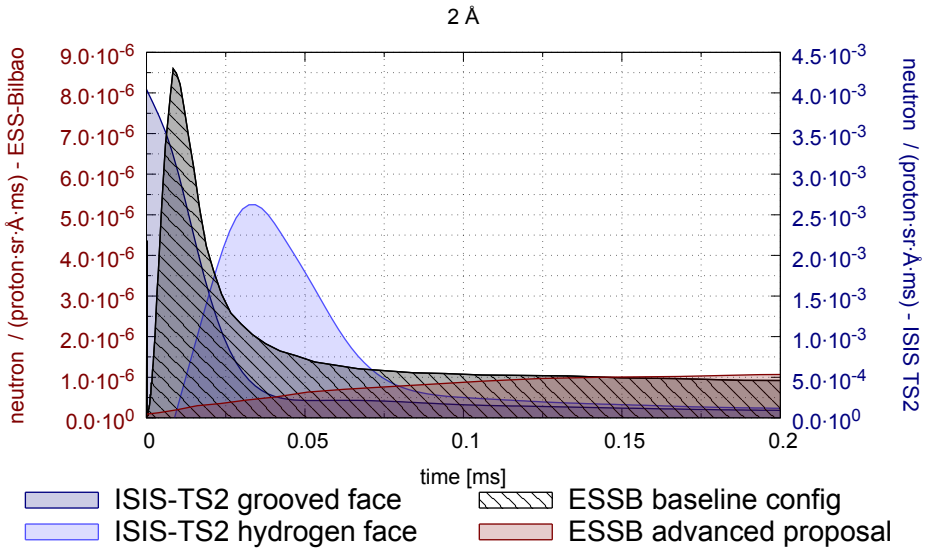

Figure B.1-2: Intrinsic moderator response: ESSB vs ISIS-TS2 at 2 Å.

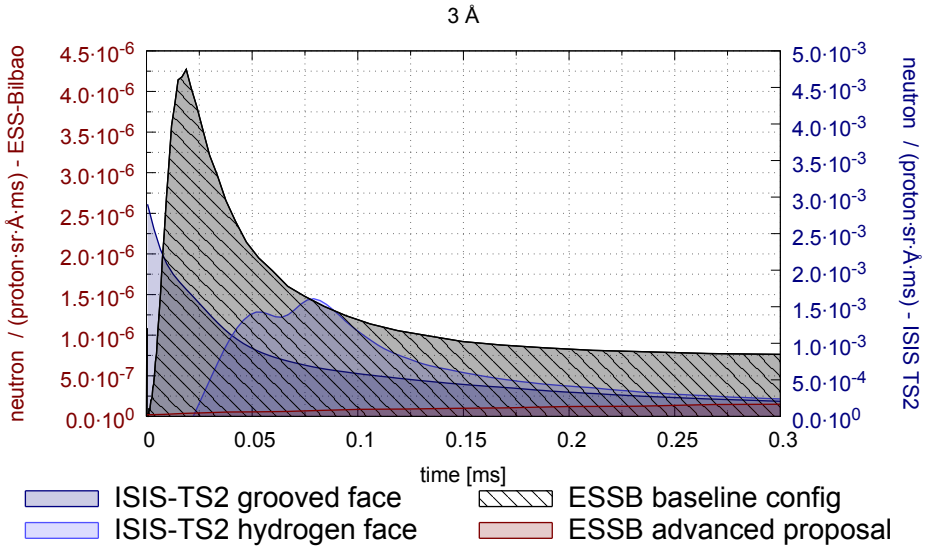

Figure B.1-3: Intrinsic moderator response: ESSB vs ISIS-TS2 at 3 Å.

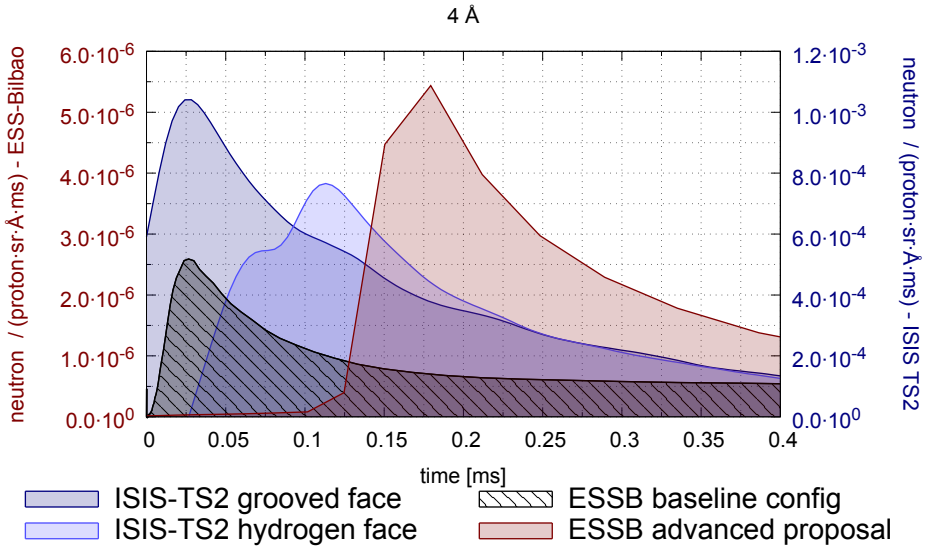

Figure B.1-4: Intrinsic moderator response: ESSB vs ISIS-TS2 at 4 Å.

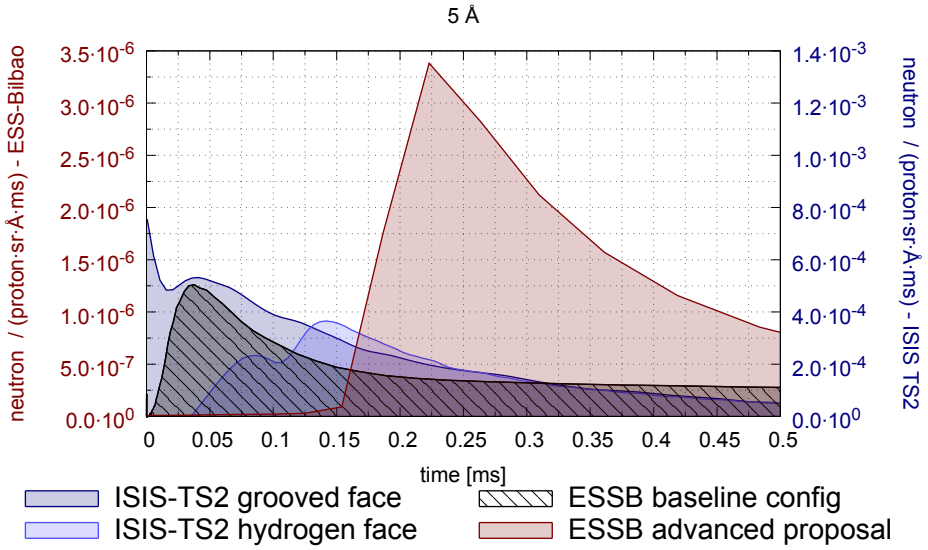

Figure B.1-5: Intrinsic moderator response: ESSB vs ISIS-TS2 at 5 Å.

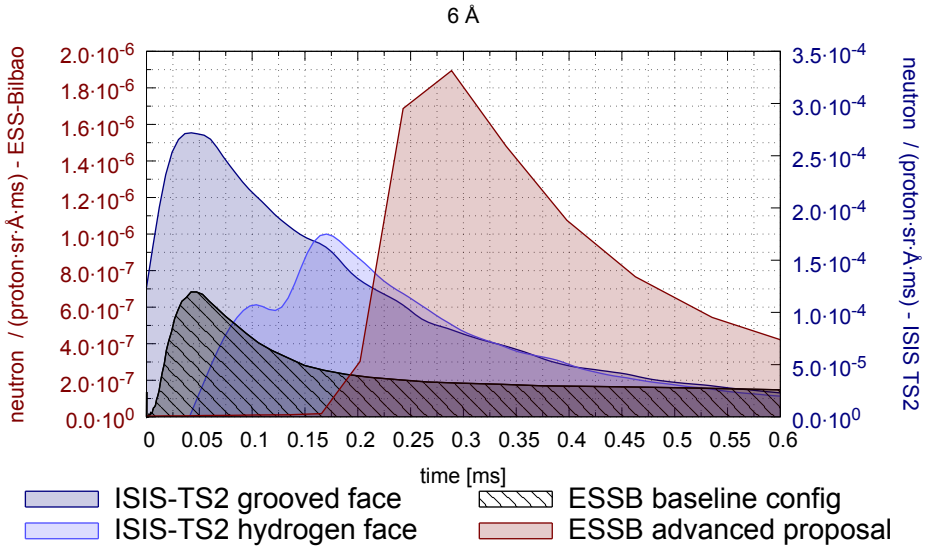

Figure B.1-6: Intrinsic moderator response: ESSB vs ISIS-TS2 at 6 Å.

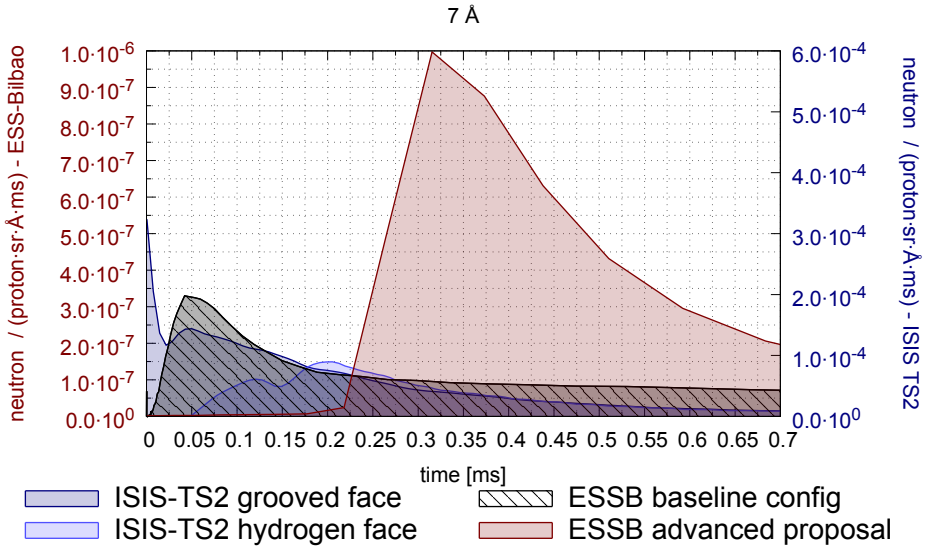

Figure B.1-7: Intrinsic moderator response: ESSB vs ISIS-TS2 at 7 Å.

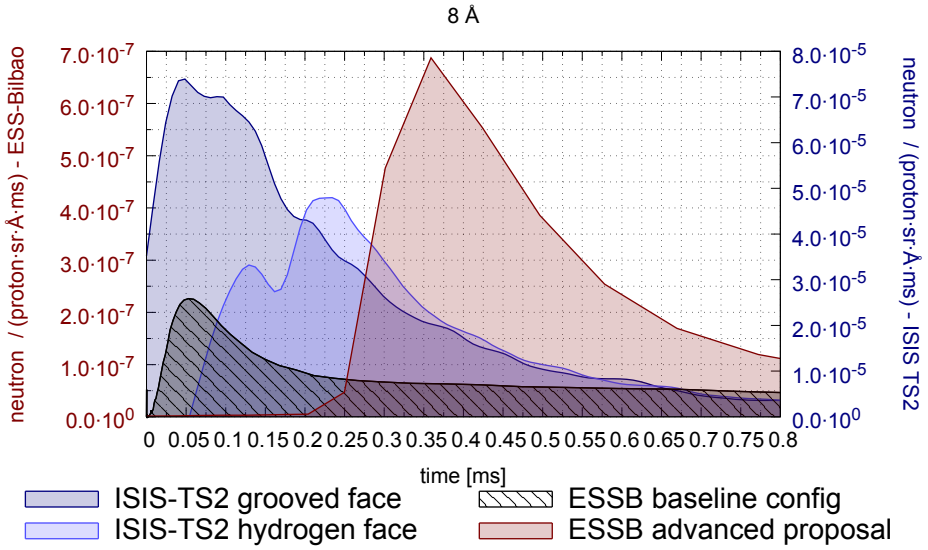

Figure B.1-8: Intrinsic moderator response: ESSB vs ISIS-TS2 at 8 Å.

APPENDIX C

THE ESSB NEUTRON PULSES

C.1 SHORT-PULSE MODE

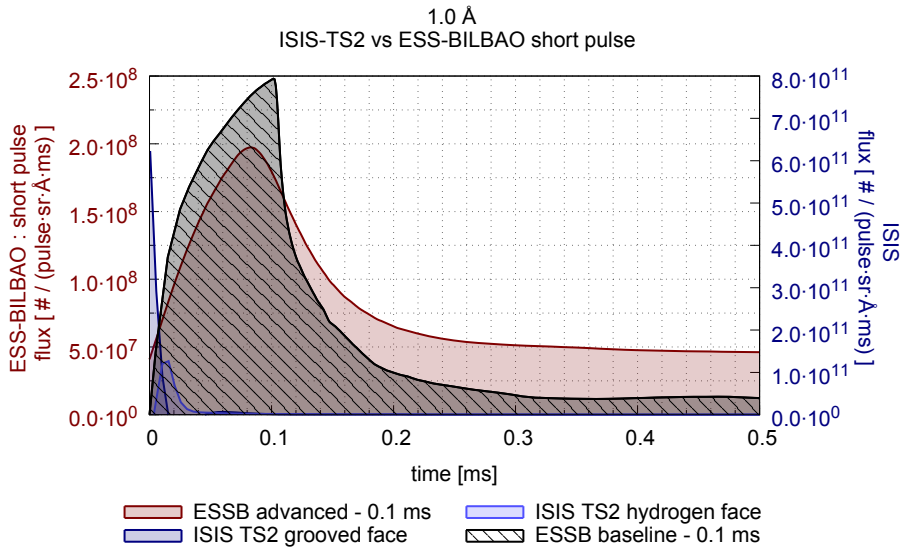

Figure C.1-1: ESSB-SPM vs ISIS-TS2 at 1 Å.

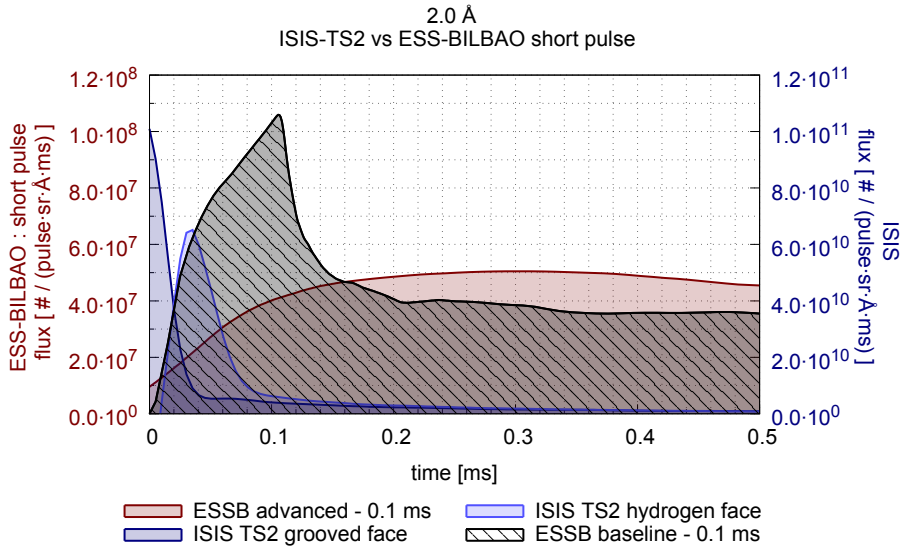

Figure C.1-2: ESSB-SPM vs ISIS-TS2 at 2 Å.

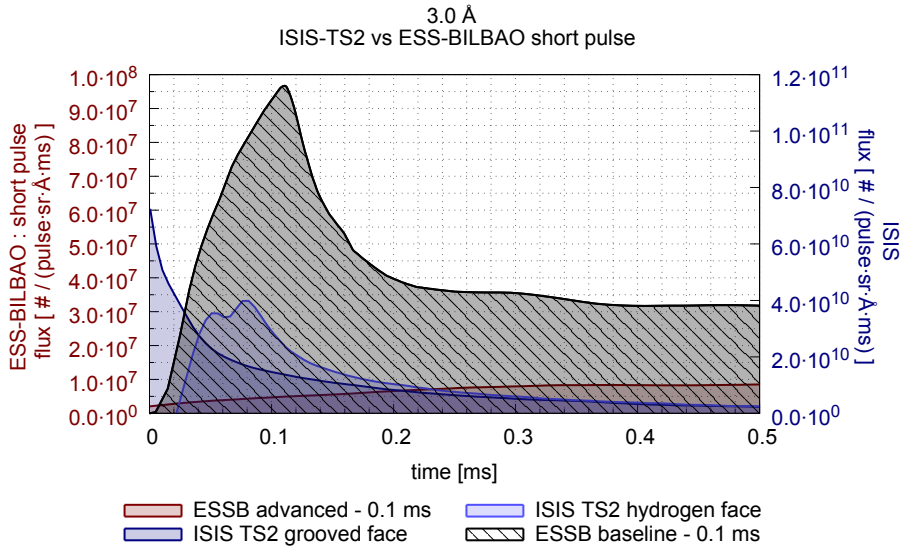

Figure C.1-3: ESSB-SPM vs ISIS-TS2 at 3 Å.

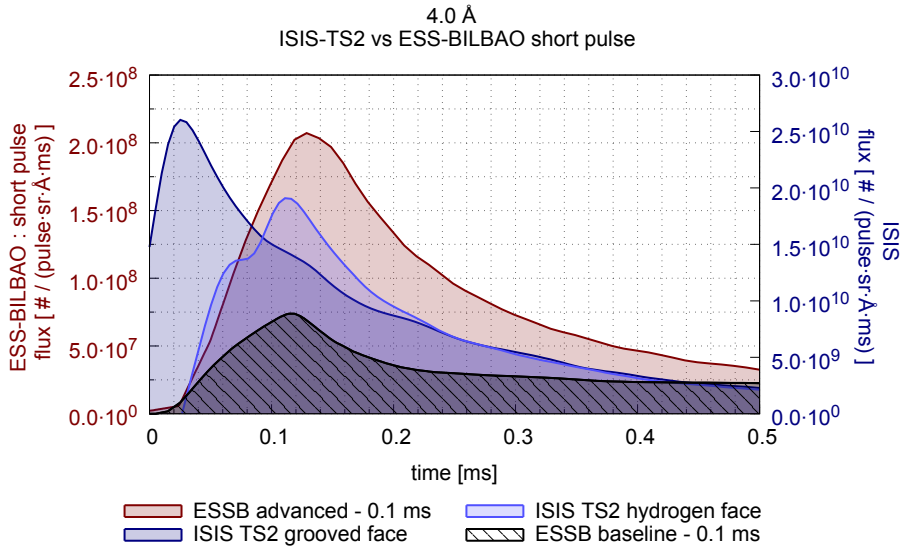

Figure C.1-4: ESSB-SPM vs ISIS-TS2 at 4 Å.

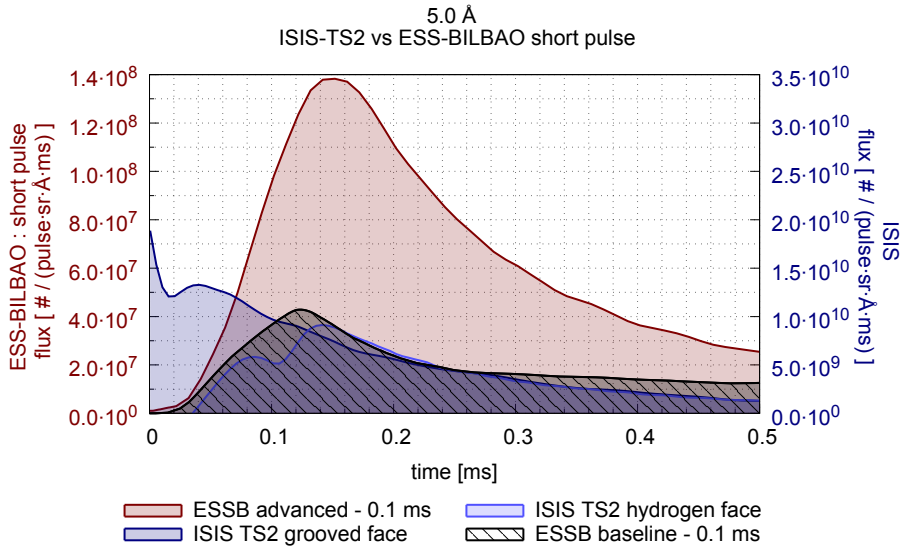

Figure C.1-5: ESSB-SPM vs ISIS-TS2 at 5 Å.

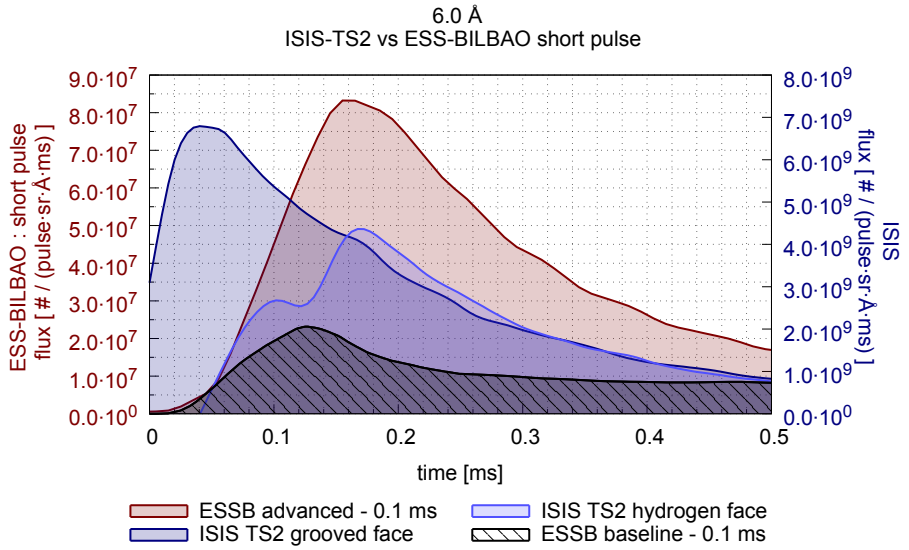

Figure C.1-6: ESSB-SPM vs ISIS-TS2 at 6 Å.

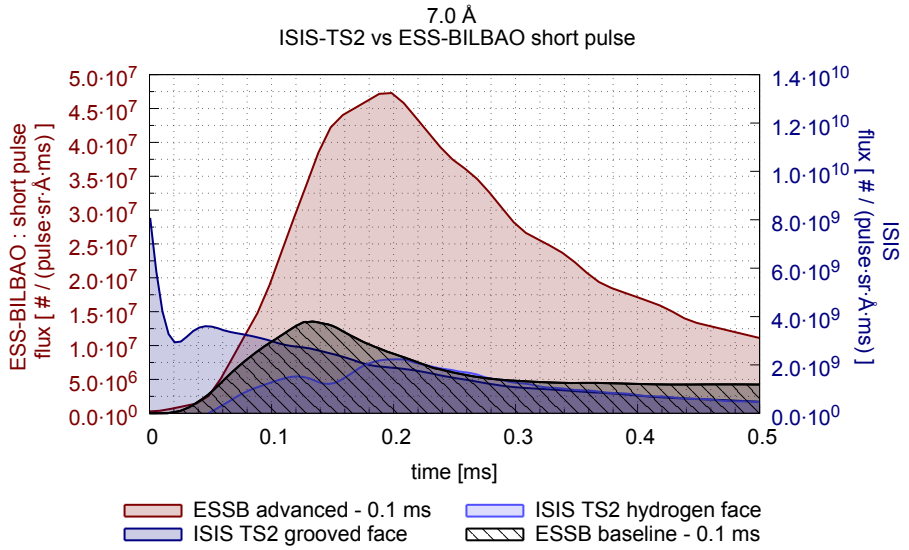

Figure C.1-7: ESSB-SPM vs ISIS-TS2 at 7 Å.

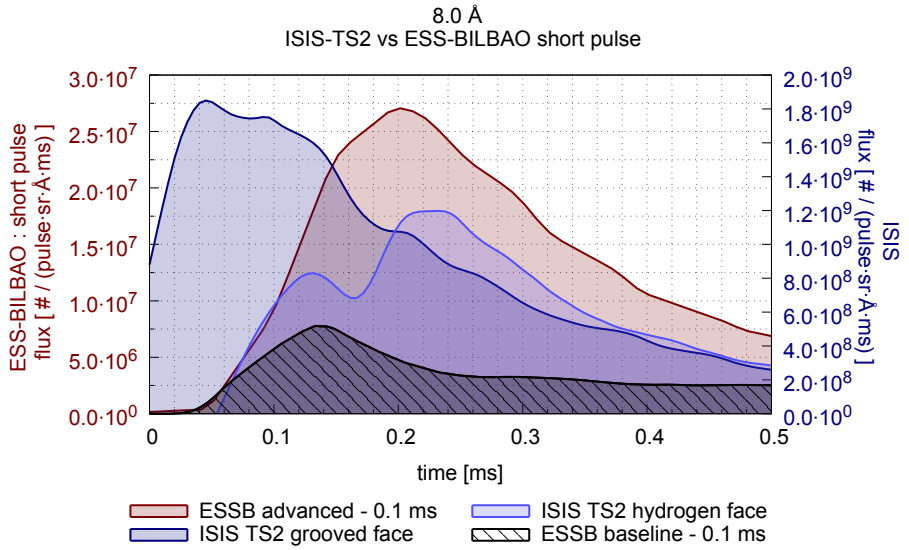

Figure C.1-8: ESSB-SPM vs ISIS-TS2 at 8 Å.

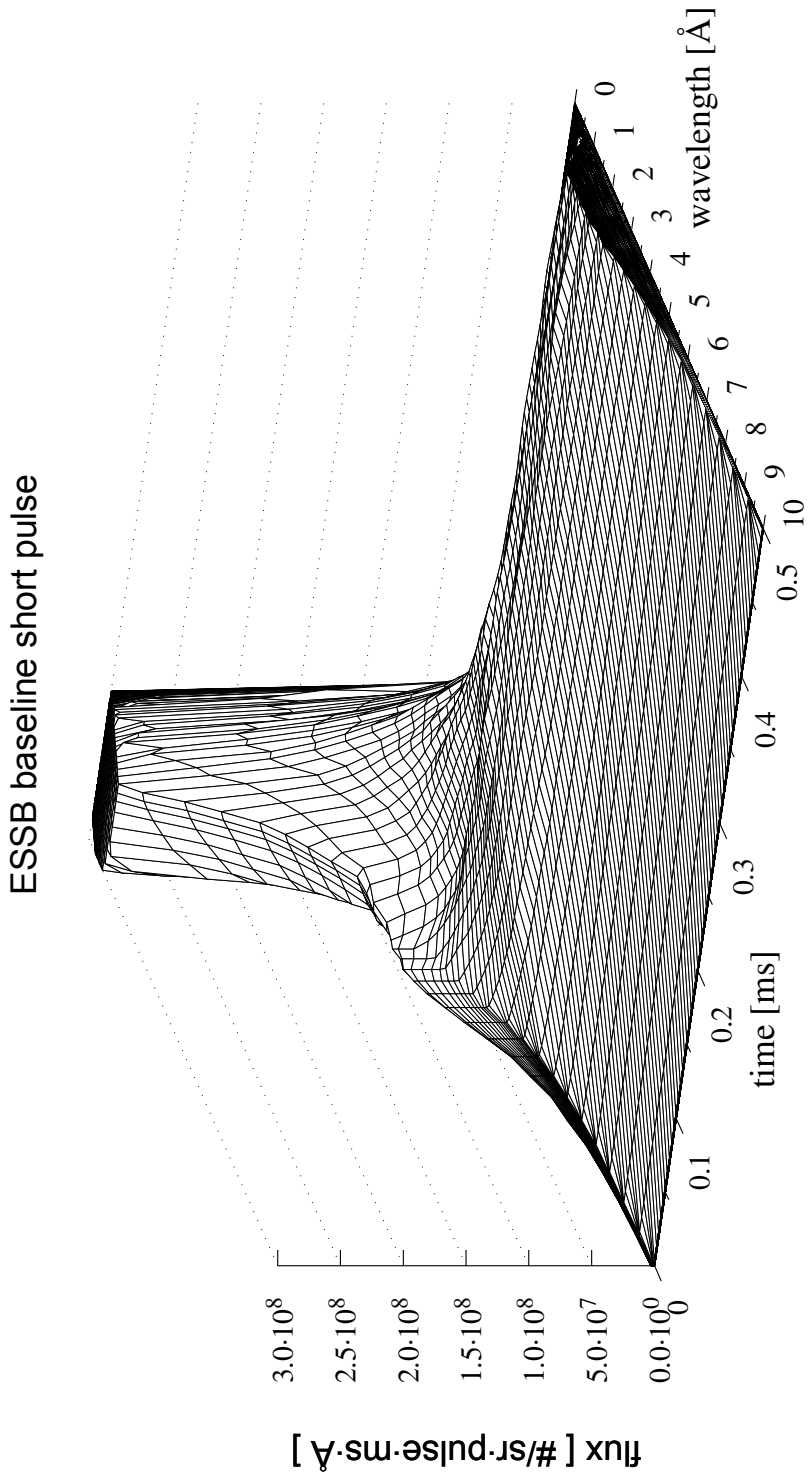

Figure C.1-9: Time-wavelength flux distribution for ESSB-SPM (baseline configuration).

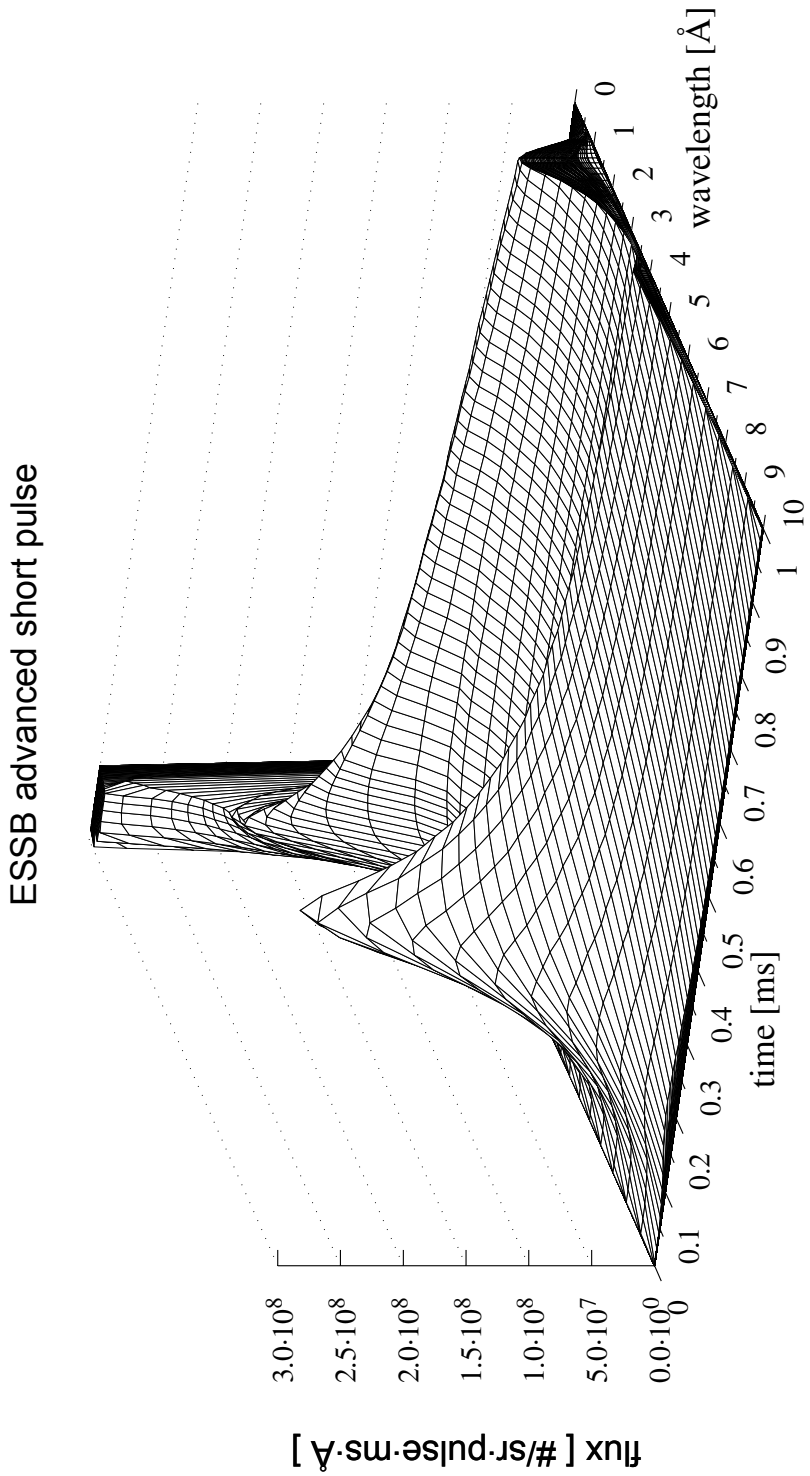

Figure C.1-10: Time-wavelength flux distribution for ESSB-SPM (advanced configuration).

C.2 LONG-PULSE MODE

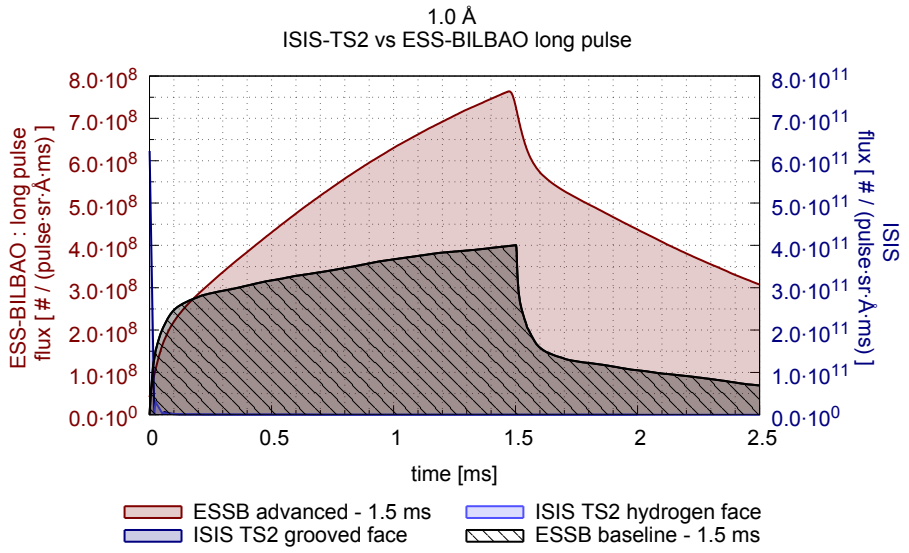

Figure C.2-1: ESSB-LPM vs ISIS-TS2 at 1 Å.

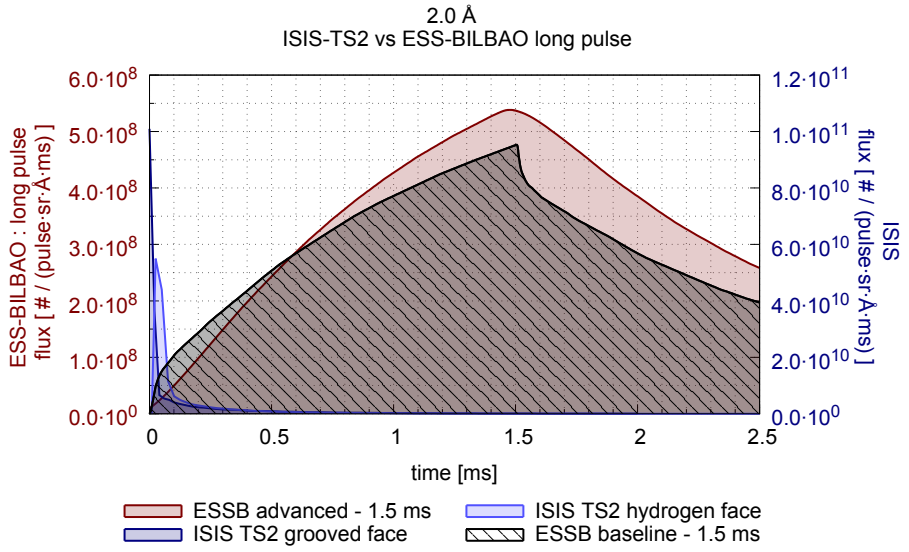

Figure C.2-2: ESSB-LPM vs ISIS-TS2 at 2 Å.

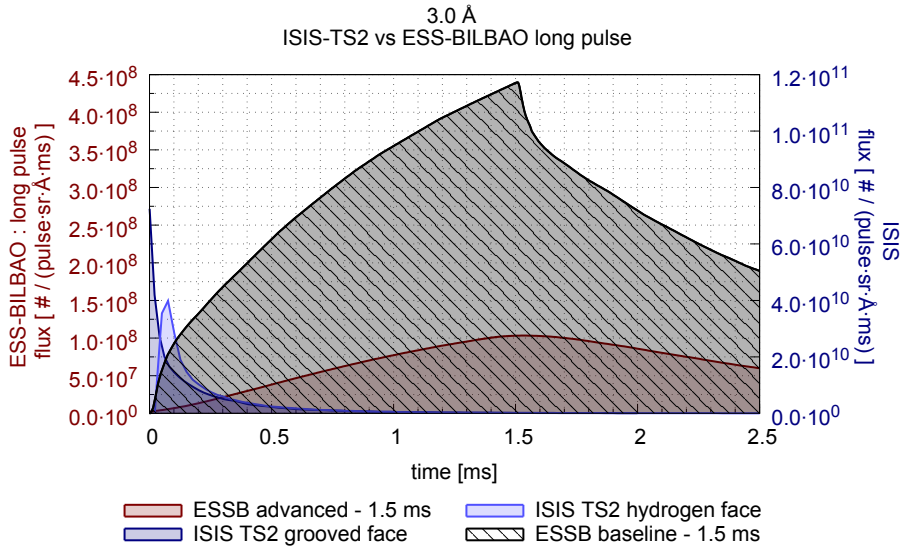

Figure C.2-3: ESSB-LPM vs ISIS-TS2 at 3 Å.

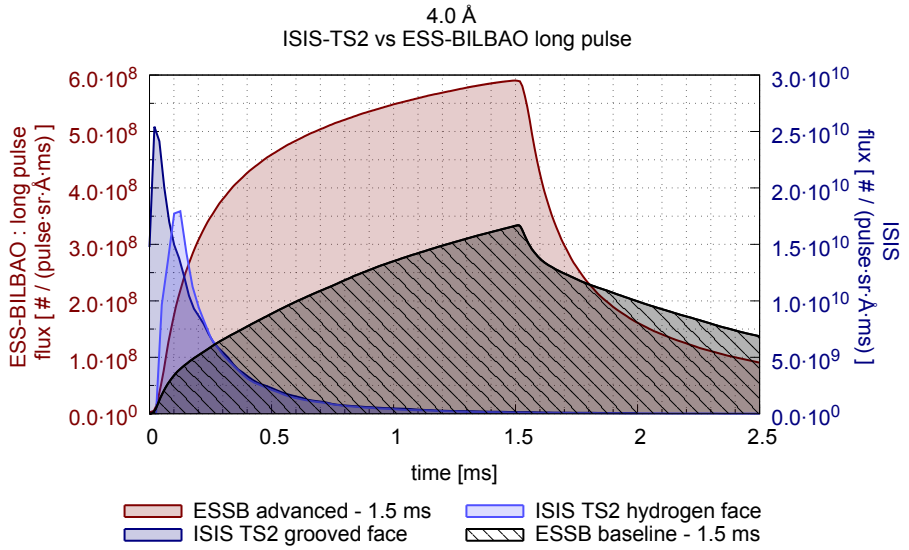

Figure C.2-4: ESSB-LPM vs ISIS-TS2 at 4 Å.

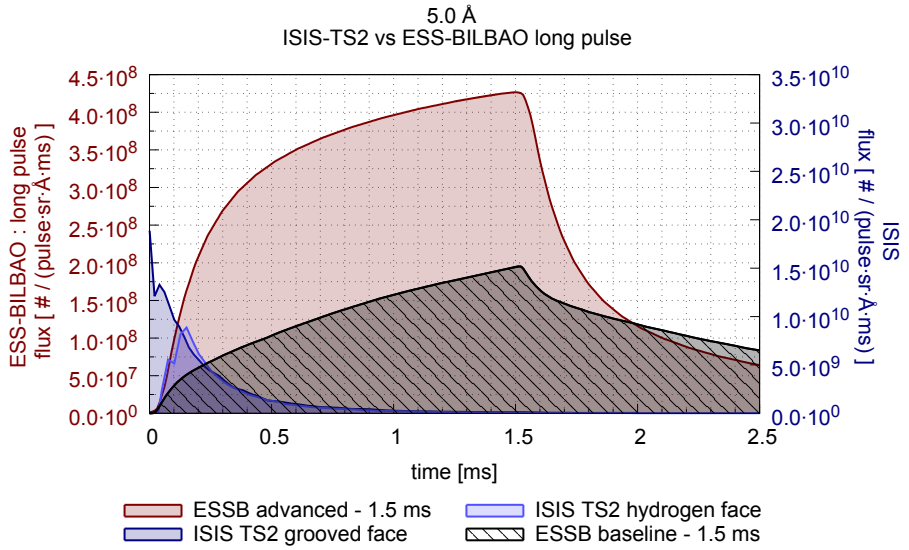

Figure C.2-5: ESSB-LPM vs ISIS-TS2 at 5 Å.

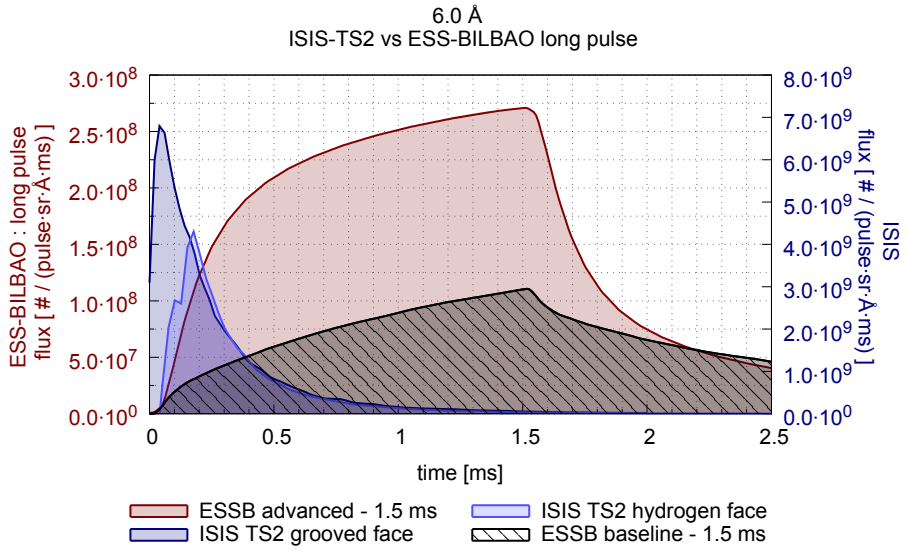

Figure C.2-6: ESSB-LPM vs ISIS-TS2 at 6 Å.

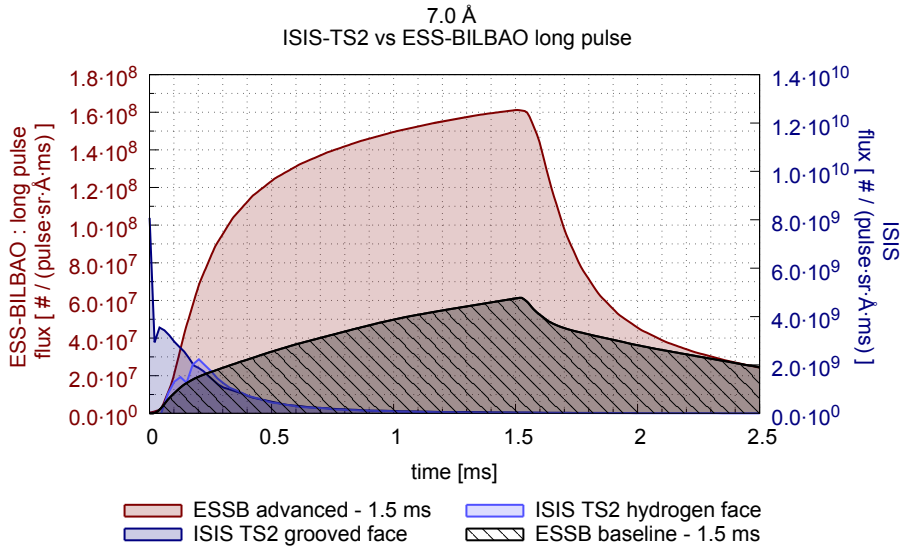

Figure C.2-7: ESSB-LPM vs ISIS-TS2 at 7 Å.

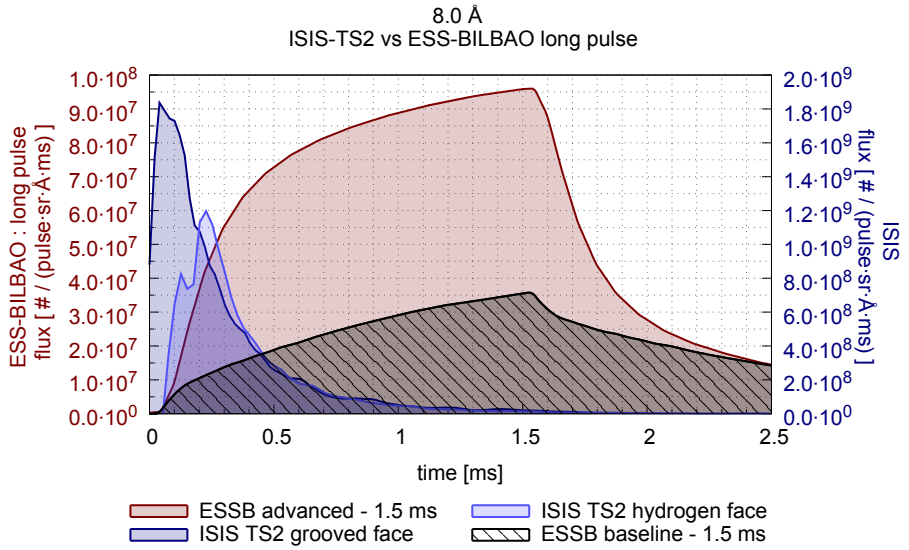

Figure C.2-8: ESSB-LPM vs ISIS-TS2 at 8 Å.

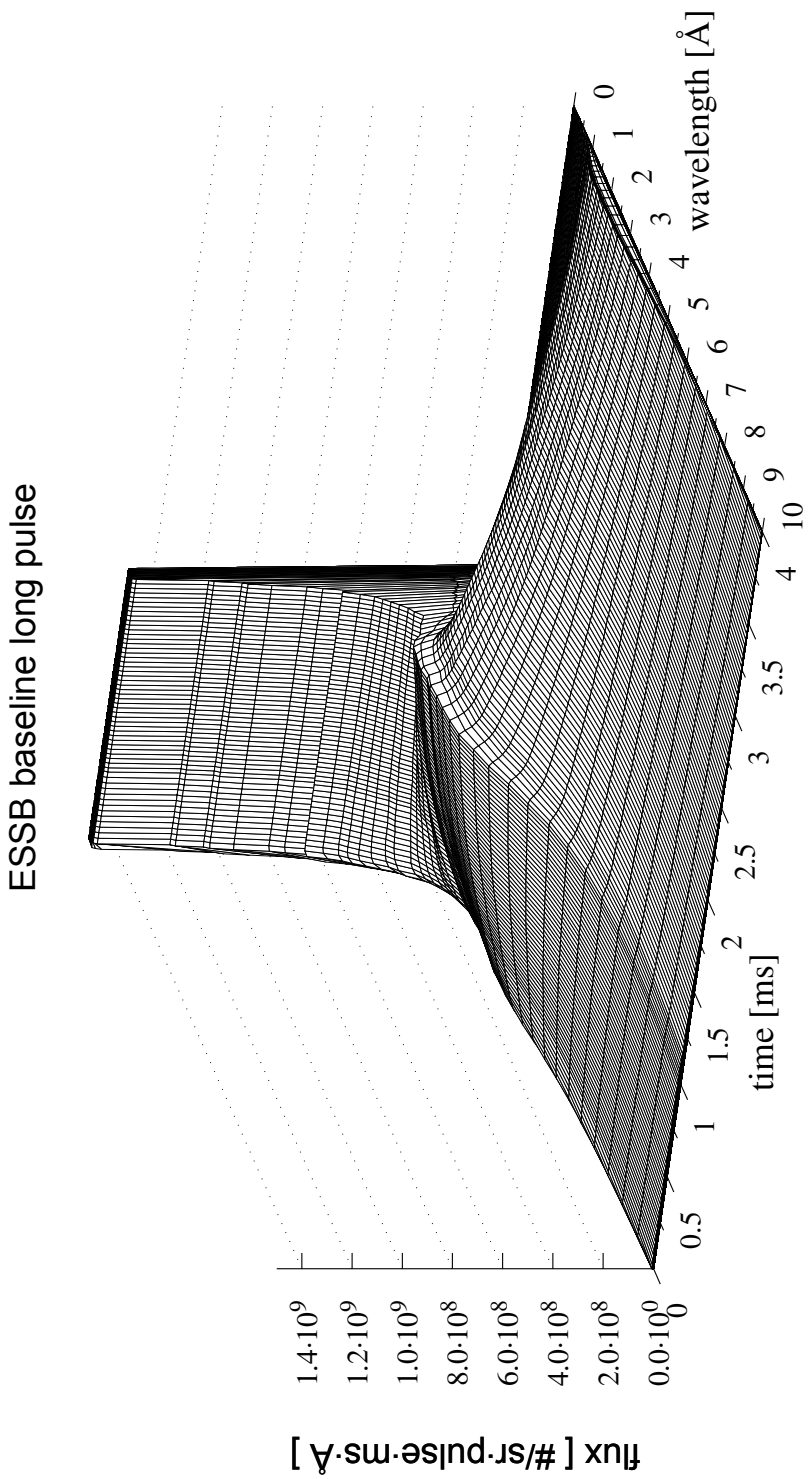

Figure C.2-9: Time-wavelength flux distribution for ESSB-LPM (baseline configuration).

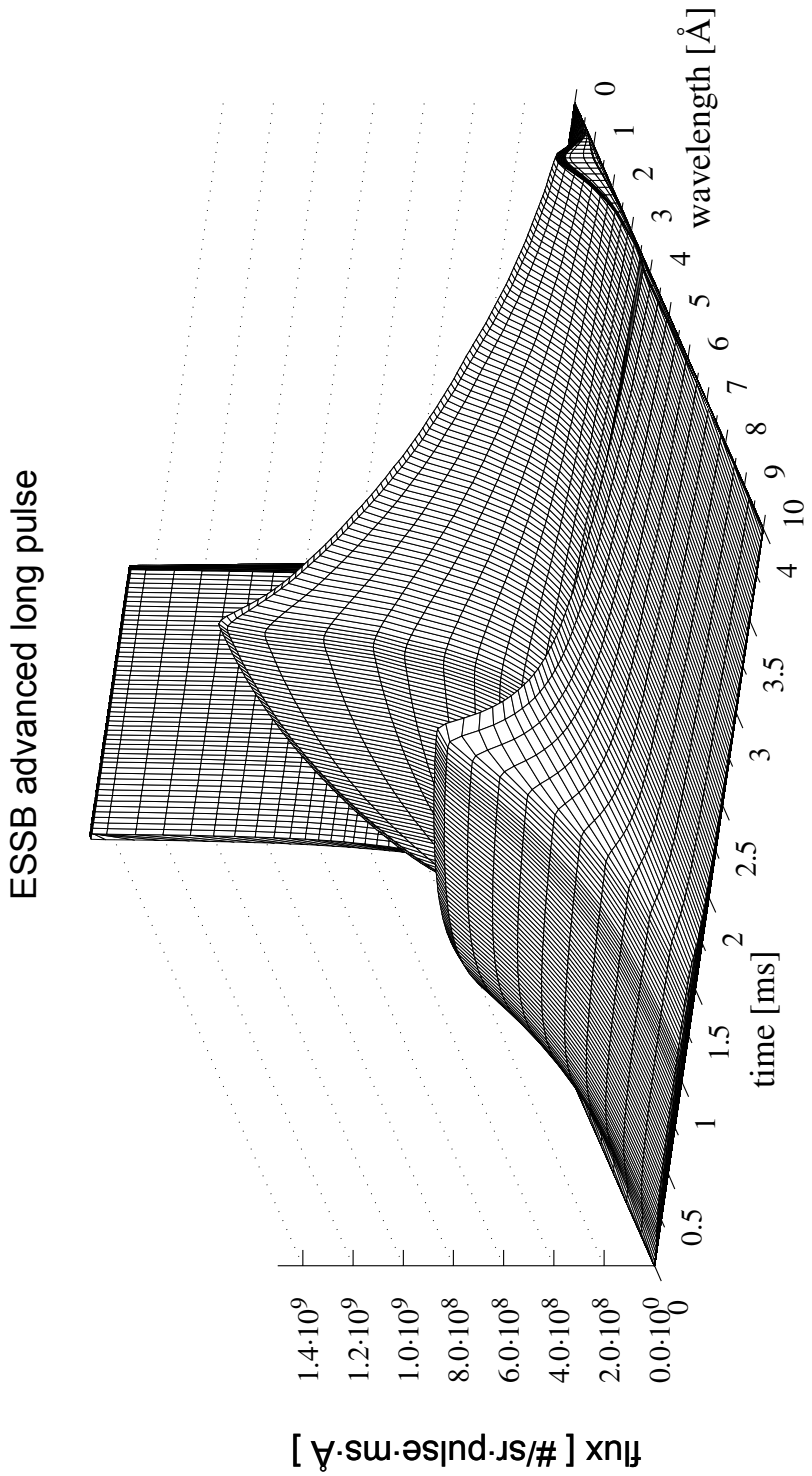

Figure C.2-10: Time-wavelength flux distribution for ESSB-LPM (advanced configuration).

APPENDIX D

THE T_0-CHOPPER

D.1 GENERAL CONSIDERATIONS

This Appendix provides estimates of the required depth of the T_0-chopper blades to block high-energy neutrons and gamma radiation from the target. We assume that the mean free paths of high-enery neutrons are longer than those characteristic of gamma-radiation backgrounds. With this approximation in mind, the thickness of this device can be calculated on the basis of neutron penetration depths.

Our analytical estimates assume 50-MeV neutrons. No detailed simulations of the neutron beam were carried out because these would require knowledge of the the exact position of the T_0-chopper relative to the TMR assembly. The chopper blades are made of Inconel X-750 (see chemical composition in Table D.1-1), following the specification developed at KEK for J-PARC [39] . This material exhibits good properties in terms of mechanical strength and radiological activation.

Table D.1-1: Chemical composition (%) of the Ni-based superalloy Inconel X-750.

Ni	Cr	Fe	Co	Ti	Al	Nb + Ta
73.8	15	7	-	2.5	0.7	1.0

Figure D.1-1 shows an sketch of the T_0-chopper from KEK. In this particular design, the required depth of the blades is specified to be ca. 30 cm. In the following section, we provide a means of estimating this parameter without recourse to detailed simulations.

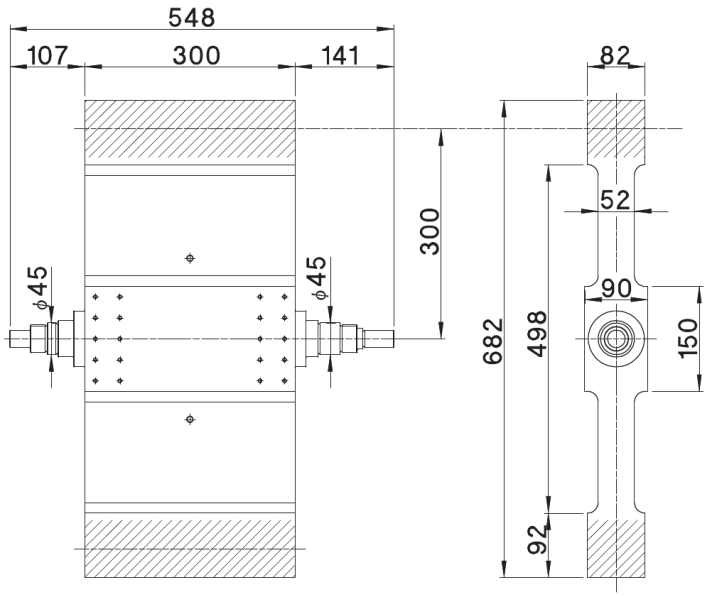

Figure from S. Ithoh et al. [39]

Figure D.1-1: Sketch of the T_0-chopper developed at KEK (all distances in millimeters).

D.2 ANALYTICAL ESTIMATION OF CHOPPER THICKNESS

Figure D.2-1 shows the elastic, inelastic, radiative capture, and total cross sections of Inconel X-750. Above a few hundred meV, nuclear scattering is predominantly elastic. Below this range, the elastic channel competes with radiative capture leading to the emission of gamma radiation. As a first step, we can estimate the penetration range of 9 MeV-neutrons, corresponding to the mean neutron energy for the ESSB target (baseline configuration), followed by subsequent estimates all the way down to a few eV [40] . These processes are dominated by elastic nuclear scattering. We also note that the contribution of nickel to the (macroscopic) elastic cross section dominates because this element is the main component in Inconel X-750.

To proceed, we also need to account for the mean energy loss per collision, as this parameter also determines the overall stopping power of the material. This loss can be quantified via recourse to the mean variation of lethargy, as shown by Eq. D-1:

$$\xi = \Delta \langle u \rangle = ln \frac{E_i}{E_f} = 1 + \frac{(A-1)^2}{2A} ln \left(\frac{A-1}{A+1} \right) \tag{D-1}$$

where,

ξ, *is the mean variation of lethargy*
u, *is the lethargy*
E_i, *is the neutron energy before collision*
E_f, *is the neutron energy after collision*
A, *is the atomic mass of the nucleus*

It is important to note that the mean lethargy variation ξ is a dimensionless quantity independent of the absolute value of the neutron energy (it only depends on the ratio of initial and final energies). A direct measure of the neutron stopping power of the material can be obtained from a lethargy-weigthed macroscopic cross section of the form [41]

$$e^{\xi} \cdot \Sigma = \frac{E_i}{E_f} \cdot \Sigma \tag{D-2}$$

Figure D.2-2 shows the weighted lethargy defined above and confirms that nickel is the component with the highest (predominant) neutron-stopping power in Inconel X-750. Our estimates below will therefore only consider this element.

Since the mean lethargy variation does not depend on the neutron energy, Eq. D-3 can be used to obtain the mean number of collisions required to reduce the neutron energy from E_i to E_f [42]

$$n = \frac{u}{\xi} = \frac{1}{\xi} \cdot ln \frac{E_i}{E_f} \tag{D-3}$$

Taking into account that ξ for nickel is 0.034, then ca. 335 collisions are required to stop neutrons from 9 MeV to 100 eV. Given that the mean macroscopic elastic cross section for nickel is around 11 cm^{-1}, this number of collisions will happen across a characteristic distance of $335/11 \approx 30$ cm. We note that this thickness represents an upper conservative bound because other nuclear processes have been neglected in this simplified analysis. More accurate estimates may be obtained through detailed Monte Carlo simulations to account for solid-angle effects or maximum radiation dose.

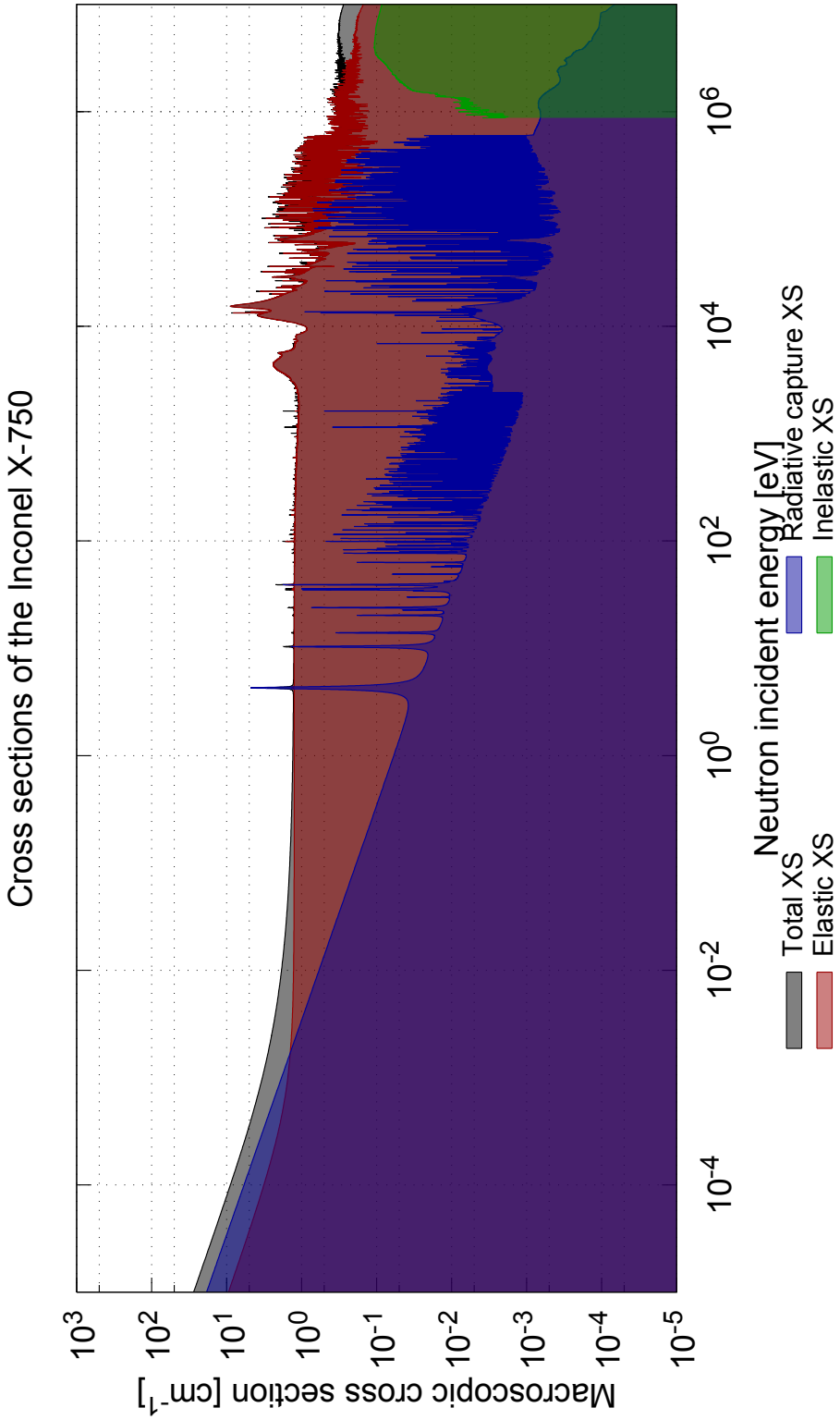

Data from the Chinese Nuclear Data Library v2.1 & v3.1

Figure D.2-1: Total, elastic, inelastic, and radiative capture cross sections of Inconel X-750.

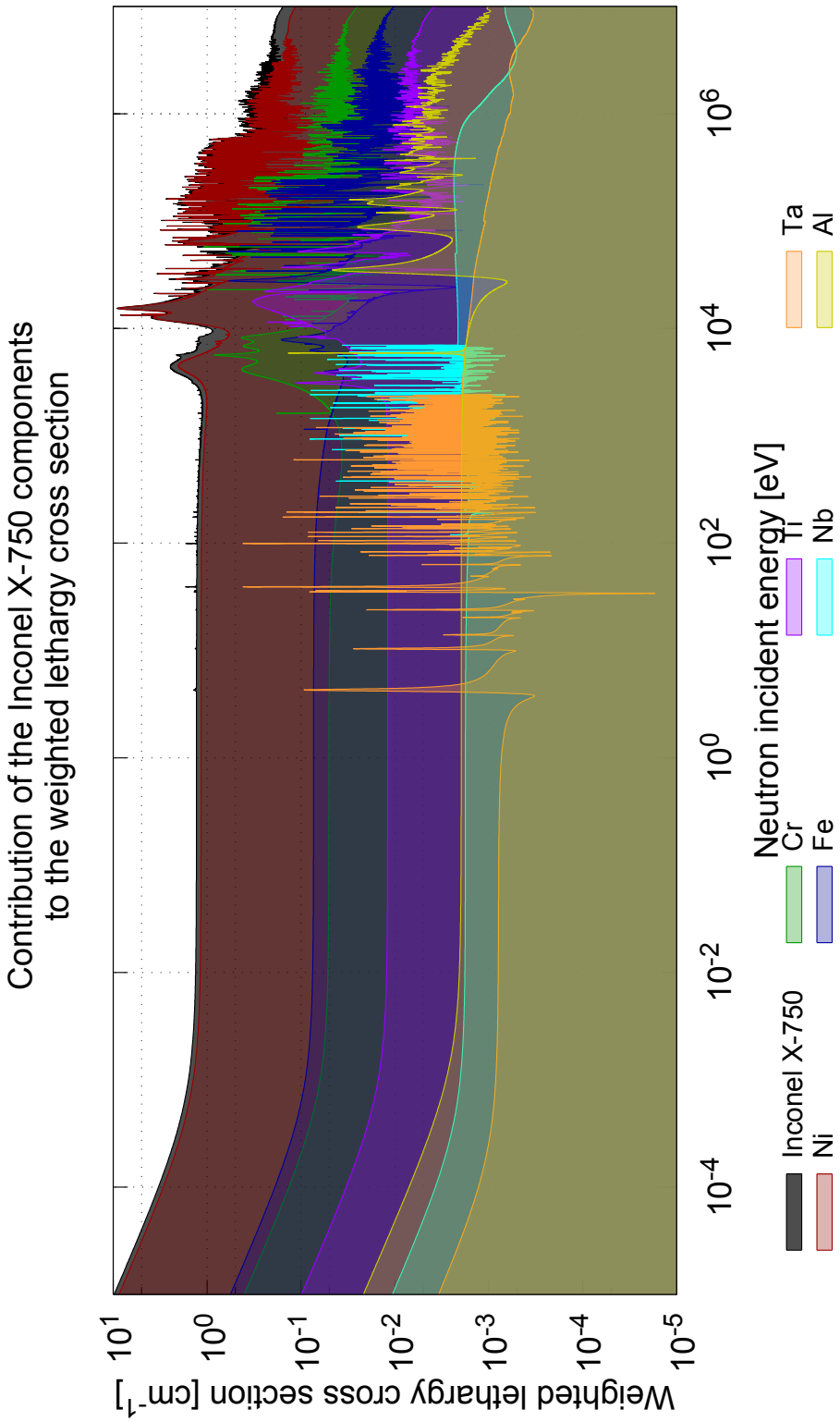

Data from the Chinese Nuclear Data Library v2.1 & v3.1

Figure D.2-2: Relative contributions of Inconel X-750 components to the weighted lethargy cross section, as defined in the main text.